LATE-MAGMATIC TO HYDROTHERMAL PROCESSES

IN THE ILÍMAUSSAQ INTRUSION,

SOUTH GREENLAND

DISSERTATION

zur Erlangung des Grades eines Doktors der Naturwissenschaften

der Geowissenschaftlichen Fakultät

der Eberhard-Karls-Universität Tübingen

vorgelegt von

Gesa Graser

aus Bremen

2008

Tag der mündlichen Prüfung: 11.02.2008

Dekan: Prof. Dr. Peter Grathwohl

1. Berichterstatter: Prof. Dr. Gregor Markl

2. Berichterstatter: PD Dr. Thomas Wenzel

ACKNOWLEDGMENTS

TABLE OF CONTENT

LIST OF FIGURES

LIST OF TABLES

FREQUENTLY USED ABBREVIATIONS

apfu: atoms per formula unit

aq: in aqueous solution

BSE: backscatter electron

c: composition

cm^{-1}: wavenumber

FMQ: fayalite-magnetite-quartz buffer

fO_2: oxygen fugacity

Ga: billion years

HFSE: high field strength elements

HM: hematite-magnetite buffer

ICP-MS: inductively coupled plasma - mass spectrometry

K: (in logK) distribution coefficient

kg: kilogram

km: kilometre

kV: kilo volt

L: litre

log: logarithm

LREE: light rare earth elements

Ma: million years

min: minute

mm: millimetre

mol: mole

n: number

nA: nano ampere

$NaCl_{equiv.}$: sodium chloride equivalents

P: pressure

P.I.: peralkalinity index

pers. com.: personal communication

ppm: parts per million

REE: rare earth elements

s: second

T: temperature

T_f, T_{fm}, $T_{m(ice)}$, and other: abbreviations concerning microthermometry, see Table 8

VPDB: Vienna PeeDee belemnite

VSMOW: Vienna standard mean ocean water

wt.: weight

X_{Mg}: mole fraction

$\delta^{18}O$, δD, $\delta^{13}C$: Isotope ratio of oxygen, hydrogen and carbon, respectively, with respect to a standard

μm: micrometer

°C: degree Celsius

%: percent

‰: permil

Chemical elements are abbreviated according to their atom symbol in the periodic table.

Mineral names are abbreviated according to Kretz (1983).

ABSTRACT

The 1.16 Ga old, persodic Ilímaussaq intrusion in South Greenland solidified at a depth of about 3 to 4 km, between the granitic basement and the sandstones and pillow-bearing basalts of the Eriksfjord Formation. The intrusion consists of alkali granite, syenites, and agpaitic nepheline syenites, which are cut by late-magmatic veins. This thesis deals with late-magmatic to hydrothermal processes in the Ilímaussaq complex and focuses on the fluid phase. The late-stage fluids are of major interest, since they are capable of mobilising, transporting, and redistributing trace elements. Their special nature may lead to a local enrichment of rare and incompatible elements like Zr, Nb, Ta, and REEs even to economic levels. The first part of this study concerns an endoskarn assemblage, whose occurrence is quite extraordinary regarding the Na-dominated intrusion and the lack of carbonate rocks. The second part deals with the geochemical and isotopic composition of the late-magmatic to hydrothermal fluid present at Ilímaussaq.

The endoskarn assemblages comprising the Ca-silicates ilvaite, epidote and Ca-rich garnet occur along fracture zones within the Ilímaussaq intrusion. In contrast to typical skarn assemblages, the Ilímaussaq endoskarns contain albite as a main phase and they did not form in metacarbonate rocks, as these are completely lacking in the vicinity of the intrusion. Instead, the studied endoskarns record late-magmatic to hydrothermal interaction of possibly external Ca-rich fluids with the alkaline to agpaitic rocks and still clearly reflect the magmatic textures of the precursor rocks. Phase relations in the two endoskarn varieties with epidote + albite + Ca-rich garnet ± ilvaite ± retrograde prehnite suggest formation conditions of about 500 °C at high oxygen fugacities slightly above the HM oxygen buffer (FMQ +5 to +7), with later small modifications due to fluid influx or cooling of the original fluid at about 300-350 °C (formation of prehnite) and at about 200-250 °C (oxygen isotopic reequilibration of the albite).

One model for the formation of the observed assemblages suggests the decomposition of Ca-bearing minerals like primary eudialyte, clinopyroxene or ternary feldspar and redistribution of the Ca by a metasomatizing late-magmatic fluid. Stable isotope (O, H) investigations, however, favour a model in which seawater was the metasomatizing fluid, which entered the Eriksfjord basalts above the intrusion, reacted with them (spilitization) and brought about 10^{-3} mol/L Ca along fractures into the metasomatized rocks. Fluid-rock interaction in the Eriksfjord basalts is documented by abundant chlorite-epidote-quartz

assemblages while high fluid/rock ratios allowed the fluid to retain its seawater oxygen isotope composition.

Late-magmatic veins, which were investigated in terms of fluid inclusions and stable isotopes in the second part of this study, consist of albite, aegirine, ussingite ($Na_2AlSi_3O_8(OH)$), fluorite, or, very rarely, quartz and are common in the Ilímaussaq intrusion. The oxygen isotopic composition of the minerals indicates different origins for the quartz veins: while the veins in the alkali granite are orthomagmatic ($\delta^{18}O_{qtz}= 8.5 \text{‰}$), the veins in augite syenite ($\delta^{18}O_{qtz} \sim 10 \text{‰}$) were either derived from fluids that entered the intrusion from the granitic country rocks or they formed by digestion of, or reaction with, sandstone xenoliths in this rock unit. While albite and aegirine do not contain fluid inclusions suitable for investigations, ussingite contains pure hydrocarbon fluid inclusions and fluorite saline brine inclusions of primary and secondary origin. Quartz comprises predominantly primary and secondary NaCl-dominated brine inclusions with up to 29.7 wt.% $NaCl_{equiv.}$ or CH_4-H_2O-NaCl mixtures. These fluids are interpreted to reflect the fluids in equilibrium with the late-stage melts at Ilímaussaq.

The carbon and hydrogen isotope composition of the methane in fluid inclusions in quartz ($\delta^{13}C = -43$ to -23 ‰, $\delta D = -176$ to -121 ‰) resembles the signature of thermogenic methane, but the higher hydrocarbons are mostly ^{13}C-depleted in relation to CH_4, which is typical of abiogenically-derived hydrocarbons. The carbon and hydrogen isotope composition of methane in ussingite ($\delta^{13}C = -6$ to -3 ‰, $\delta D = -121$ ‰), is similar to earlier analyses of Ilímaussaq methane, and suggests a magmatic origin.

Ion-chromatography of fluid inclusion leachates from the late-stage veins reveals Cl/Br ratios of about 100. As such values seem to be a typical feature of peralkaline magmatic rocks, at least in the Gardar Province of South Greenland, it is suggested that this ratio is typical of Gardar magmatic fluids and may be characteristic of the Cl/Br ratio of the lithospheric mantle from which these alkaline melts were derived. The geochemical composition of the late-stage aqueous fluids shows some variability, but is dominated by sodium chloride (108 621 to 149 655 ppm chloride, 77 505 to 254 657 ppm sodium) and minor to trace amounts of, for example, calcium (3 299 to 34 193 ppm), potassium (3 966 to 21 966 ppm), iron (212 to 584 ppm), uranium (188 ppm), and fluorine (52 to 20 731 ppm).

ZUSAMMENFASSUNG

Die 1,16 Ga alte persodische Ilímaussaq Intrusion in Südgrönland erstarrte in einer Tiefe von 3 bis 4 km zwischen dem granitischen Grundgebirge und der Wechselfolge von Sandsteinen und Basalten der Eriksfjord Formation. Die Intrusion besteht aus Alkaligraniten, Syeniten und agpaitischen Nephelinsyeniten, die von spätmagmatischen Adern durchdrungen werden. Die vorliegende Arbeit befasst sich mit spätmagmatischen bis hydrothermalen Prozessen innerhalb der Ilímaussaq Intrusion mit Schwerpunkt auf der Fluidphase. Das Verständnis solcher Prozesse ist von großem Interesse, da auf diesem Weg seltene und inkompatible Elemente wie Zr, Nb, Ta und REEs remobilisiert, transportiert und bis zu ökonomisch relevanten Größenordnungen angereichert werden können. Im ersten Teil der Arbeit wird die Entstehung einer Endoskarn-Paragenese untersucht, deren Auftreten innerhalb dieser Na-dominierten Intrusion äußerst ungewöhnlich ist, da es in deren Umfeld keine Karbonatgesteine gibt. Der zweite Teil behandelt die geochemische und isotopische Zusammensetzung des spätmagmatisch bis hydrothermalen Ilímaussaq Fluids.

Die Endoskarn-Paragenese tritt entlang von Bruchstrukturen innerhalb der Intrusion auf und umfasst die Ca-Silikate Ilvait, Epidot und Ca-reichen Granat. Im Gegensatz zu typischen Skarnen haben die Endoskarne in Ilímaussaq jedoch Albit als Hauptbestandteil und bildeten sich nicht in Zusammenhang mit Metakarbonaten, da diese im direkten Umfeld der Intrusion nicht auftreten. Stattdessen spiegeln sie eine spätmagmatische bis hydrothermale Wechselwirkung eines Ca-reichen, möglicherweise externen Fluids mit den alkalinen bis agpaitischen Gesteinen der Intrusion wider. Die Texturen der Endoskarne zeigen noch deutlich die magmatischen Texturen ihrer Vorgängergesteine. Phasenbeziehungen der zwei Endoskarn-Varietäten, die aus Epidot + Albit + Ca-reichem Granat ± Ilvait ± retrogradem Prehnit bestehen, lassen Bildungsbedingungen von ca. 500 °C bei hoher Sauerstofffugazität leicht oberhalb des HM Puffers (FMQ +5 bis +7) vermuten. Durch erneuten Fluid-Einfluss oder durch Wechselwirkung mit dem noch vorhandenen, abgekühlten Fluid wurde der Mineralbestand bei 300 bis 350 °C (Bildung von Prehnit) und die Sauerstoffisotopie bei ca. 200 bis 250 °C (Reequilibrierung des Albits) nochmals verändert.

Ein möglicher Prozess, der zur Bildung der Paragenesen führen könnte, ist der Zerfall von kalziumhaltigen Mineralen, wie den primären Mineralen Eudialyt, Klinopyroxen und ternärem Feldspat und die Umverteilung des Kalziums durch ein spätmagmatisches, metasomatisches Fluid. Die Untersuchung stabiler Isotope (O, H) legt jedoch nahe, dass Meerwasser das wechselwirkende Fluid war. Das Meerwasser drang in die Basalte oberhalb

der Intrusion ein, führte zu deren Spilitisierung und transportierte ca. 10^{-3} mol/L Ca entlang von Rissen in die alterierten Gesteine. Eine Wechselwirkung zwischen Fluid und Gestein innerhalb der Eriksfjord Basalte ist durch das Auftreten der Paragenese Chlorit-Epidot-Quarz belegt. Hohe Fluid/Gesteins-Verhältnisse ermöglichten, dass das Meerwasser die Sauerstoffisotopie beibehielt.

Spätmagmatische Adern, die im zweiten Teil dieser Arbeit hinsichtlich ihrer Fluideinschlüsse und Isotopie untersucht wurden, gehören zum typischen Erscheinungsbild der Ilímaussaq Intrusion. Die Adern beinhalten Albit, Ägirin, Ussingit ($Na_2AlSi_3O_8(OH)$), Fluorit und in seltenen Fällen auch Quarz. Die Sauerstoffisotopie der Minerale deutet auf verschiedene Entstehungen der Quarz-Adern hin: während die Adern im Alkaligranit orthomagmatischen Ursprungs sind ($\delta^{18}O_{qtz}$= 8.5 ‰), entstanden die Quarz-Adern im Augit-syenit ($\delta^{18}O_{qtz}$ ~10 ‰) entweder aus Fluiden, die aus dem granitischen Umgebungsgestein in die Intrusion eingedrungen sind oder aus der Aufarbeitung, oder einer Reaktion mit Sandsteinxenolithen innerhalb der Gesteinseinheit.

Albit und Ägirin enthalten keine analysierbaren Fluideinschlüsse. Ussingit hingegen beinhaltet reine Kohlenwasserstoffeinschlüsse und Fluorit salinare Lösungen primären und sekundären Ursprungs. Quarz enthält vorwiegend primäre und sekundäre NaCl-dominierte Einschlüsse, die bis zu 29.7 Gew.% $NaCl_{equiv.}$ enthalten oder aus CH_4-H_2O-NaCl-Gemischen bestehen. Diese Fluideinschlüsse repräsentieren höchstwahrscheinlich das Fluid, das mit den späten Ilímaussaq Schmelzen im Gleichgewicht stand.

Die Kohlenstoff- und Wasserstoffisotopie von im Quarz eingeschlossenem Methan ($\delta^{13}C$ = –43 to –23 ‰, δD = –176 to –121 ‰) gleicht der Signatur von thermogenem Methan, aber die höheren Kohlenwasserstoffe sind im Vergleich zum Methan meist an ^{13}C verarmt, was typisch für abiogen entstandene Kohlenwasserstoffe ist. Die Kohlenstoff- und Wasserstoffisotopie des Methans in Ussingit ($\delta^{13}C$ = –6 to –3 ‰, δD = –121 ‰) ähnelt der Signatur bereits existierender Analysen von Methan der Ilímaussaq Intrusion und deutet auf seinen magmatischen Ursprung hin.

Ionenchromatographische Untersuchungen der Fluide erbrachte Cl/Br-Verhältnisse um 100. Da Werte um 100 typisch für peralkaline magmatische Gesteine zu sein scheinen, zumindest in der Gardar Provinz in Südgrönland, deutet das darauf hin, dass das Verhältnis charakteristisch für den lithospherischen Mantel ist, aus dem die alkalinen Schmelzen stammen. Die chemische Zusammensetzung der späten wässrigen Fluide zeigt eine gewisse Variabilität, ist aber charakterisiert durch Natriumchlorid (108 621 bis 149 655 ppm Chlorid, 77 505 bis 254 657 ppm Natrium) und geringeren Mengen von unter anderem Kalzium (3 299

bis 34 193 ppm), Kalium (3 966 bis 21 966 ppm), Eisen (212 bis 584 ppm), Uran (188 ppm) und Fluorid (52 bis 20 731 ppm).

1 INTRODUCTION

Peralkaline intrusive rocks represent just a small fraction of the total volume of igneous rocks of the Earth's crust. Nevertheless, there are some extraordinary features, which have attracted the curiosity of geologists for a long time. The crystallization conditions and the chemical evolution are of major interest since some of the intrusions show extreme fractionation trends with particularly long crystallization intervals of between 1000 and 400 °C (Sood & Edgar, 1970; Edgar & Parker, 1974; Larsen & Sørensen, 1987). Moreover, the unusual enrichment of high field strength elements (HFSE) such as Zr, Hf, Nb, Ta, or REEs in some of the complexes, the occurrence of pegmatites enriched in rare elements, liquid immiscibility features, and the Ivigtut cryolite deposit evoked the interest of many petrologists (Sørensen, 1992; 1997; Pauly & Bailey, 1999; Markl, 2001a; Sørensen *et al.*, 2003; Veksler, 2004). Late-magmatic metasomatic processes such as fenitization and autometasomatism are also common features of alkaline intrusions (Ferguson, 1964; Sørensen *et al.*, 1974; Salvi & Williams-Jones, 1990; 1996; 2006; Ranløv & Dymek, 1991; Boily & Williams-Jones, 1994; Finch, 1995; Rae *et al.*, 1996; Coulson, 1997; 2003; Salvi *et al.*, 2000; Sindern & Kramm, 2000; Sørensen & Larsen, 2001; Marks *et al.*, 2003, Liferovich & Mitchell, 2006; Mitchell & Liferovich, 2006). Salvi & Williams-Jones (1990; 2006) and Salvi *et al.* (2000) showed that the involved late-magmatic to hydrothermal fluids are not only able to mobilize rare and incompatible elements but may also redeposit and concentrate them up to economic levels. Salvi & Williams-Jones (1990; 1996) and Salvi *et al.* (2000) suggested the Zr enrichment to be related to late-magmatic to hydrothermal F-rich, HFSE-bearing fluid phases, which led to the formation of Ca-rich Zr-silicates. The details of the late-magmatic to hydrothermal processes as a whole, like transport capability, the effect of redox conditions and fluid composition, fluid unmixing, metasomatic reactions and precipitation mechanisms are still poorly understood. Hence, it is of interest to understand the details of the fluid origin, its chemical evolution during late-magmatic to hydrothermal stages, fluid-rock interaction processes, and the formation of unusual Ca-rich assemblages in peralkaline intrusions.

The Ilímaussaq complex in South Greenland is a textbook example of a peralkaline intrusion (Larsen & Sørensen, 1987; Sørensen, 2001). It is one of the most reduced syenitic intrusions (Markl *et al.*, 2001; Marks & Markl, 2001), for the most part remained a closed system during fractionation (Markl *et al.*, 2001; Marks *et al.*, 2004), and hosts one of the major Zr, Nb, Ta, and REE (rare earth element) deposits of the world (Bohse *et al.*, 1971; Sørensen, 1992). Its study enables to further constrain the geochemical evolution of the

magma and the evolution of the coexisting fluid phases (Stevenson *et al.*, 1997; Markl & Baumgartner, 2001; Marks *et al.*, 2004). Phenomena of the late-magmatic to hydrothermal stage in the evolution of the intrusion are immiscibility features of extremely Th-, Nb- and REE-rich residual melts (Markl, 2001a) and Be-rich hydrothermal veins (Engell *et al.*, 1971; Markl, 2001b). The occurrence of different late-stage veins allows to reconstruct quantitatively the pH evolution of hydrothermal fluids (Markl & Baumgartner, 2001; Sørensen *et al.*, 2003) and the enrichment of Na (Sørensen, 1962; Engell *et al.*, 1971; Schönenberger *et al.*, 2006; Müller-Lorch *et al.*, 2007).

A so far little studied late-stage phenomenon in the Ilímaussaq intrusion are Ca-rich assemblages including epidote, Ca-rich garnet, ilvaite and prehnite (Ussing, 1912; Petersen *et al.*, 1995), which resemble assemblages known from skarns in contact metamorphic carbonates (Einaudi *et al.*, 1981; Einaudi & Burt, 1982; Meinert *et al.*, 2005). However, carbonate rocks are absent in the vicinity of the Ilímaussaq complex. Examples of skarn assemblages with no relation to carbonate rocks are scarce. Only the Sasano copper skarn, Yoshioka Mine, Japan, is believed to have formed from aluminous sedimentary rocks by interaction with Ca- and Fe-rich hydrothermal solutions (Shimazaki, 1982). Skarn-like assemblages are very unusual for a persodic intrusion like Ilímaussaq. Thus, detailed petrographic and geochemical investigations can be used to quantitatively understand the late-stage metasomatic interaction of the intrusion with fluids and the physico-chemical conditions during this interaction. The results of this study are presented in the first part of this thesis.

The second part focuses on the fluid, which coexisted with the late-stage Ilímaussaq melts. Investigations in peralkaline rocks have shown that the magmatic fluid is commonly H_2O-CO_2 or CH_4-dominated depending on the redox state (Petersilie & Sørensen, 1979; Markl *et al.*, 2001; Potter *et al.*, 2004; Nivin *et al.*, 2005). Studies on peralkaline complexes like Khibina, Lovozero, and Kovdor of the Kola peninsula, Russia have been published by Potter *et al.* (1998, 2004) and Beeskow *et al.* (2006), and on the Strange Lake Complex, Canada, by Salvi & Williams-Jones (1990; 1992; 1997; 2006). All of these studies indicate that hydrocarbon-bearing fluid inclusions are a peculiar but typical feature of peralkaline and agpaitic rocks. However, the origin of these highly reduced fluids has been controversial. The late-magmatic reduction of a primary CO_2-H_2O fluid was suggested for the Ilímaussaq intrusion (Petersilie & Sørensen, 1979; Konnerup-Madsen & Rose-Hansen, 1982; Konnerup-Madsen, 2001) whereas Salvi & Williams-Jones (1997; 2006), Potter & Konnerup-Madsen (2003), and Potter *et al.*

(2004) supposed a post-magmatic Fischer-Tropsch-type reaction[1] to account for the hydrocarbons in the Strange Lake complex, Canada, and the Khibina and Lovozero complexes, Russia. A prerequisite of both models is the presence of a primary CO_2-rich fluid, which was reduced to hydrocarbons. However, such a fluid would not be stable at the low oxygen fugacity (fO_2) conditions known from the Ilímaussaq and Khibina magmas (FMQ –2 to –5 (fayalite-quartz-magnetite oxygen buffer), Markl *et al.*, 2001; Ryabchikov & Kogarko, 2006). Furthermore, such models are only applicable if considerable amounts of CO_2 were present which, however, is neither the case in Ilímaussaq nor in Khibina (e.g. Beeskow *et al.*, 2006). The recent studies of Krumrei *et al.* (2007) on fluid inclusions from the cores of sodalite crystals of the Ilímaussaq complex demonstrated that at least some of the hydrocarbon-rich fluid inclusions appear to be of primary magmatic origin. Calculations performed by Ryabchikov & Kogarko (2006) indicate a melt will be in equilibrium with almost pure CH_4 at magmatic conditions of 900°C and 1 kbar and under redox conditions corresponding to FMQ –3. But they also showed that a CO_2-H_2O fluid close to the FMQ buffer can produce significant amounts of methane by simple closed-system cooling between 800 and 400 °C.

Since the existence of high-temperature magmatic methane in the Ilímaussaq intrusion was proven by Krumrei *et al.* (2007), it is now of interest to study the geochemistry and the stable isotopic composition of the fluid, especially during late-magmatic mineralization, after more fluid separated from the melt. In the second part of this study various fluid inclusion types in quartz, ussingite and fluorite of the Ilímaussaq complex were investigated using petrography, microthermometry, Laser-Raman spectroscopy, ion-chromatography and gas chromatography-mass spectrometry. The results of this study expand the investigations on Ilímaussaq fluid inclusions done by Konnerup-Madsen (1980; 2001) Konnerup-Madsen & Rose-Hansen (1982), and Konnerup-Madsen *et al.* (1979; 1988), which could not constrain the geochemical composition of the fluid in terms of major, minor and trace elements. It details the composition of a reduced, persodic fluid, which coexisted with late-stage alkaline melts.

---

[1] Which means in this case the reduction of exsolved magmatic CO_2 with H_2 from hydrothermal reaction to hydrocarbons. This reaction needs to take place in the presence of catalysts, which are native transition metals like Fe from e.g. Fe-oxides and Fe-silicates (Potter & Konnerup-Madsen, 2003).

2 GEOLOGICAL SETTING

The 1.16 Ga old Ilímaussaq intrusive complex is part of the mid-Proterozoic (1.1-1.3 Ga) Gardar failed rift province in South Greenland (Upton & Emeleus, 1987; Krumrei *et al.*, 2006). During a period of about 200 Ma, 12 major and several minor alkaline complexes intruded the early Proterozoic Ketilidian basement (Garde *et al.*, 2002; Upton *et al.*, 2003). The mantle melts forming the Ilímaussaq magmas intruded at a depth of about 3 to 4 km (Konnerup-Madsen & Rose Hansen, 1984; Larsen & Sørensen, 1987), between the contact of the early Proterozoic Ketilidian (1.7-1.8 Ga) basement granites, the so-called Julianehåb batholith, and the overlying sandstones and basalts of the late-Gardar Eriksfjord Formation (Fig. 1; Poulsen, 1964).

Crystallization temperatures in the Ilímaussaq intrusion range from about 900 °C to 450 °C (Sørensen, 1969; Piotrowsky & Edgar, 1979; Markl *et al.*, 2001), indicating an extraordinarily long crystallization interval (Sood & Edgar, 1970; Larsen, 1976; Edgar & Parker, 1974; Larsen & Sørensen, 1987). The rocks show a strong fractionation trend of an initially silica saturated alkaline magma towards silica-undersaturation. Four magma batches intruded successively producing first an alkaline, barely silica-saturated augite syenite, in the second stage a peralkaline granite, and finally two sets of silica-undersaturated agpaitic nepheline syenites (Fig. 1; Sørensen *et al.*, 2006; Krumrei *et al.*, 2007). The agpaites form the major part of the intrusion and are divided into sodalite foyaite and naujaite of stage three, and the layered kakortokites and the lujavrites of stage four. All of them are texturally different varieties of nepheline or sodalite syenites. They contain nepheline, sodalite, eudialyte, alkali feldspar, arfvedsonite, and aegirine in various proportions as well as rare minerals like, for example, aenigmatite and rinkite.

During fractionation, the oxygen fugacity in the augite syenite decreased from FMQ –1 to below FMQ –4 but increased during further fractionation and cooling in the agpaitic stage to FMQ +2 to +4 (Markl *et al.*, 2001). Crystallization in a closed system is believed to be responsible for this peculiar redox trend (Markl *et al.*, 2001).

Depending on the predominance or presence of a mineral, lujavrites are divided into black (arfvedsonite), green (aegirine), naujakasite, steenstrupine, or villiaumite lujavrites (Ferguson, 1964; Bohse & Andersen, 1981; Sørensen & Larsen, 2001; Andersen & Sørensen, 2005; Sørensen, 2006). The dominance of a certain mineral mainly depends on the oxygen fugacity, water activity, and the Na/Si ratio in the melt at the time of formation (Andersen & Sørensen, 2005). A low oxygen fugacity at elevated water activity favours the formation of
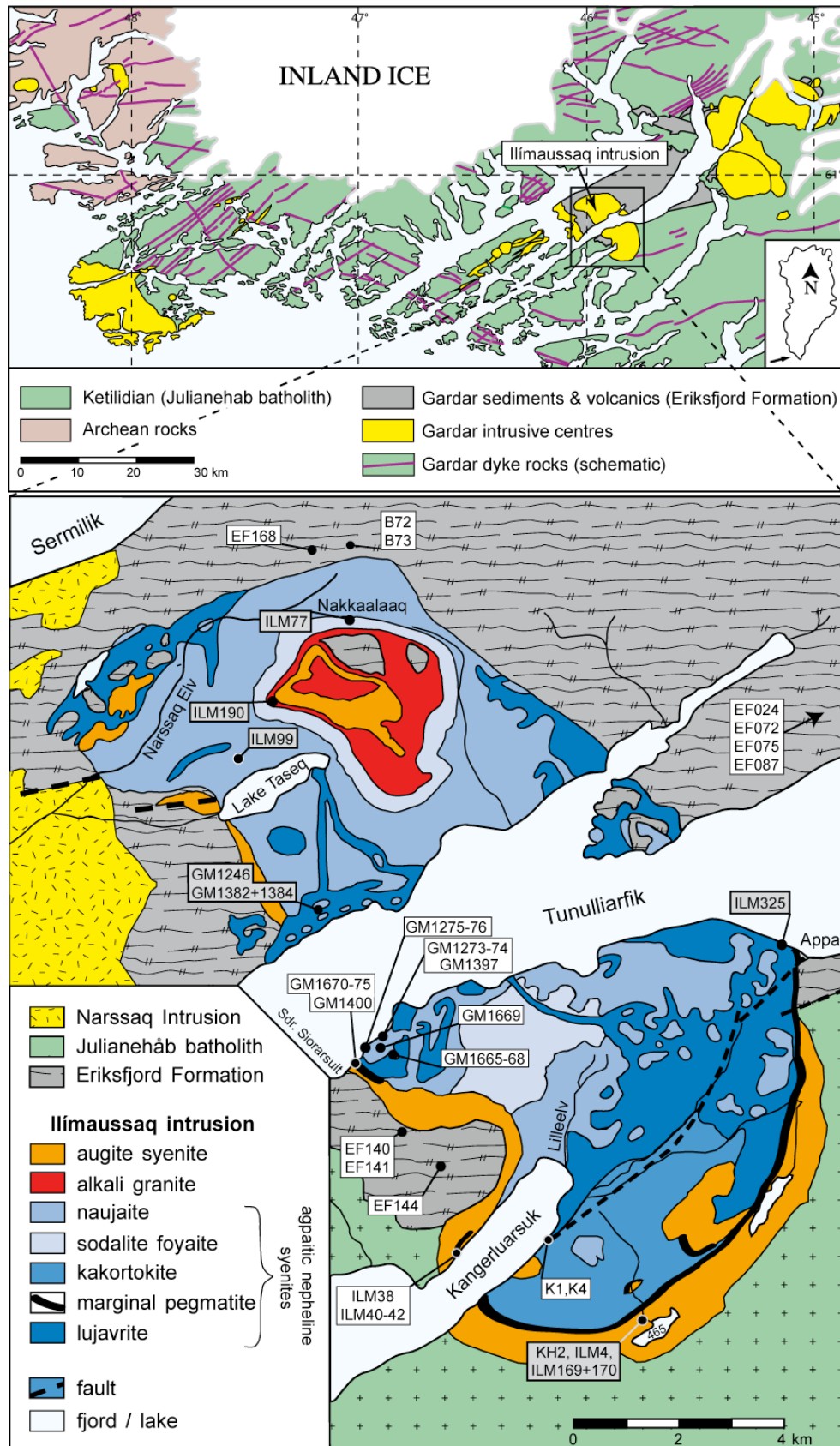
Fig. 1: Simplified geological maps of the Gardar Province (top, after Esche & Watt, 1976) and the Ilímaussaq intrusion (bottom, after Ferguson, 1964; Anderson, *et al.*, 1988) with sample locations. Samples are marked with different boxes depending on whether they were used in the first (white boxes) or in the second part (grey boxes) of this study.

naujakasite + arfvedsonite, whereas a higher oxygen fugacity stabilizes arfvedsonite + aegirine.

The agpaitic rocks in the southern part of the intrusion are separated from the augite syenite by an up to 100 m thick marginal pegmatite comprising pegmatitic veins in an agpaitic matrix (Bohse *et al.*, 1971; Sørensen, 2006; Fig. 2a). Mineralogically, it is similar to the kakortokites, but in parts much coarser and texturally extremely heterogeneous (Bohse *et al.*, 1971). Andersen *et al.* (1988) and Petersen *et al.* (1995) described occurrences of this marginal pegmatite on the north coast of the Kangerluarsuk fjord and on the south coast of the Tunulliarfik fjord (see Fig. 1). Sørensen (2006) gave a detailed overview of the different outcrops of marginal pegmatite.

Early workers like Lorenzen (1881), Bøggild (1902) and Ussing (1912) documented the presence of ilvaite ($CaFe^{3+}(Fe^{2+})_2O(Si_2O_7)(OH)$) in altered nepheline syenites, augite syenite and marginal pegmatite (Ferguson, 1964; Petersen *et al.*, 1995) in the Ilímaussaq intrusion. Although the occurence of ilvaite in the absence of quartz is quite unusual (Bartholomé & Dimanche, 1967), the Ilímaussaq ilvaite and its mode of formation has not been studied in detail. Ferguson (1964) reported the occurrence of ilvaite associated with grossular and explained it by conversion of aegirine and/or arfvedsonite but he did not explain the gain and the source of Ca. Petersen *et al.* (1995) described bavenite ($Ca_4Be_2Al_2Si_9O_{26}(OH)_2$) from the Ilímaussaq ilvaite-bearing assemblage and noted that the ilvaite occurrences belong to a zone of pneumatolytic alteration.

Late-magmatic to hydrothermal veins are present in all Ilímaussaq rock types. The lujavrites are believed to be the source of the late-stage fluids (Engell *et al.*, 1971), which led to the formation of Na-rich veins. These veins contain aegirine, arfvedsonite, albite, analcime, ussingite ($Na_2AlSi_3O_8OH$), or rare Be-silicates like chkalovite or tugtupite (Engell *et al.*, 1971; Markl, 2001). Some veins also formed by fluid-rock interaction between Ilímaussaq rocks and a Na-rich autometasomatic hydrothermal fluid (Markl & Baumgartner, 2002). Depending on the rock type it reacted with, the fluid could evolve completely differently with regard to pH and salinity and, hence, could precipitate variable mineral assemblages (Markl & Baumgartner, 2002). Fluid inclusion data and phase equilibria indicate formation temperatures of 300 to 500 °C at 1 kbar for the veins (Sobolev *et al.*, 1970; Konnerup-Madsen & Rose-Hansen, 1982; Markl & Baumgartner, 2002).

3   CA-RICH ILVAITE - EPIDOTE - HYDROGARNET ENDOSKARNS: A RECORD OF LATE-MAGMATIC FLUID INFLUX INTO THE PERSODIC ILíMAUSSAQ COMPLEX, SOUTH GREENLAND

3.1   Field observations

Endoskarns were investigated in two areas in the southern part of the intrusion at its western margins (Fig. 1): on the south coast of the Tunulliarfik fjord and along the coast of the Kangerluarsuk fjord. Ilvaite was found at two localities associated with the marginal pegmatite (samples GM1273, GM1275, GM1276, GM1400, GM1670 to GM1675 and ILM38, and ILM40 to ILM42). All other endoskarns are free of ilvaite and are, based on field relations and petrography, interpreted as altered naujaites (sample GM1274, GM1397, GM1666 to GM1667, and GM1669), altered foyaite (GM1665), and altered augite syenite (GM1668). A small locality at the Kangerluarsuk's south coast within the kakortokites close to the major fault zone through the Lakseelv valley comprises similarly altered rocks (K1, K4) with naujaitic textures, even though unaltered naujaite is not known from this particular locality. An ilvaite-bearing locality in the Lakseelv valley mentioned by Bohse *et al.* (1971) was not sampled during the present study. In general, ilvaite in Ilímaussaq is only found where augite syenite and marginal pegmatite have been exposed to secondary alteration (H. Sørensen, pers. com.).

Ussing (1912) already described the field relations of the ilvaite locality on the south coast of Tunulliarfik. Here, the rocks have been intensely altered over an area of about a quarter of a square kilometre and the pristine mineralogical composition of augite syenite, naujaite, lujavrite, and marginal pegmatite is partially or wholly replaced. Ussing (1912) interpreted the alteration as due to "pneumatolytical action" of varying intensity. Thus, the alteration in this region, which is responsible for the endoskarn formation with or without ilvaite, not only affects different rock types, but is also of variable intensity. The suite of newly formed minerals identified by Ussing (1912) comprises epidote, garnet, hematite, fluorite, well-crystallized albite, and ilvaite.

Both altered augite syenite and the pegmatitic veins on the north coast of Kangerluarsuk contain amongst others ilvaite and green garnet (Ussing, 1912). Petersen *et al.* (1995) studied bavenite, a Be-silicate, from this ilvaite occurrence which comprises besides augite syenite also marginal pegmatite and they also described calcite and a sodium zeolite from this place.

The ilvaite-bearing rocks studied here are very heterogeneous in texture and mineral distribution and thereby perfectly reflect the texture of the mixed zone of pegmatite veins and agpaitic rocks called marginal pegmatite (Fig. 2a, b; Bohse *et al.*, 1971). In these areas ilvaite mainly occurs as up to 3 cm large crystals in the pegmatitic parts of the rocks (Fig. 2b, c), whereas finer grained rocks lack ilvaite and must have been richer in eudialyte and poorer in amphibole. The coarse-grained rocks show vugs up to several cm in size lined by euhedral crystals of ilvaite, garnet, epidote or albite.

The ilvaite-free epidote-bearing assemblages south of the Tunulliarfik occur within augite syenite, naujaite, and foyaite close to the ilvaite-bearing rocks. Except for the lack of ilvaite they are quite similar mineralogically. Fresh rocks could only be sampled along the coast, but the endoskarn assemblage also occurs in boulders further inland. The typical textures of the precursor rock types (e.g. naujaite) are commonly preserved, but original mineral grains are now pseudomorphed by fine-grained mineral assemblages.

_____

Fig. 2: Textures of the unaltered marginal pegmatite and of the ilvaite-bearing assemblage. (a) Outcrop photograph of the marginal pegmatite at Sdr. Siorarsuit. Pegmatitic veins (lower left side to centre) in the fine grained matrix (upper left and lower right side) are clearly visible. Photograph courtesy of Henning Sørensen. (b) The pegmatitic ilvaite-bearing assemblage in the field at the south coast of the Tunulliarfik fjord. Scale is the Swiss army knife left from the centre. (c) Specimen with ilvaite and amphibole. The dashed line indicates the alteration front from amphibole to ilvaite. (d) Thin section of GM1674 with dark minerals (ilvaite and amphibole), light grey feldspar and grey hydrogarnet. (e) The enlargement of the section marked in (d) with a box shows on the left side alteration from amphibole to ilvaite. Hydrogarnet and zircon occur between the albite grains on the right side of the thin section. (f) Backscattered electron (BSE) image of amphibole (bottom) reacting to ilvaite (top) from the box section in (e). The bright needles in the lower right are zircons. (g) REE-rich epidote to allanite enclosed by hydrogarnet and spindle-shaped zircon in sample GM1275.
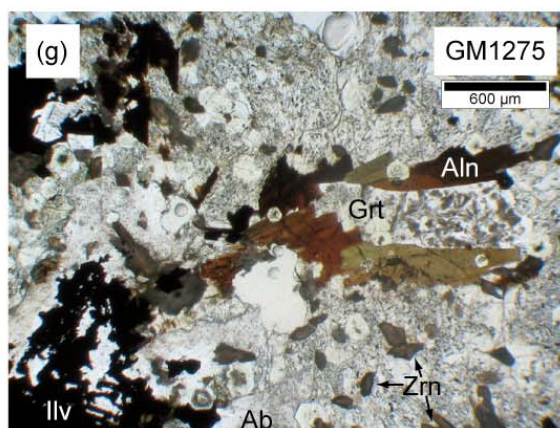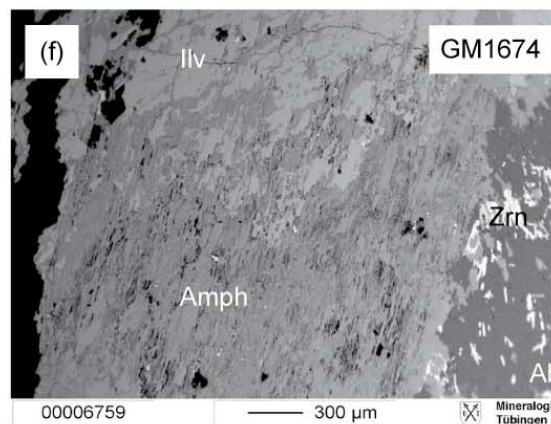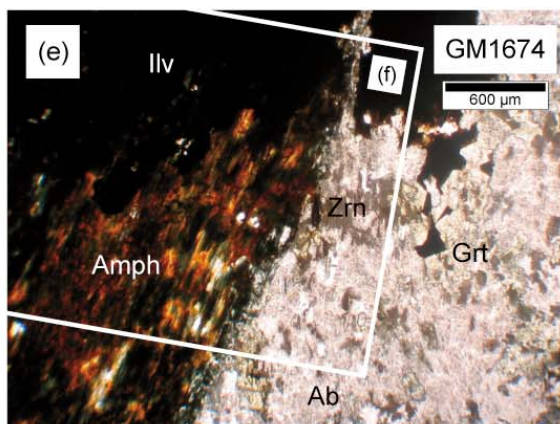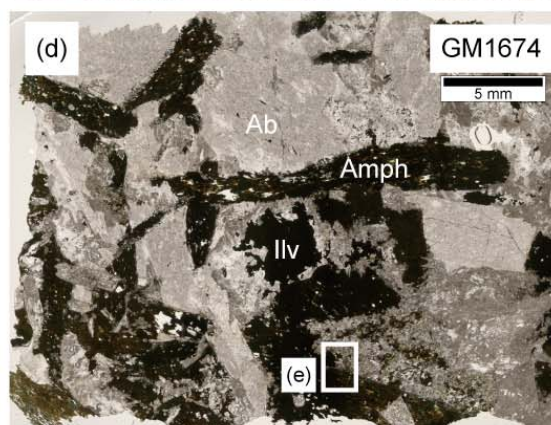
3.2 Petrography

Ilvaite-bearing assemblage

Black, lustrous ilvaite occurs as mm- to cm-sized subhedral lath-like crystals and is intergrown with small crystals of albite or potassium feldspar and more rarely with garnet, epidote and aegirine. In places, ilvaite may have a dendritic shape, and it commonly replaces other minerals, mainly large amphiboles (Fig. 2c-f).

Macroscopically, amphibole is green to brown and up to 5 cm long. A conversion reaction to ilvaite is common (Fig. 2b-f). Lamellae of secondary, pleochroic olive- to brown-green or blue-green amphiboles are intergrown with albite tracing the former shape of the primary magmatic amphibole.

The light green anhedral grains of epidote are typically smaller than 1 mm. They are intergrown with ilvaite or associated with garnet and zircon. REE-rich varieties may reach the proper allanite composition. The green to brown pleochroic allanite lamellae or grains occur together with epidote, garnet and zircon (Fig. 2g). Epidote and REE-rich epidote/allanite occur as separate phases next to each other but also as zoned grains with variable amounts of REEs.

Garnet occurs as small (usually < 0.5 mm) green, euhedral grains or anhedral masses (Fig. 2f). Some of the grains are zoned with a greenish or inclusion-rich core and a colourless rim. The inclusions comprise zircon and other minerals, which are too small for identification. The garnet shows anomalous birefringence with a sector-zoned extinction caused by a minor hydrogrossular component (Rossman & Aines, 1986).

Pyroxenes are rare and occur as small relict grains overgrown by ilvaite or as fine greenish needles in albite. In both cases the pyroxenes are only some micrometers large. In a few samples only, green to brownish pleochroic felt-like chlorite is intergrown with feldspar and/or ilvaite.

The matrix of these rocks consists mainly of white to greyish or pinkish pure albite (Fig. 2c-f), which commonly contains clusters of very small but empty inclusions, rarely small needles of aegirine and even more rarely titanite. Only BSE images revealed the presence of potassium feldspar as irregularly shaped zones in albite, which are less clouded by inclusions than albite. Potassium feldspar also occurs as grains along skeleton-like margins of ilvaite.

Zircon is a very common constituent of all samples (Fig. 2e-f). It occurs as small euhedral grains distributed throughout the rock. It is associated with garnet and/or epidote/allanite. Hematite is found as very small grains in albite. Titanite, violet fluorite and bavenite are rare

accessories. Petersen *et al.* (1995) also described zeolites, calcite and REE-bearing minerals like cerite-(Ce).
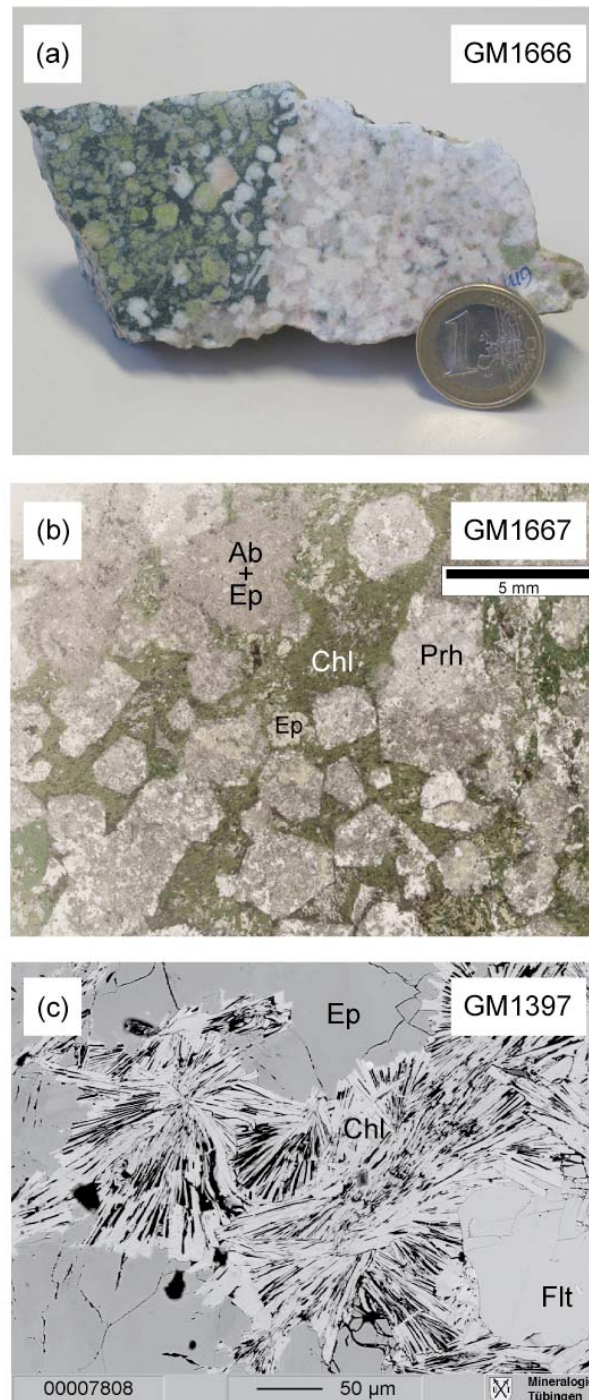
Fig. 3: Naujaite-like textures of ilvaite-free assemblages in hand specimen of sample GM1666 (a) and thin section of GM1667 (b). The left part of the hand specimen in (a) is rich in dark chlorite and epidote, whereas the right part is rich in bright prehnite and feldspar. (c) Fluorite in chlorite surrounded by epidote in sample GM1397, BSE image.

Ilvaite-free assemblage

Even though the samples of the ilvaite-free assemblage are from two different localities they are very similar in their mineralogical composition and resemble in part the ilvaite-bearing rocks. The composition and appearance of feldspar in the matrix is similar to the feldspar from the ilvaite-bearing assemblage. In some samples, sericitization of feldspar is common. The pure albite is grey to whitish or pinkish if altered.

Greenish epidote, albite, potassium feldspar and later prehnite replace former sodalite crystals (Fig. 3a, b). Prehnite was described before from the southern part of the intrusion by Metcalf-Johansen (1983) forming spherulitic incrustations. In the samples presented here, it occurs as a rock-forming mineral. It is restricted to some samples and occurs in irregular patches, which almost exclusively consist of prehnite. It appears to overgrow earlier pure albite crystals.

Epidote forms laths up to 1 mm in length and is commonly intimately intergrown with all other minerals.

Garnet is very similar to that in the ilvaite-bearing assemblage showing anomalous birefringence with a sector-zoned extinction. It is associated with epidote, allanite, chlorite, zircon or fluorite and replaces former interstitial eudialyte.

Allanite, chlorite and zircon appear as described before in the ilvaite-bearing rocks, but chlorite as alteration product of arfvedsonite is more common and is in places intergrown with feldspar, epidote, fluorite, garnet and/or zircon (Fig. 3c). Fluorite is violet to colourless and occurs as rounded grains of up to 1 mm in size.

Amphibole is absent in the ilvaite-free samples. Characteristic of most ilvaite-free samples is the still clearly visible macroscopic naujaitic texture.

3.3 Analytical methods

Mineral compositions were analyzed using a JEOL 8900 electron microprobe at the Institut für Geowissenschaften, Universität Tübingen. Natural and synthetic standards were used for calibration. The beam current was 15 nA and acceleration voltage was 15 kV for all minerals except epidote for which 40 nA and 20 kV were used. The measurements were performed with a focused electron beam. Counting time on the peak was 16 s for major elements and 30-120 s for minor elements. Background counting times were half the peak counting time. The raw data were corrected using the internal $\phi\rho Z$ procedures of JEOL (Armstrong, 1991). The detection limits and the typical average standard deviations (1σ) for each element depend on

the error based on count statistic. The average standard deviations govern the number of the decimals listed in Tables 1 to 3.

Whole-rock analyses were performed according to the methods described in Bailey *et al.* (2006). 1.5 to 2.0 kg of the most homogeneous samples were taken for crushing. The samples were crushed and milled in an agate mill and analyzed in the laboratories of the University of Copenhagen and the Rock and Geochemistry Laboratory of the Denmark and Greenland Geological Survey using X-ray fluorescence, instrumental neutron activation analysis, inductively coupled plasma - mass spectrometry (ICP-MS), and atomic absorption spectroscopy. These labs are particularly experienced in analyzing rocks of such unusual bulk compositions in terms of their minor and trace elements.

Whole-rock oxygen isotope compositions were analyzed according to a modified version of the conventional method of Clayton & Mayeda (1963) and Vennemann & Smith (1990) with BrF_5 as reagent and the conversion of oxygen to CO_2 before loading into the mass spectrometer. Mineral separates were analyzed using a method adapted from Sharp (1990) and Rumble & Hoering (1994) as described in Marks *et al.* (2003). NBS-28 quartz and UWG-2 garnet (Valley *et al.*, 1995) were used as standards.

Hydrogen isotope data were obtained using the method of Vennemann & O'Neil (1993) for the quantitative conversion of H_2O to H_2 from minerals and whole rocks on a Zn reagent (University of Indiana). An internal laboratory standard (kaolinite 17, $\delta D = -125\,‰$) was used for calibration.

Oxygen and hydrogen isotopic compositions of minerals and whole rocks were measured on a Finnigan MAT 252 isotope ratio mass spectrometer at the Universität Tübingen. The results are in δ-notation in permil [‰] relative to Vienna standard mean ocean water (VSMOW). The analytical precision is about $\pm\,0.2\,‰$ for $\delta^{18}O$ and about $\pm\,2\,‰$ for δD.

Different ilvaite-bearing and ilvaite-free whole-rock samples and hand picked separates of ilvaite, garnet, epidote and albite of the ilvaite-bearing assemblage were analyzed for their stable isotope compositions. The ilvaite-free assemblage is much finer grained which made it impossible to separate enough pure material of single minerals. For comparison, two augite syenite whole-rock samples (GM1330, GM1857), some whole-rock Eriksfjord basalts in different degrees of alteration - from fresh (EF024, EF072, EF168) to epidotized (EF075, EF087, EF140, EF141, EF144) - and two grains of epidote from cavities in the Eriksfjord basalts (B72, B73) were analyzed as well (Fig. 1).

3.4 Results

3.4.1 Mineral composition

Ilvaite-bearing assemblage

<u>Feldspar</u> is commonly pure albite or, in smaller amounts, pure potassium feldspar.

Table 1 shows representative microprobe analyses of <u>ilvaite</u>. It may contain up to 4.2 wt.% MnO, corresponding to 0.25 atoms per formula unit (apfu). Minor elements are Na_2O (< 0.42 wt.%), MgO (< 0.1 wt.%), Al_2O_3 (0.01 – 1.2 wt.%) and K_2O (< 0.18 wt.%).

Representative <u>epidote</u> analyses (Table 2, Fig. 4) show a solid solution between epidote and <u>allanite</u> with up to 22.4 wt.% $LREE_2O_3$ (light-REEs, here: $La_2O_3 + Ce_2O_3 + Nd_2O_3$, which are the predominant REE_2O_3 in the studied samples). The name allanite is used if REEs are dominant on the A2 site (Gieré & Sorensen, 2004). Analyses with more than 3 wt.% $LREE_2O_3$ but less than 0.5 REE apfu are referred to as REE-rich epidote.
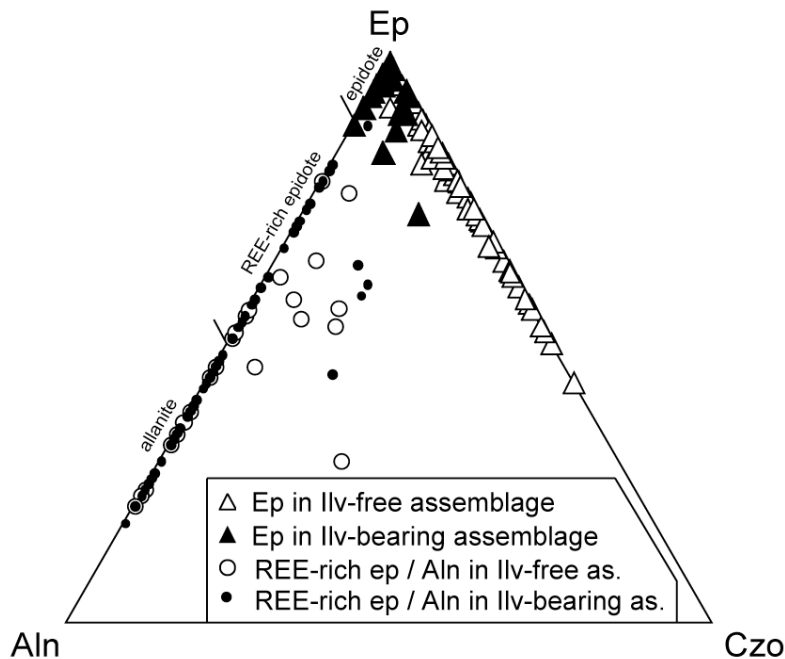
Fig. 4: Classification of the epidote-group minerals in the epidote - allanite - clinozoisite triangle. The proportion of clinozoisite was calculated as Al (apfu) –2 (if Al > 2, otherwise the proportion it taken as 0), the proportion of allanite is equal to REE (apfu), and epidote is 1–(allanite+clinozoisite). Mineral name abbreviations after Kretz (1983).

The garnets are almost pure granditic garnets with variable H_2O (≤ 2.0 wt.%) and F (≤ 1.9 wt.%) contents (Valley *et al.*, 1983; Lager *et al.*, 1989; Fig. 5). They vary in composition between Adr_{44} and Adr_{100} (Adr: andradite, Table 3, Fig. 5) and their spessartine component is ≤ 3 mol%. BSE images commonly show concentric or patchy zonation due to variable contents of Al and Fe^{3+}.
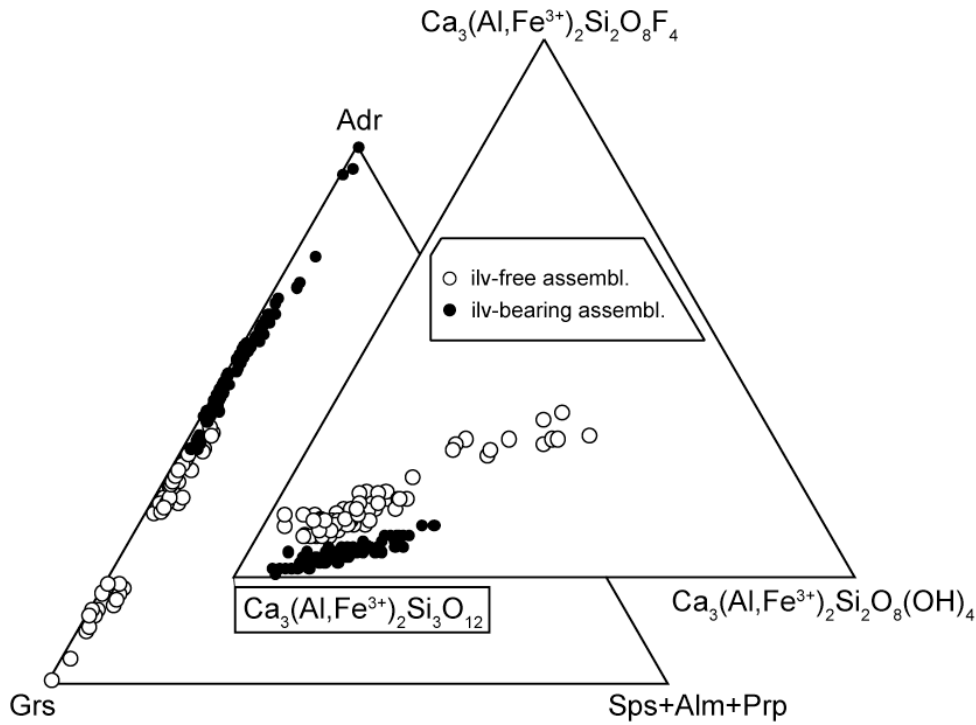
Fig. 5: Composition of the Ilímaussaq hydrogarnets in the grossular - andradite - (spessartine + almandine + pyrope) triangle and in the grandite - hydrograndite - fluorograndite triangle. Abbreviations after Kretz (1983).

Two types of secondary amphiboles, which are, however, texturally identical, can be distinguished according to their compositions: arfvedsonite to ferric-ferronyböite and potassic-hastingsite to potassic-ferritaramite (Leake *et al.*, 1997; 2004, Table 1). The ferric-ferronyböites contain about 1.15 wt.% F, whereas the other sodic amphiboles have less than 1 wt.%. The F content of the calcium amphiboles is close to the detection limit.

The only clinopyroxene present is aegirine (Aeg, Table 1) with compositions between $Aeg_{84}Jd_9QUAD_7$ and $Aeg_{93}Jd_5QUAD_2$ (Jd: jadeite, the QUAD-component comprises enstatite, ferrosilite, diopside, and hedenbergite). The aegirine may contain up to about 1 wt.% Al_2O_3, 0.106 to 0.214 wt.% MnO, and 0.14 to 0.9 wt.% ZrO_2.

In the ilvaite-bearing samples chlorite is Fe-rich chamosite ($X_{Mg} = 0.01$ to 0.29; Fig. 6, Table 1) with the average composition $chamosite_{82}clinochlore_{16}pennantite_2$.

Table 1: Electron microprobe analyses of minerals from the ilvaite-bearing assemblage.

Assemblage	ilv-bearing	ilv-bearing	ilv-bearing	ilv-bearing	ilv-bearing	ilv-bearing	ilv-bearing	ilv-bearing	ilv-bearing	ilv-bearing	ilv-bearing	ilv-bearing	ilv-bearing	ilv-bearing	ilv-bearing
Sample no.	ILM41	GM1670	GM1670	GM1275	ILM42	GM1400	GM1400	GM1671	GM1675	GM1400	ILM42	ILM42	GM1670	GM1670	GM1672
Mineral	ilvaite	ilvaite	ilvaite	arfvedsonite	arfvedsonite	arfvedsonite/ferric-ferronyböite	potassic-ferritaramite	potassic-ferritaramite	potassic-hastingsite/	aegirine	aegirine	aegirine	chlorite	chlorite	chlorite
wt.%															
SiO_2	29.75	29.57	29.78	48.0	49.6	46.9	37.6	38.7	38.1	51.2	52.3	51.9	28.08	23.91	24.53
TiO_2	0.045	0.073	0.130	0.50	0.46	0.70	0.158	0.057	<0.02	0.419	0.417	0.376	<0.02	<0.02	0.027
Al_2O_3	0.059	0.084	0.240	2.38	1.218	2.69	10.07	10.22	9.21	0.767	1.011	0.886	15.41	18.2	16.62
FeO	51.5	47.6	50.2	33.2	33.0	33.4	32.9	33.0	33.1	28.3	28.6	28.8	36.8	45.6	47.6
MnO	0.256	4.11	1.58	0.61	0.86	0.65	0.60	0.404	0.372	0.214	0.115	0.106	1.04	0.98	0.50
MgO	<0.01	0.026	0.026	0.366	0.173	0.581	0.584	0.743	1.20	0.088	0.017	0.023	7.14	1.44	0.521
CaO	13.9	13.9	13.9	2.09	0.392	2.57	7.72	7.93	9.28	4.06	1.62	2.38	0.288	0.047	0.030
Na_2O	<0.01	0.010	<0.01	7.8	8.7	7.9	3.41	3.42	2.29	11.3	12.9	12.5	0.159	0.078	0.024
K_2O	0.014	<0.01	0.023	1.69	2.33	1.61	3.05	3.02	2.99	0.015	<0.01	0.010	0.343	0.019	0.010
ZrO_2				0.25	<0.02	0.26	0.23	0.09	<0.02	0.9	0.45	0.20	<0.02	<0.02	<0.02
Cl				<0.01	<0.01	<0.01	<0.01	<0.01	<0.01				0.036	0.054	0.014
F				0.36	0.64	1.15	0.044	0.051	0.060				<0.02	<0.02	<0.02
Total	95.5	95.4	95.9	97.2	97.4	98.4	96.4	97.6	96.6	97.3	97.4	97.2	89.3	90.3	89.9
	Based on 6 cations and 8.5 oxygens			*Based on 16 cations and 23 oxygens*						*Based on 4 cations and 6 oxygens*			*Based on 20 cations and 28 oxygens*		
Si	2.03	2.01	2.02	7.71	7.92	7.50	6.17	6.27	6.29	1.99	2.00	2.00	6.27	5.52	5.76
Al	0.01	0.01	0.02	0.45	0.23	0.51	1.95	1.95	1.79	0.03	0.04	0.04	4.05	4.95	4.60
Ti	0.00	0.00	0.01	0.06	0.06	0.08	0.02	0.01	0.00	0.01	0.01	0.01	0.00	0.00	0.00
Fe^{3+}	0.94	0.96	0.93	0.76	0.97	1.04	1.35	1.19	1.00	0.81	0.89	0.89	0.00	0.06	0.00
Mg	0.00	0.00	0.00	0.09	0.04	0.14	0.14	0.18	0.29	0.01	0.00	0.00	2.37	0.49	0.18
Fe^{2+}	1.99	1.76	1.92	3.69	3.43	3.42	3.18	3.28	3.58	0.11	0.03	0.03	6.87	8.74	9.34
Mn	0.01	0.24	0.09	0.08	0.12	0.09	0.08	0.05	0.05	0.01	0.00	0.00	0.20	0.19	0.10
Ca	1.02	1.02	1.01	0.36	0.07	0.44	1.36	1.37	1.64	0.17	0.07	0.10	0.07	0.01	0.01
Na	0.00	0.00	0.00	2.44	2.69	2.43	1.09	1.07	0.73	0.85	0.95	0.93	0.07	0.03	0.01
K	0.00	0.00	0.00	0.34	0.47	0.33	0.64	0.62	0.63	0.00	0.00	0.00	0.10	0.01	0.00
Zr	0.00	0.00	0.00	0.02	0.00	0.02	0.02	0.01	0.00	0.01	0.01	0.00	0.00	0.00	0.00
Total	6.00	6.00	6.00	16.00	16.00	16.00	16.00	16.00	16.00	4.00	4.00	4.00	20.00	20.00	20.00
Cl				0.00	0.00	0.00	0.00	0.00	0.00				0.01	0.02	0.01
F				0.18	0.32	0.58	0.02	0.03	0.03				0.00	0.00	0.00

Table 2: Electron microprobe analyses of epidotes, REE-rich epidotes and allanites of the endoskarn assemblages. Low totals may be caused by the occurrence of other REEs that were not included in the analyses.

| Assemblage | ilv-bearing | ilv-bearing | ilv-bearing | ilv-bearing | ilv-bearing | ilv-bearing | ilv-free | ilv-free | ilv-free | ilv-free | ilv-free | ilv-free |
| Sample no. | ILM42 | GM1670 | GM1675 | ILM38 | GM1670 | GM1275 | GM1667 | GM1665 | GM1669 | GM1669 | GM1669 | K1 |
Mineral	epidote	epidote	epidote	REE-rich ep	REE-rich ep	allanite	epidote	epidote	epidote	REE-rich ep	REE-rich ep	allanite
wt.%												
SiO_2	36.5	36.6	36.5	34.9	33.1	31.2	37.1	37.2	38.0	35.2	35.1	33.2
TiO_2	0.082	0.065	0.023	<0.02	0.550	0.098	0.046	0.043	0.087	<0.02	0.036	0.913
Al_2O_3	18.6	19.6	21.4	19.0	11.2	9.8	22.6	20.6	24.9	20.4	20.3	17.2
FeO	17.90	15.9	12.97	15.30	23.30	20.71	12.62	15.08	10.63	13.94	13.3	13.88
MnO	<0.02	0.07	0.191	0.038	0.69	3.15	0.207	0.251	<0.02	0.106	0.135	0.21
MgO	<0.01	<0.01	<0.01	<0.01	<0.01	<0.01	<0.01	<0.01	0.010	<0.01	<0.01	0.011
CaO	21.9	22.6	22.7	18.1	15.4	12.2	22.7	22.3	23.2	19.5	18.0	13.7
Na_2O	0.030	<0.01	0.018	<0.01	0.025	<0.01	<0.01	0.024	<0.01	<0.01	0.024	0.040
K_2O	<0.01	<0.01	<0.01	<0.01	<0.01	<0.01	<0.01	<0.01	<0.01	<0.01	<0.01	0.059
La_2O_3	0.14	0.13	0.15	2.0	3.0	5.5	0.25	<0.01	<0.01	1.6	2.7	3.7
Ce_2O_3	0.44	0.34	0.27	4.3	7.1	10.4	0.30	0.022	<0.01	3.2	5.1	9.2
Nd_2O_3	0.6	0.13	0.08	1.6	2.7	3.0	0.05	<0.01	<0.01	1.0	1.5	3.0
Total	96.2	95.4	94.3	95.2	97.1	96.0	95.9	95.5	96.8	94.9	96.2	95.1
Based on 8 cations and 12.5 oxygens												
Si	3.00	3.00	3.00	3.03	3.01	3.01	3.00	3.03	3.00	2.99	3.02	3.07
Al	1.81	1.89	2.07	1.94	1.20	1.12	2.15	1.98	2.32	2.05	2.06	1.87
Ti	0.01	0.00	0.00	0.00	0.04	0.01	0.00	0.00	0.01	0.00	0.00	0.06
Fe^{3+}	1.17	1.08	0.91	0.76	1.28	1.18	0.83	0.97	0.66	0.79	0.61	0.35
Mg	0.00	0.00	0.00	0.00	0.00	0.00	0.00	0.00	0.00	0.00	0.00	0.00
Fe^{2+}	0.07	0.02	0.00	0.35	0.49	0.49	0.03	0.06	0.04	0.20	0.35	0.73
Mn	0.00	0.01	0.01	0.00	0.05	0.26	0.02	0.02	0.00	0.01	0.01	0.02
Ca	1.92	1.99	2.00	1.67	1.50	1.26	1.96	1.94	1.97	1.78	1.65	1.36
Na	0.00	0.00	0.00	0.00	0.00	0.00	0.00	0.00	0.00	0.00	0.00	0.00
K	0.00	0.00	0.00	0.00	0.00	0.00	0.00	0.00	0.00	0.00	0.00	0.00
La	0.00	0.00	0.00	0.06	0.10	0.20	0.01	0.00	0.00	0.05	0.09	0.13
Ce	0.01	0.01	0.01	0.14	0.24	0.37	0.00	0.00	0.00	0.10	0.16	0.31
Nd	0.01	0.00	0.00	0.05	0.09	0.10	0.00	0.00	0.00	0.03	0.05	0.10
Total	8.00	8.00	8.00	8.00	8.00	8.00	8.00	8.00	8.00	8.00	8.00	8.00
czo	0.00	0.00	0.07	0.00	0.00	0.00	0.15	0.00	0.32	0.05	0.06	0.00
aln	0.02	0.02	0.02	0.25	0.42	0.67	0.02	0.00	0.00	0.18	0.29	0.54
ep	0.98	0.98	0.91	0.75	0.58	0.33	0.83	1.00	0.68	0.77	0.65	0.46

Table 3: Electron microprobe analyses of minerals from the ilvaite-bearing and -free assemblages.

Prehnite and chlorite analyses

Assemblage	ilv-free	ilv-free	ilv-free	ilv-free	ilv-free	ilv-free
Sample no.	K4	K11	GM1666	K11	GM1397	GM1666
Mineral	prehnite	prehnite	prehnite	chlorite	chlorite	chlorite
wt.%						
SiO_2	43.7	43.8	44.2	24.84	23.40	23.68
TiO_2	<0.02	<0.02	0.027	1.74	0.053	<0.02
Al_2O_3	23.7	23.1	24.1	17.2	20.0	19.0
FeO	0.051	0.997	0.302	41.1	44.5	45.8
MnO	0.078	0.122	<0.01	1.49	0.94	0.91
MgO	<0.01	<0.01	<0.01	0.947	0.353	0.181
CaO	26.5	26.8	26.0	1.91	0.141	0.015
Na_2O	0.152	0.134	0.014	0.223	0.068	0.015
K_2O	0.012	0.015	<0.01	0.021	0.014	<0.01
ZrO_2	<0.02	<0.02	<0.02	0.53	<0.02	<0.02
Cl	0.017	<0.01	<0.01	<0.01	0.033	0.025
F	<0.02	<0.02	<0.02	<0.02	<0.02	<0.02
Total	94.2	95.0	94.6	90.0	89.5	89.6
	Based on 14 cations and 22 oxygens			Based on 20 cations and 28 oxygens		
Si	6.09	6.07	6.14	5.76	5.46	5.54
Al	3.90	3.77	3.94	4.70	5.49	5.24
Ti	0.00	0.00	0.00	0.30	0.01	0.00
Fe^{3+}	0.00	0.12	0.00	0.00	0.00	0.00
Mg	0.00	0.00	0.00	0.33	0.12	0.06
Fe^{2+}	0.01	0.00	0.04	7.97	8.67	8.96
Mn	0.01	0.02	0.00	0.29	0.18	0.18
Ca	3.95	3.98	3.87	0.48	0.03	0.00
Na	0.04	0.04	0.01	0.10	0.03	0.01
K	0.00	0.00	0.00	0.01	0.00	0.00
Zr	0.00	0.00	0.00	0.06	0.00	0.00
Total	14.00	14.00	14.00	20.00	20.00	20.00
Cl	0.00	0.00	0.00	0.00	0.01	0.01
F	0.00	0.00	0.00	0.00	0.00	0.00

Garnet analyses

Assemblage	ilv-bearing	ilv-bearing	ilv-bearing	ilv-free	ilv-free	ilv-free
Sample no.	ILM41	ILM41	GM1671	K1II	K4	GM1668
Mineral	garnet	garnet	garnet	garnet	garnet	garnet
wt.%						
SiO_2	34.3	36.1	34.7	35.6	33.07	36.3
TiO_2	<0.02	0.484	0.474	0.240	0.020	0.617
Al_2O_3	0.146	11.3	7.2	10.2	20.0	14.0
FeO calc	0.0	0.0	0.0	0.0	0.0	0.0
Fe2O3 calc	31.0	14.5	20.9	17.4	3.0	11.3
MnO	0.139	0.39	0.33	0.37	0.52	0.78
MgO	0.010	<0.01	0.024	0.016	0.013	<0.01
CaO	33.0	34.7	34.3	35.6	36.7	35.6
ZrO_2				<0.02	<0.02	<0.02
Cl				<0.01	<0.01	<0.01
F	0.276	0.350	0.764	1.480	4.32	1.370
H_2O calc.	0.51	0.53	1.02	0.89	1.88	0.69
Total	99.4	98.4	99.7	101.8	99.5	100.7
	Based on the 5 cations of the X and Y-site°					
Si	2.91	2.91	2.81	2.79	2.50	2.83
H/4	0.07	0.07	0.14	0.12	0.24	0.09
F/4	0.02	0.02	0.05	0.09	0.26	0.08
Cl/4	0.00	0.00		0.00	0.00	0.00
Al	0.01	1.07	0.69	0.94	1.79	1.29
Fe^{3+}	1.98	0.88	1.27	1.03	0.20	0.66
Ti	0.00	0.03	0.03	0.01	0.00	0.04
Zr	0.00	0.00	0.00	0.00	0.00	0.00
Cr	0.00	0.00	0.00	0.00	0.00	0.00
Fe^{2+}	0.00	0.00	0.00	0.00	0.00	0.00
Mg	0.00	0.00	0.00	0.00	0.00	0.00
Mn	0.01	0.03	0.03	0.03	0.03	0.05
Ca	3.00	2.99	2.99	2.99	2.98	2.96
Total	8.00	8.00	8.00	8.00	8.00	8.00
Spessartine	0	1	1	1	1	2
Grossular	1	55	35	47	89	65
Andradite	99	44	64	52	10	33
(after Deer, Howie & Zussman, 1992)						
Hydrograndite*	7	7	14	12	24	9
Fluorograndite*	2	2	5	9	26	8
Grandite	91	91	81	79	50	83

* Hydrograndite: $Ca_3(Al,Fe^{3+})_2Si_2O_8(OH)_4$, Fluorograndite: $Ca_3(Al,Fe^{3+})_2Si_2O_8F_4$
° Si is assumed to be present only on the Si-site

Ilvaite-free assemblage

Feldspar occurs as pure albite and pure potassium feldspar.

Representative analyses of epidote and allanite (Table 2, Fig. 4) show a solid solution between epidote and allanite with up to 22.8 wt.% $LREE_2O_3$ ($La_2O_3+Ce_2O_3+Nd_2O_3$).

The garnets are richer in Al and poorer in Fe^{3+} than in the ilvaite-bearing assemblage and vary between Adr_{01} and Adr_{52} (Table 3, Fig. 5). They contain up to 5 wt.% F and commonly less than 2 wt.% H_2O (calculated).

In the ilvaite-free samples, chlorite is a chamosite with a lower average X_{Mg} (range: 0 to 0.35) than in the ilvaite-bearing assemblage (Fig. 6) and with the average composition $chamosite_{93}clinochlore_4pennantite_3$.

Prehnite is close to the pure endmember composition (Table 3).
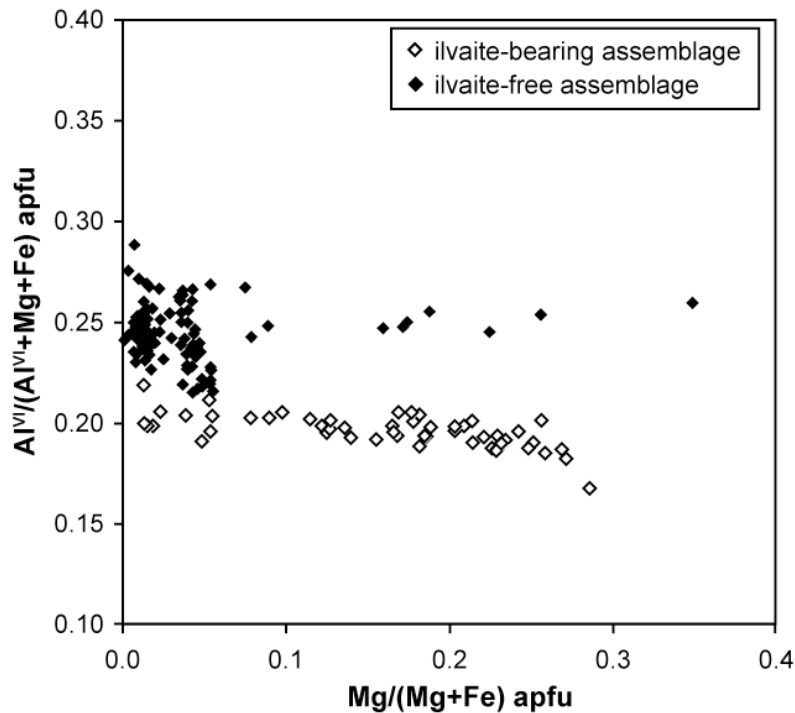
Fig. 6: Atomic ratios of Mg/(Mg+Fe) versus $Al^{VI}/(Al^{VI}+Mg+Fe)$ for chlorites in the ilvaite-bearing and ilvaite-free assemblages.

3.4.2 Whole-rock composition

Five representative samples of the ilvaite-bearing assemblage and four of the ilvaite-free assemblage were selected for whole-rock analysis (Table 4). When compared to their marginal pegmatite precursor rock (Sørensen, 2006), the ilvaite-bearing assemblages are invariably enriched in Ca. The other element concentrations are similar to their precursor, with small depletions in K and Al and possibly with an enrichment in Fe, Ti, and Zr (Fig. 7). The peralkalinity index (P.I. = molar (Na_2O + K_2O)/Al_2O_3) varies between 0.83 and 0.94 (Fig. 8).
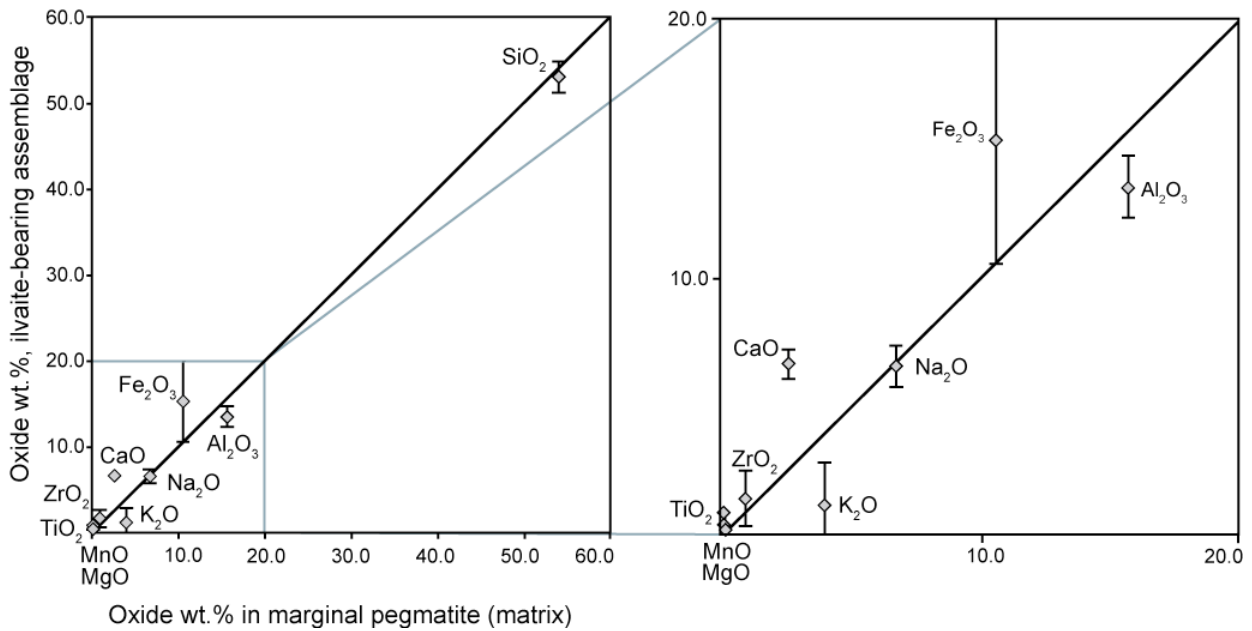
Fig. 7: Major element isocon-like plot of the average ilvaite-bearing assemblage versus the marginal pegmatite (Sørensen, 2006). Bars indicate standard deviation of the mean.

The variation in major element concentrations of the ilvaite-free assemblages (Table 4) is larger because of different precursor rock types for these samples. Nevertheless, Ca is strongly enriched in GM1666 and K1 and slightly enriched in GM1668 and GM1669 with respect to their average precursor rocks (Fig. 9).

Fig. 10 shows a comparison of primitive-mantle normalized trace element data (after McDonough & Sun, 1995) of the endoskarns, major average Ilímaussaq rock types (Bailey *et al.*, 2001) and the marginal pegmatite (Sørensen, 2006). Several trace elements of the ilvaite-bearing assemblage lie within the range of Ilímaussaq trace elements but scatter around the marginal pegmatite pattern (Fig. 10a). Interestingly, all ilvaite-bearing samples are depleted in

Cs, Rb, and Ba with respect to the marginal pegmatite. The trace elements of the ilvaite-free assemblages (Fig. 10b) vary, with exceptions, within the range of the common Ilímaussaq trace element distribution. Sample K1 is distinct in terms of its enrichment in several trace elements with respect to the other ilvaite-free samples (Fig. 10b).
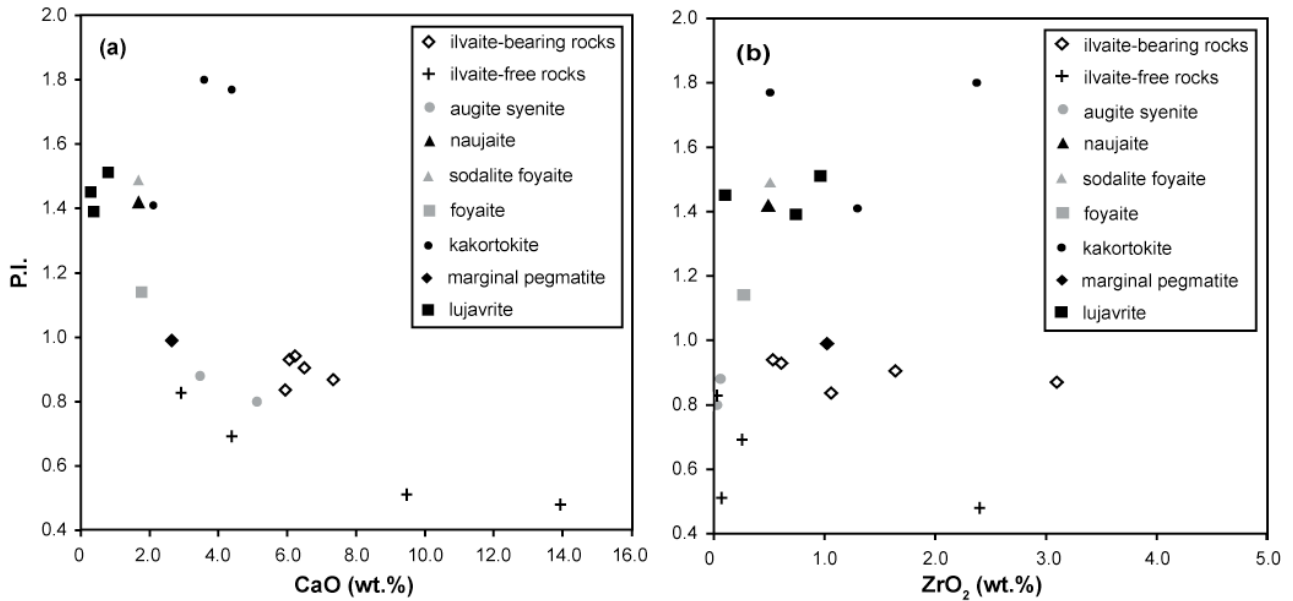
Fig. 8: CaO (a) and ZrO_2 (b) concentration versus the peralkalinity index (P.I.) of the ilvaite-bearing and -free assemblages in comparison to different Ilímaussaq rocks of Sørensen (2006; marginal pegmatite) and Bailey *et al.* (2001; all other rocks).

Table 4: Whole-rock analyses of skarn-like rocks in the Ilímaussaq intrusion and reference data.

Sample no.	GM1273	ilvaite-bearing assemblage GM1670	GM1671	GM1674	ILM42	ilvaite-free assemblage GM1666	GM1668	GM1669	K1	marginal pegmatite Sørensen (2006)	augite syenite (coarse) Bailey et al. (2001)	foyaite Bailey et al. (2001)	naujaite Bailey et al. (2001)
SiO$_2$	53.36	53.38	55.44	50.22	53.61	53.93	55.48	62.25	49.43	54.10	56.97	58.50	48.25
TiO$_2$	0.18	0.20	0.19	0.27	0.16	0.12	0.10	0.05	0.13	0.20	1.27	0.32	0.32
ZrO$_2$	1.03	0.59	1.63	0.53	3.12	0.07	0.24	0.02	2.43	1.02	0.06	0.27	0.49
Al$_2$O$_3$	14.21	12.97	14.80	11.77	14.15	20.71	18.71	19.61	18.29	15.72	16.82	16.21	19.30
Fe$_2$O$_3$	7.29	7.43	6.35	9.15	7.00	1.99	5.50	1.33	4.06	7.96	1.47	3.03	4.07
FeO	6.84	9.31	3.14	11.24	3.82	3.17	4.35	1.12	1.25	2.43	6.68	3.80	3.08
MnO	0.58	0.68	0.36	0.66	0.39	0.12	0.31	0.06	0.26	0.26	0.22	0.19	0.21
MgO	0.43	0.08	0.27	0.26	0.27	0.14	0.21	0.11	0.23	0.26	0.76	0.11	0.10
CaO	5.86	6.06	6.37	6.29	7.48	9.43	4.29	2.88	13.94	2.64	3.47	1.76	1.68
Na$_2$O	7.13	7.22	5.47	5.81	7.04	4.27	7.94	8.29	3.52	6.79	5.65	7.56	14.37
K$_2$O	0.05	0.31	3.57	1.17	0.15	3.19	0.04	2.58	2.50	4.09	5.16	5.64	3.41
P$_2$O$_5$	0.06	0.12	0.06	0.06	0.13	0.03	0.12	0.41	0.09	0.05	0.34	0.04	0.06
H$_2$O$^+$	0.93	0.90	0.72	1.39	0.71	1.51	1.71	0.47	0.81	n.r.	0.56	1.26	1.25
H$_2$O$^-$	0.16	0.07	0.05	0.07	0.17	0.05	0.33	0.07	0.04	n.r.	0.19	0.21	0.17
S	< 0.01	< 0.01	0.01	0.01	0.01	< 0.01	< 0.01	< 0.01	< 0.01	n.r.	0.07	0.02	0.08
Cl	0.03	0.06	0.07	0.07	0.09	0.04	0.02	0.04	0.04	0.03	0.04	0.12	2.34
F	0.06	0.09	0.16	0.06	0.10	0.25	0.06	0.04	0.45	0.23	0.14	0.20	0.16
others	1.11	0.35	0.79	0.42	1.25	0.33	0.39	0.40	1.57	n.r.	0.06	0.17	0.01
sum	99.32	99.80	99.46	99.45	99.62	99.35	99.80	99.72	99.04	98.71	99.98	99.45	99.55
–O	0.03	0.05	0.09	0.05	0.07	0.11	0.03	0.03	0.20	0.11	0.1	0.12	0.65
sum	99.29	99.75	99.37	99.40	99.56	99.24	99.77	99.69	98.85	98.60	99.88	99.33	98.9
P.I.	0.83	0.94	0.87	0.92	0.83	0.51	0.70	0.84	0.46	0.99	0.88	1.14	1.42
Cs	0.1	0.1	0.7	0.2	1.9	0.2	0.1	0.1	0.6	3.8	1.2	5.3	6.2
Rb	4.5	51	379	118	23	268	4.4	103	152	456	68	315	334
Tl	< 0.5	< 0.5	< 0.5	0.6	< 0.5	< 0.5	< 0.5	< 0.5	< 0.5	n.r.	<0.5	1.3	2.3
Ba	15	29	79	28	42	231	26	228	1282	379	2320	42	11
Pb	341	14	133	86	99	11	8	52	182	62	15	45	94
Sr	889	220	343	130	480	1171	760	1158	2866	269	395	27	10
La	1229	292	682	286	1181	119	413	327	987	541	77	244	594
Ce	2480	570	1296	539	2338	228	613	623	1846	930	163	512	1180
Pr	311	72	170	67	313	28	67	78	234	n.r.	n.r.	n.r.	n.r.
Nd	1072	259	591	233	1133	92	202	264	805	426	76	219	540
Sm	197	54.0	121	44.8	241	15.2	27.4	36.7	158	79	13.9	38.2	96.1
Eu	17.8	5.0	11.3	4.7	21.6	1.4	2.4	3.1	15.2	7.3	4.53	3.60	9.63
Gd	188	53.3	149	45.5	246	14.8	29.2	33.4	170	n.r.	n.r.	n.r.	n.r.
Tb	25.3	8.2	20.7	6.8	40.9	1.8	3.6	3.4	28.0	13.6	1.88	5.82	16.1
Dy	139	48.9	129	41.3	254	9.8	21.0	15.5	176	n.r.	n.r.	n.r.	n.r.
Ho	27.4	10.6	28.6	8.7	56.7	1.9	4.5	2.3	39.8	n.r.	n.r.	n.r.	n.r.
Er	72.6	28.5	79.9	24.4	157	5.2	13.2	5.3	113	n.r.	n.r.	n.r.	n.r.
Tm	10.2	4.4	11.8	3.7	23.3	0.7	2.0	0.6	17.0	n.r.	n.r.	n.r.	n.r.
Yb	64.7	28.9	77.7	25.3	148	5.2	13.2	3.1	110	50.2	5.30	19.7	38.3
Lu	8.4	4.1	10.4	3.7	20.0	0.8	1.8	0.4	15.0	7.0	0.80	2.43	5.24
Y	933	295	684	241	1249	64	172	62	897	471	45	184	461
Th	86	41	57	35	42	27	79	36	37	50	7.9	27.8	41.0
U	63	18	22	14	22	8	18	6	14	14	1.9	9.8	19.5
Zr	7634	4340	12073	3925	23066	552	1779	160	17973	8145	272	2070	4360
Hf	103	85.0	255	79.5	461	13.0	27.1	3.5	404	184	11.4	42.5	75.2
Nb	329	466	956	607	1387	169	349	104	1459	830	93	325	742
Ta	40.8	23.3	68.5	23.6	115	5.0	7.5	2.1	137	54.7	6.0	19.2	51.8
Li	1	4	2	1	1	27	49	12	11	n.r.	80	132	161
Zn	1009	206	638	629	1092	182	180	146	1478	300	117	276	505
Cu	38	38	5	6	4	5	17	17	11	n.r.	16	10	9
Co	1.8	2.7	2.6	2.9	2.6	3.3	1.0	0.9	5.5	n.r.	3.8	3.6	0.29
Ni	1.7	1.7	3.6	1.0	0.8	1.8	1.0	0.2	2.0	n.r.	<0.5	0.5	0.8
Sc	2.7	4.7	7.9	3.0	13	0.2	1.4	2.7	12	7	18	0.52	<0.01
Ge	1.8	2.1	1.7	2.0	0.9	1.5	1.7	0.8	0.7	n.r.	1.9	1.4	2.0
Be	21	35	18	55	37	22	28	11	16	n.r.	3.5	16	22
Mo	1.3	0.8	6.7	1.0	4.8	2.4	0.3	0.8	13	n.r.	4.4	<0.5	9
As	10	20	7.5	9.8	11	9.5	1.8	8.9	11	n.r.	3.3	2.8	11
Br	1.4	2.1	3.0	2.1	3.0	1.8	1.8	2.9	1.9	n.r.	1.5	2.9	119

P.I.: peralkalinity index: molar (Na$_2$O+K$_2$O)/Al$_2$O$_3$ n.r. = not reported
others: sum of other trace elements as oxides.
Analysts: J.C. Bailey, V. Moser and the Rock Geochemistry Laboratory of the Denmark and Greenland Geological Survey.
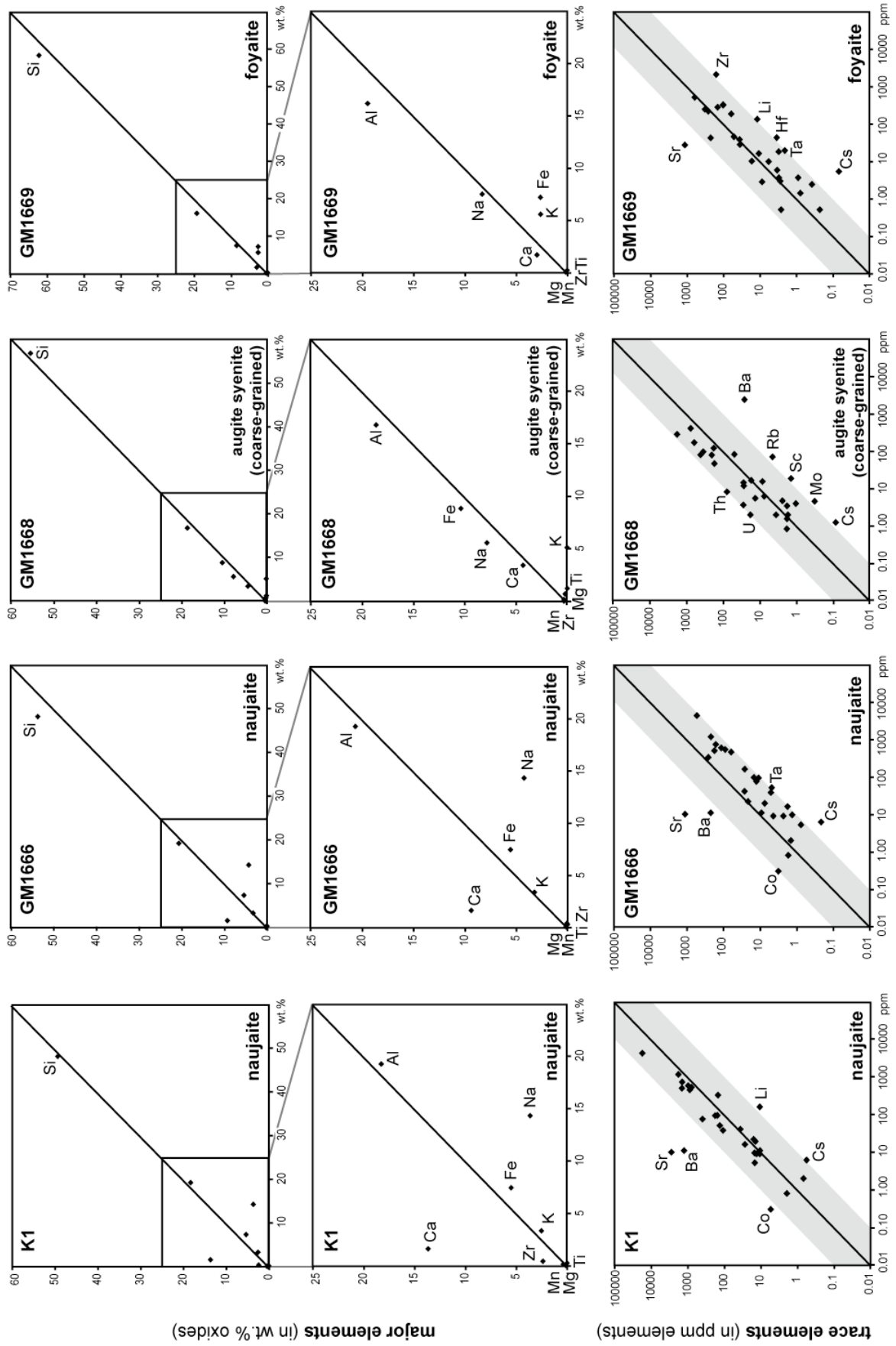
Fig. 9: Isocon-like plots of the ilvaite-free rocks versus their precursor rocks (data from Bailey *et al.*, 2001) for major and trace elements.
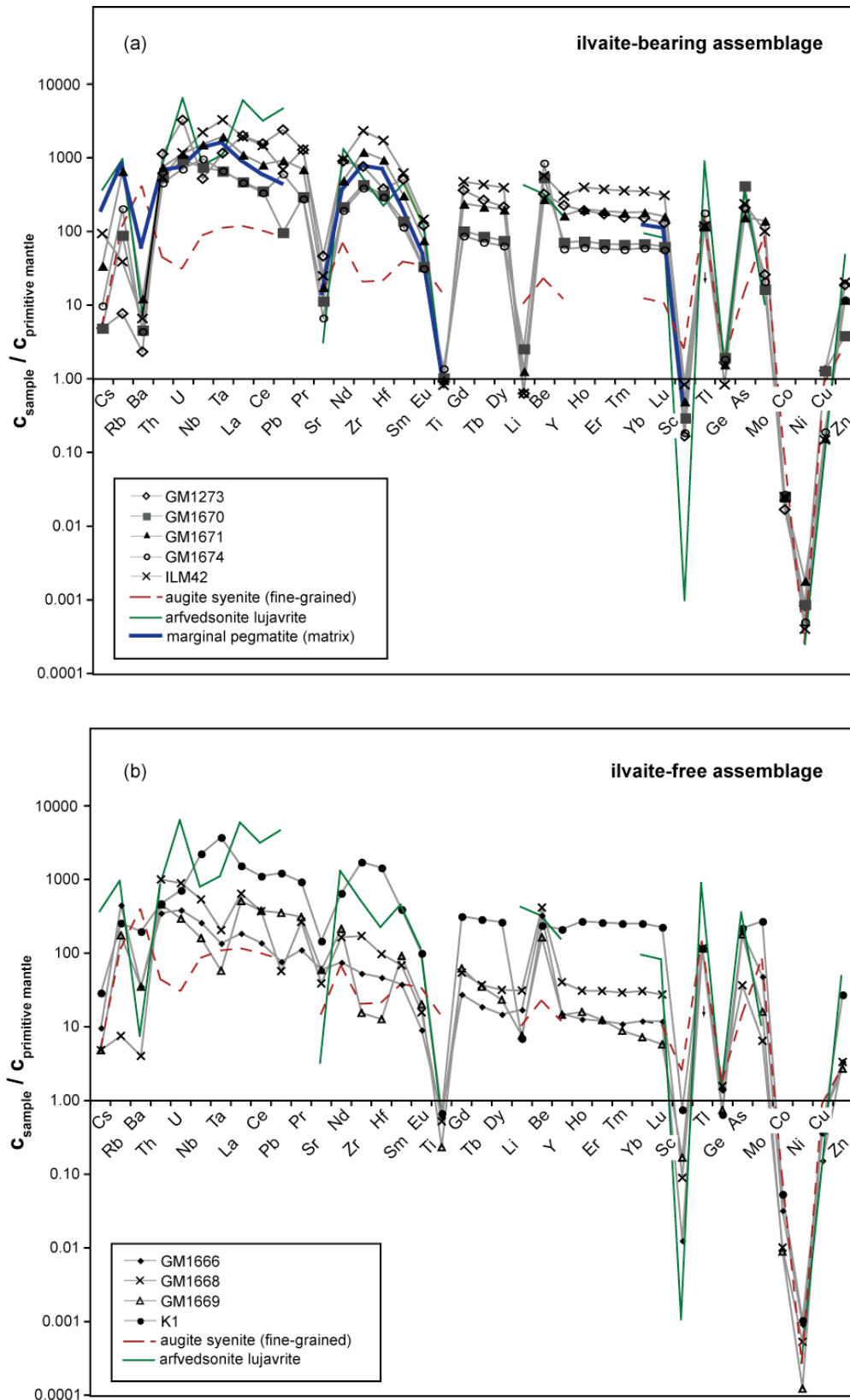
Fig. 10: Trace element whole-rock data normalized to primitive mantle (McDonough & Sun, 1995) of the ilvaite-bearing (a) and -free (b) assemblages. Data for augite syenite and lujavrite from Bailey *et al.* (2001) give the maximum range of the trace element composition of whole-rocks in the Ilímaussaq complex; data for the matrix of the marginal pegmatite (Sørensen, 2006) are added for comparison. Unfortunately, reference data are only available for selected elements. Arrows indicate element concentrations below detection limit.

3.4.3 Stable isotopes

The $\delta^{18}O$ values of the ilvaite-bearing whole-rock samples range between 3.0 and 6.2 ‰ and of the ilvaite-free assemblage between 4.5 and 6.8 ‰ relative to VSMOW (Table 5, Fig. 11). In the ilvaite-bearing assemblage, ilvaite values range between −4.7 and −3.6 ‰, garnet between −3.3 and −1.8 ‰ and albite between 5.9 and 7.2 ‰. The epidote has a value of −1.1 ‰. The Ilímaussaq augite syenite whole-rock samples have a $\delta^{18}O$ of 6.4 and 6.7 ‰, the basalts of the Eriksfjord formation range between −1.8 and 5.5 ‰ and the epidote from the cavities in the Eriksfjord basalts between −1.9 and 0.5 ‰.

Table 5: Results of stable isotope analyses of whole-rocks and minerals of the endoskarn assemblages and some comparing whole-rocks.

Sample no.	Sample type	Rocktype	δD [‰]	$\delta^{18}O$ [‰]
ILM42	w.r.	Ilv-bearing assemblage	-130	6.2
GM1273	w.r.	Ilv-bearing assemblage	-118	4.7
GM1670	w.r.	Ilv-bearing assemblage	-131	3.5
GM1671	w.r.	Ilv-bearing assemblage	-123	4.7
GM1674	w.r.	Ilv-bearing assemblage	-136	3.0
GM1670	Ilv	Ilv-bearing assemblage	-136	-4.7
GM1674	Ilv	Ilv-bearing assemblage	-145	-3.6
ILM40	Ilv	Ilv-bearing assemblage	-148	-4.0
ILM40	Ep	Ilv-bearing assemblage	-	-1.1
ILM40	Grt	Ilv-bearing assemblage	-	-1.8
GM1670	Grt	Ilv-bearing assemblage	-	-3.3
ILM40	Fsp	Ilv-bearing assemblage	-	7.2
GM1670	Fsp	Ilv-bearing assemblage	-	5.9
GM1674	Fsp	Ilv-bearing assemblage	-	7.2
K1	w.r.	Ilv-free assemblage	-74	4.8
GM1666	w.r.	Ilv-free assemblage	-55	4.5
GM1668	w.r.	Ilv-free assemblage	-86	4.9
GM1669	w.r.	Ilv-free assemblage	-67	6.8
GM1330	w.r.	augite syenite	-94	6.7
GM1857	w.r.	augite syenite	-88	6.4
EF024	w.r.	EF-basalt	-103	4.3
EF072	w.r.	EF-basalt	-92	5.5
EF075	w.r.	EF-basalt, much Ep	-65	1.9
EF087	w.r.	EF-basalt, slightly Ep	-84	-0.1
EF140	w.r.	EF-basalt, slightly Ep	-94	1.8
EF141	w.r.	EF-basalt, slightly Ep	-93	-0.8
EF144	w.r.	EF-basalt, complete Ep	-64	-1.8
EF168	w.r.	EF-basalt	-73	3.8
B72	Ep	Ep-Qtz-cavity in EF-basalt	-35	0.5
B73	Ep	Ep-Qtz-cavity in EF-basalt	-44	-1.9

w.r.: whole rock   EF: Eriksfjord

The δD values of ilvaite-bearing whole-rock samples range from –136 to –118 ‰, those of the ilvaite-free assemblages from –86 to –55 ‰. Pure, hand-picked ilvaite varies from –148 to –136 ‰. Epidote could not be analyzed because of the impossibility to pick a large enough clean separate of the very fine-grained material. The Ilímaussaq augite syenites range from –94 to –88 ‰, the Eriksfjord basalts from –103 to –64 ‰ and the epidotes from the cavities have values of –44 and –35 ‰, respectively.
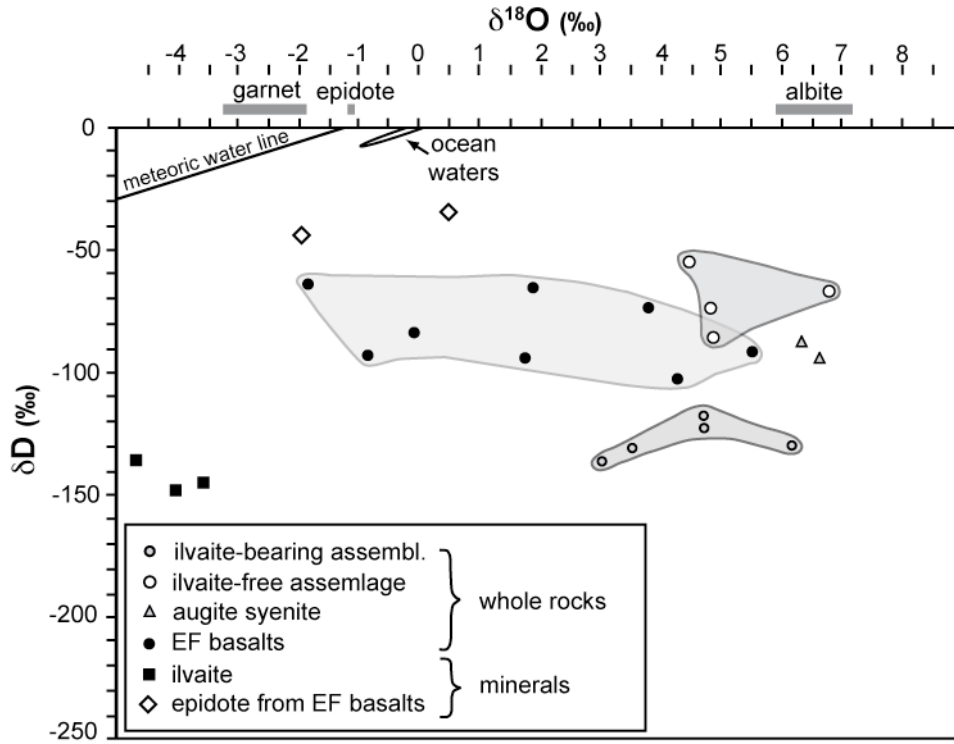
Fig. 11: $\delta^{18}O$ and δD values of whole-rock samples and minerals. Albite, garnet and epidote from the ilvaite-bearing assemblage are shown as bars because of the lack of hydrogen isotope data. For comparison, other Ilímaussaq and Eriksfjord (EF) samples are plotted.

3.5   Discussion

3.5.1   Activity calculations

The stability of the ilvaite-bearing assemblage in terms of T and fO_2 at constant P was investigated in the simplified chemical system Ca-Fe-Si-Al-O-H considering the phases grossular (Grs), epidote (Ep), ferro-actinolite (Fac), hedenbergite (Hd), hematite (Hem) and a fluid consisting of $SiO_{2(aq)}$, H_2O and O_2. Grossular was chosen instead of andradite since another Al-bearing component was needed to balance epidote-involving reactions.

To estimate the position of relevant phase equilibria, a Schreinemakers analysis was performed for the following reactions in this system (Fig. 12):

$$Grs + Hem + SiO_2 + H_2O = Ep + Hd + O_2 \quad [Fac] \qquad (1)$$
$$Hd + Hem + SiO_2 + H_2O = Fac + O_2 \qquad\qquad [Grs,Ep] \quad (2)$$
$$Ep + Hd + SiO_2 + H_2O = Fac + Grs + O_2 \quad [Hem] \qquad (3)$$
$$Ep + Hd = Fac + Hem + Grs + O_2 \qquad\qquad [SiO_2,H_2O] \quad (4)$$
$$Hem + Grs + SiO_2 + H_2O = Ep + Fac + O_2 \quad [Hd] \qquad (5)$$
$$Ep + Hd = Fac + Hem + Grs + SiO_2 + H_2O \quad [O_2] \qquad (6)$$
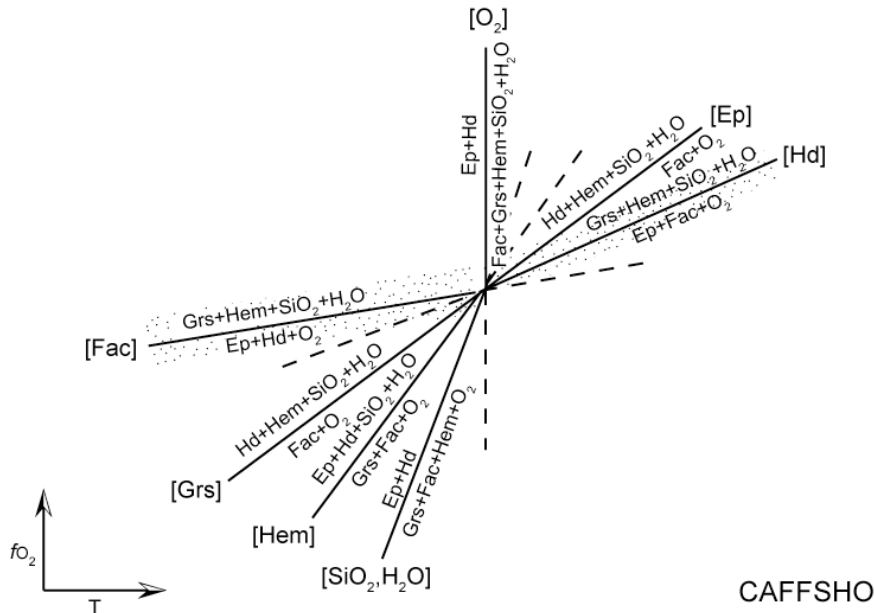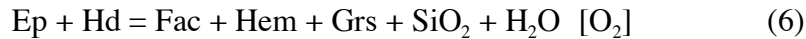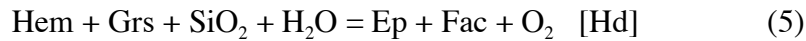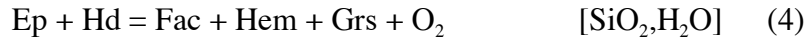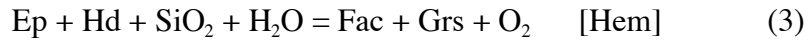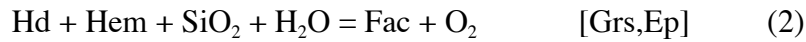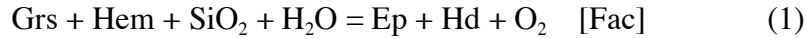
Fig. 12: Schreinemakers analysis of the Al_2O_3-CaO-FeO-Fe_2O_3-SiO_2-H_2O-system including the phases grossular, epidote, ferro-actinolite, hedenbergite, hematite, and a fluid consisting of $SiO_{2(aq)}$, H_2O and O_2. Abbreviations after Kretz (1983).

The rock texture shows amphibole and pyroxene to be in disequilibrium with the other phases because they are in reaction textures with ilvaite. The field in which the endoskarn mineral assemblage is stable in an fO_2 versus T diagram is thus close to or above reactions (1) and reaction (5) where amphibole and pyroxene, respectively, are not stable or become unstable in contact with epidote (Fig. 12).

Mineral endmember activities were calculated for 400 °C. The activity of epidote was calculated after Bird & Helgeson (1980), that of hedenbergite after Holland (1990) and that of grossular was estimated using the program Ax of Holland & Powell (2000). The activity of $SiO_{2(aq)}$ was calculated to be temperature-dependent. The lower limit of the $SiO_{2(aq)}$ activity is given by the reaction nepheline + 2 SiO_2 = albite ($SiO_{2(aq)}$= 0.0002 at 200°C; 0.0079 at 500 °C), the upper limit by quartz saturation ($SiO_{2(aq)}$= 0.0027 at 200°C, 0.0367 at 500 °C). Variation of water activity results in just small changes of the position of the reactions in the fO_2-T-field.

Oxygen fugacity during cooling was calculated by determining the activity-corrected log$K$s with *Unitherm*, the database program of HCh (Shvarov & Bastrakov, 1999; SUPCRT92-routine of Johnson *et al.*, 1992), for 1 and 2 kbar and variable activities of H_2O and SiO_2. The results for 1 kbar (Fig. 13) constrain the stability field of both the ilvaite-bearing and the ilvaite-free assemblages. Reaction (1) is invariably close to the hematite-magnetite (HM) buffer and spans the grey field in Fig. 13 if calculated with two different $SiO_{2(aq)}$ activities. The activity-corrected reaction (5) plots far away from geologically realistic fO_2-T-conditions and beyond the conditions of Fig. 13. The occurrence of hematite in the endoskarn assemblage restricts the field to the hematite-stable side of the buffer curve and, hence, to the range of FMQ +5 to +7. Gustafson (1974) performed ilvaite stability experiments at 2 kbar. Since the position of the calculated reaction curves and invariant points of this study (Fig. 13) does not change significantly between 1 and 2 kbar the ilvaite reaction of Gustafson (1974) is regarded to be at least an approximation also for the here studied assemblages. However, it is important to note that Gustafson's experiments were done in the pure C-F-S-O-H system, whereas the ilvaites of the present study contain up to 4.2 wt.% MnO, which may change the precise location of the reaction curve in T-fO_2 space. The isotope fractionation temperatures detailed below, suggested that the uncertainty of the curve in Fig. 13 is about 50 to 100 °C, implying that (based on Fig. 13) the main endoskarn formation probably occurred between 400 and 500 °C. Phase relations after Liou *et al.* (1983), plotted in Fig. 13, indicate that the formation of prehnite in the ilvaite-free assemblage occurred between 300 and 340 °C and at logfO_2 values between –26 and –29. Hence, it is inferred that prehnite did not grow during the

main-stage endoskarn formation, but later at lower temperatures (see below). It is interesting to note that the temperature results for the formation of prehnite in the ilvaite-free assemblage agree well with T-fO_2 data derived from hydrothermal sulphide assemblages in Ilímaussaq late-stage veins determined by Karup-Møller (1978, Fig. 13).

In summary, phase relations indicate that the Ca-rich assemblages formed at temperatures below about 500 °C at $SiO_{2(aq)}$ activities between 0.001 and 0.02 and at fO_2 values slightly above HM (between FMQ +5 and +7). The formation of ilvaite in the endoskarns is limited to Fe-rich precursor whole-rock compositions.
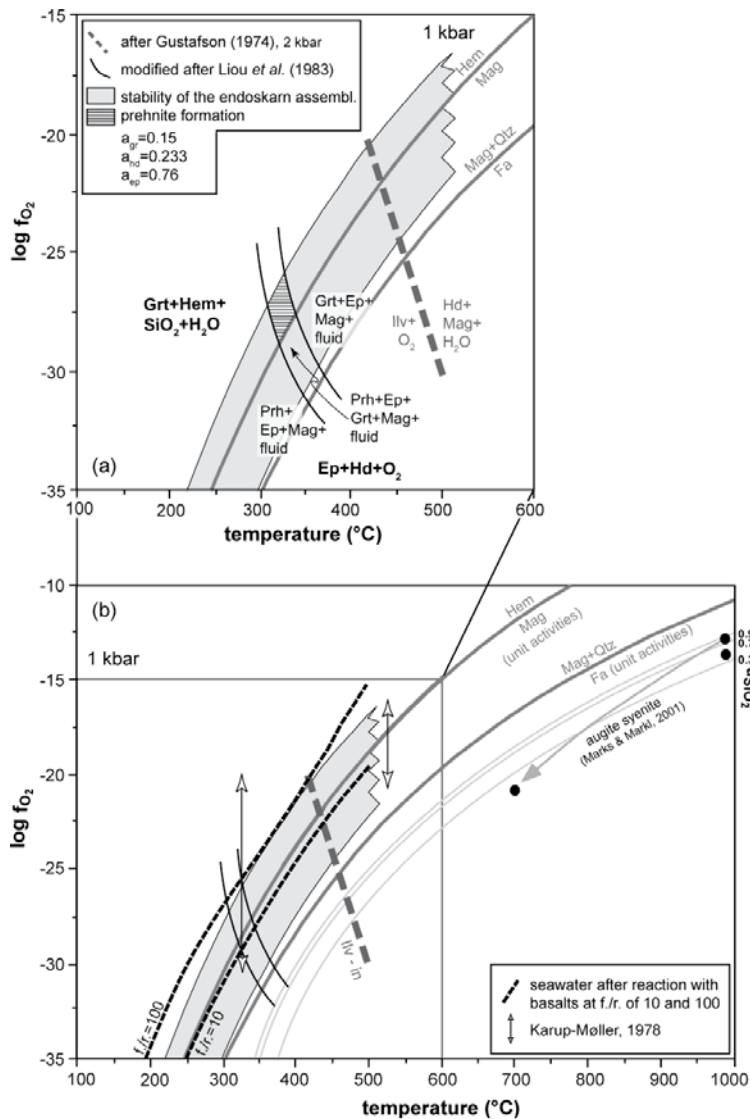
Fig. 13: (a) Stability constraints for the endoskarn assemblages in a T - logfO_2-diagram. Unit activities were used unless specified otherwise. Stability constraints of Gustafson (1974) and Liou et al. (1983) were added for ilvaite and prehnite-bearing assemblages, respectively. The ilvaite stability curve after Gustafson (1974) is plotted as a thick dashed line, to illustrate an uncertainty, since it is for the pure system, whereas the ilvaites of the present study contain additional Mn. (b) Stability constraint for the endoskarn assemblages in comparison to the fO_2-T-evolution during fractionation of Ilímaussaq melts, after Marks & Markl (2001). The thin dashed lines for different fluid/rock ratios (f./r.) constrain seawater composition after spilitization reactions with the basalts (see text for details). Mineral name abbreviations after Kretz (1983), except ilvaite (Ilv).

3.5.2 Whole-rock constraints

Based on field observations, textures and whole-rock compositions, the endoskarn assemblages are not related to carbonate rocks. Furthermore, textures and the similarity between the primitive mantle-normalized trace element patterns (after McDonough & Sun, 1995) of the endoskarns of this study and the range of Ilímaussaq rocks (Bailey *et al.*, 2001; Sørensen, 2006; Fig. 10) suggests that it were rocks from the peralkaline complex itself that were transformed into the endoskarns. In order to understand the mass transport of elements related to the formation of the endoskarn assemblages in the Ilímaussaq complex, isocon-like diagrams (Fig. 7, 9) were used, which show the element concentrations of the endoskarns compared to their suggested precursors. The inferred precursor rock for the ilvaite-bearing assemblages, the marginal pegmatite, is quite heterogeneous with respect to grain size and mineralogical composition: it comprises the pegmatitic Fe-richer parts with large amphibole crystals and the fine-grained matrix which is poorer in Fe but with an enrichment in eudialyte and, hence, in Ca and Zr. Accordingly, these elements are highly variable in endoskarn assemblages as well (Fig. 7, 9). The only persistent feature in all of the samples is that the Ca-content of the ilvaite-bearing assemblage is quite constant and significantly higher than in the unaltered matrix of the marginal pegmatite (Table 4). This matrix is used as best approximation to the composition of the unaltered pegmatitic part as well, since there are no whole-rock data for the pegmatitic veins available, yet. The matrix generally contains less arfvedsonite than the pegmatitic part and, hence, the ilvaite-bearing endoskarn assemblage is consistently richer in Fe than the unaltered matrix (Fig. 7). On the other hand, the matrix commonly contains more eudialyte than the pegmatitic veins and thus, it should have higher amounts of Ca. The fact that the opposite is true points to an enrichment of Ca in the studied rocks (Fig. 7).

Two of the four analyzed whole-rock samples of the ilvaite-free assemblage (GM1668 and GM1669) fit quite well with the representative analyses of the coarse-grained augite syenite and the foyaite, respectively, from Bailey *et al.* (2001; Fig. 9). Both have CaO < 5 wt.%, but slightly more than their presumed precursors. The two samples with clear naujaite texture (GM1666 and K1) fit well with the representative naujaite of Bailey *et al.* (2001) except for a strong enrichment in Ca and depletion in Na. It is evident, that the presence of the very Fe-rich amphiboles or the generally much higher Fe content of the amphibole-bearing pegmatitic parts was a necessary prerequisite for the formation of ilvaite. The Fe-richer whole-rock

composition is also reflected in the mineral compositions, for example of the garnets or the epidotes / allanites.

The source of the calcium

There are two ways to explain the gain of Ca: from internal or from external sources. Both possibilities will be explored below.

Internal sources of Ca in the intrusion from which Ca could be redistributed and enriched in the endoskarn assemblages could be clinopyroxene, feldspar and eudialyte. These minerals contain up to about 21, 4, and 10 wt.% CaO (clinopyroxen, Marks & Markl, 2001; feldspar, Larsen, 1981; and eudialyte, Johnsen & Gault, 1997, respectively), and late-magmatic metasomatic reactions involving Na-rich peralkaline fluids could release Ca according to the following reactions:

feldspar: $CaAl_2Si_2O_8 + 2\,Na^+ + 4\,SiO_2 = 2\,NaAlSi_3O_8 + \mathbf{Ca^{2+}}$

clinopyroxene: $2\,CaFeSi_2O_6 + 2\,Na^+ + 2\,H^+ + 0.5\,O_2 = 2\,NaFeSi_2O_6 + 2\,\mathbf{Ca^{2+}} + H_2O$

eudialyte (schematic): eudialyte + fluid = allanite + zircon + albite
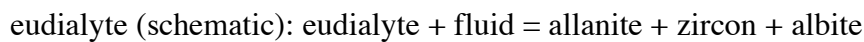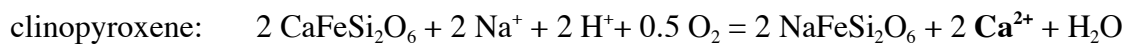
In this model, the Ca from feldspar and clinopyroxene would have been released into the fluid for redistribution and fixation in new minerals leaving behind pure albite and aegirine. Additionally, eudialyte, a major REE- and Zr-rich mineral of the agpaitic rocks in Ilímaussaq (Sørensen, 1992), was transformed releasing Ca, Zr, and REEs, which were incorporated into the zircon and the allanite present in the samples.

In principle, this would be a viable process and extensive late-magmatic fluid-rock interaction is recorded in many Ilímaussaq rocks (see e.g. Schönenberger, 2006). However, it is unclear to us, why Ca from large areas in the intrusion should be enriched at the particular point of endoskarn formation. This would be necessary, as there is no way to generate the Ca enrichment on a volume-conservative basis. Such an underlying process would remain enigmatic. Therefore, the second explanation of Ca enrichment is preferred, which involves an external source, i.e. a Ca-rich external fluid. In this case, it would be possible to derive Ca from the metasomatic alteration of the overlying Eriksfjord basalts, which display ample evidence for alteration in the greenschist facies (epidote-chlorite-quartz assemblage).

Metasomatic phenomena in and around peralkaline rocks: a comparison

Phase assemblages formed by metasomatic alteration and involving external fluids are well known from alkaline complexes (e.g. Sindern & Kramm, 2002; Savatenkov *et al.*, 2004). Boily & Williams-Jones (1994) and Salvi & Williams-Jones (1990; 1996; 2006) studied the

role of hydrothermal processes in the peralkaline Strange Lake complex, Canada, and Salvi *et al.* (2000) investigated the agpaitic rocks of the Tamazeght complex, Morocco, with respect to HFSE mobilization in, and deposition from, F- and Ca-bearing fluids. In this case, HFSE were transported as fluoride complexes in a F-rich orthomagmatic fluid and deposited by mixing with a Ca-enriched, externally derived meteoric fluid (Salvi & Williams-Jones, 1996). Khadem Allah *et al.* (1998) describe Ca enrichment in nepheline syenites of the Tamazeght Complex in contact with carbonate country rocks, which is recorded by the occurrence of, for example, pectolite and cancrinite and by an enrichment in the diopside component of clinopyroxenes. Fluid-related alteration phenomena are also known from <u>around</u> the Gardar intrusions in South Greenland. Fenitization is known from the volcanic rocks overlying the lujavrites in the northern part of the Ilímaussaq intrusion (Sørensen *et al.*, 1974; Kunzendorf *et al.* 1982; Sørensen & Larsen, 2001). Pitchblende occurs in fractures in the basement granite (Armour-Brown et al., 1983). The fracture zones are fenitized and contain perthitic feldspar and interstitial chlorite, iron oxides, carbonates, and as common accessories apatite, fluorite, and zircon. Ranløv & Dymek (1991) delineated aegirine-rich zones of metasomatic alteration on the Narssaq Peninsula in the northeastern part of the Ilímaussaq intrusion. Hansen (1968) described in the same area fractures filled with quartz, albite, microcline, aegirine, calcite, and hematite and accessories such as allanite and apatite and fenetized rocks in between the fractures. The mineralizations were related to low-temperature fluids derived from the intrusive complexes of Ilímaussaq and Igaliko. Wegmann (1938) who found abundant fluorite in the country rock of the intrusion around Tunulliarfik, concluded the F mobilization affected the entire area.

Fluid-related alteration <u>within</u> Gardar plutons are found, for example, in andradite-bearing autometasomtic assemblages described by Marks *et al.* (2003) from the peralkaline Puklen pluton. Parsons *et al.* (1991), Finch (1995), Rae *et al.* (1996) and Coulson (1997; 2003) described metasomatic alteration phenomena, which involved both late-magmatic and external fluids within other Gardar complexes. Fluid-involving alterations in the Ilímaussaq complex were mentioned by Ussing (1912), who described a broad (≤ 100 m), red, ferric oxide- and fluorite-rich band of alteration in the northern part of the intrusion. Except for feldspar, the assemblages of naujaite and lujavrite are replaced by hematite, fluorite, natrolite, chlorite, and zeolites at this place. Other regions within the Ilímaussaq intrusion where pneumatolytic alteration took place are shown on the maps of Ferguson (1964) and Bohse *et al.* (1971).

In summary, metasomatic processes involving Ca-enriched fluids are well-known from peralkaline complexes in general and from the Gardar Province in particular. The Ilímaussaq endoskarns are just a particularly spectacular and unusual example of such phenomena. The source and chemical evolution of the external metasomatizing fluid will be further characterized in the following paragraph.

3.5.3 Isotopic constraints

The large range in whole-rock $\delta^{18}O$ for the ilvaite-bearing assemblage (Fig. 11) may be caused by modal variations of ilvaite ($\delta^{18}O = -4.7$ to -3.6 ‰), epidote ($\delta^{18}O = -1.1$ ‰), garnet ($\delta^{18}O = -1.8$ and -3.3 ‰), and albite ($\delta^{18}O = 5.9$ to 7.2 ‰). The mineral data reveal a large isotopic fractionation between albite and the other minerals and a smaller one between ilvaite and garnet, ilvaite and epidote, and garnet and epidote.

To derive temperature information, mineral-mineral isotopic equilibria were studied by using mineral-H_2O fractionation coefficients of Zheng (1993a; b). Because it is well known, that some of Zheng's data do not reproduce experimental fractionation factors, various sets of mineral-H_2O fractionation factors are applied to the data and compared the respective results. Experimentally determined fractionation factors exist for albite-H_2O (Friedman & O'Neil, 1977; Matsuhisa et al., 1979) and for andradite-H_2O (Taylor, 1976; Kieffer, 1982), but not for ilvaite-H_2O and epidote-H_2O. Experimentally derived factors, however, are ascertained for distinct ranges of temperature only, and our inferred conditions do not always fall into these ranges. Our calculations therefore provide only an estimate of the temperature range in which the alteration processes took place.

Most of the equilibria not involving albite indicate that the ilvaite-bearing endoskarn assemblage formed in the range of 400 to 600 °C (Table 6). This range slightly exceeds the upper temperature limit of ilvaite stability according to Gustafson (1974), which most probably is the result of additional elements present in the endoskarn assemblage and not present in Gustafson's experiments (e. g., Mn).

Calculation of epidote-albite equilibria showed no results, regardless of the fractionation coefficients used. This means that these two minerals are not in isotopic equilibrium. Most other equilibria involving albite invariably indicate low temperatures below 285 °C, regardless of the coefficients used (Table 6). This is interpreted to indicate isotopic reequilibration of albite at low temperatures. As feldspars are known to reequilibrate to very low temperatures (Giletti et al., 1978), it is highly likely that the other three minerals record

the fluid during formation of the assemblages, whereas the feldspar probably records reequilibration with (potentially the same) fluid during cooling.

Table 6: Mineral-mineral equilibrium temperatures calculated via mineral-H_2O fractionation factors from different sources.

Mineral pairs Reference of fractionation factor min-H_2O	calculated range of equilibrium
Mineral pairs excluding albite	
Ilvaite-Andradite	
Ilvaite: Zheng (1993a), andradite: Taylor (1976)	350-490
Ilvaite: Zheng (1993a), andradite: Kieffer (1982)	490-610 °C
Ilvaite and andradite: Zheng (1993a, b)	380-600 °C
Epidote-Andradite	
Epidote: Zheng (1993a), andradite: Taylor (1976)	500 °C
Epidote and andradite: Zheng (1993a, b)	400 °C
Epidote-Ilvaite	
Epidote and ilvaite: Zheng (1993a)	500-720 °C
Mineral pairs including albite	
Andradite-Albite	
Andradite: Taylor (1976), albite: Matsuhisa *et al*. (1979)	no result
Andradite: Taylor (1976), albite: Friedman & O'Neil (1977)	300-307 °C
Andradite: Kieffer (1982), albite: Matsuhisa *et al*. (1979)	no result
Andradite: Kieffer (1982), albite: Friedmann & O'Neil (1977)	206-212 °C
Andratite and albite: Zheng (1993b)	160-166 °C
Ilvaite-Albite	
Ilvaite: Zheng (1993a), albite: Matsuhisa *et al*. (1979)	210-237 °C
Ilvaite: Zheng (1993a), albite: Friedman & O'Neil (1977)	220-285 °C
Ilvaite and albite: Zheng (1993a, b)	212-233 °C
Epidote-Albite	
all possible combinations	no result

In summary, textural observations, phase relations and oxygen isotope temperatures clearly reflect that the endoskarn assemblages were modified twice after their formation: at 300 to 350 °C, prehnite formed in the ilvaite-free assemblage (see also Fig. 13), and below about 250 °C, albite reequilibrated with a cooled fluid. In both these cases (prehnite formation and albite reequilibration), it was not possible to determine, if the same, but cooled fluid or a new fluid influx was responsible for the alteration.

It was suggested above that an external fluid was probably responsible for the Ca-enrichment and the endoskarn mineralization. An approximation to the $\delta^{18}O$ signature of this fluid in isotopic equilibrium with the analyzed minerals was calculated using the fractionation coefficients between mineral and H_2O of Zheng (1993a, b; Fig. 14). The oxygen isotopic compositions of the fluid calculated for each mineral in dependence of temperature show an intersection for epidote, ilvaite and garnet at about a minimum temperature of $\sim 450\,°C$ and a $\delta^{18}O$ value of $\sim 0\,‰$ (Fig. 14) - hence, modern seawater - whereas albite is not in isotopic equilibrium at this temperature (see above).
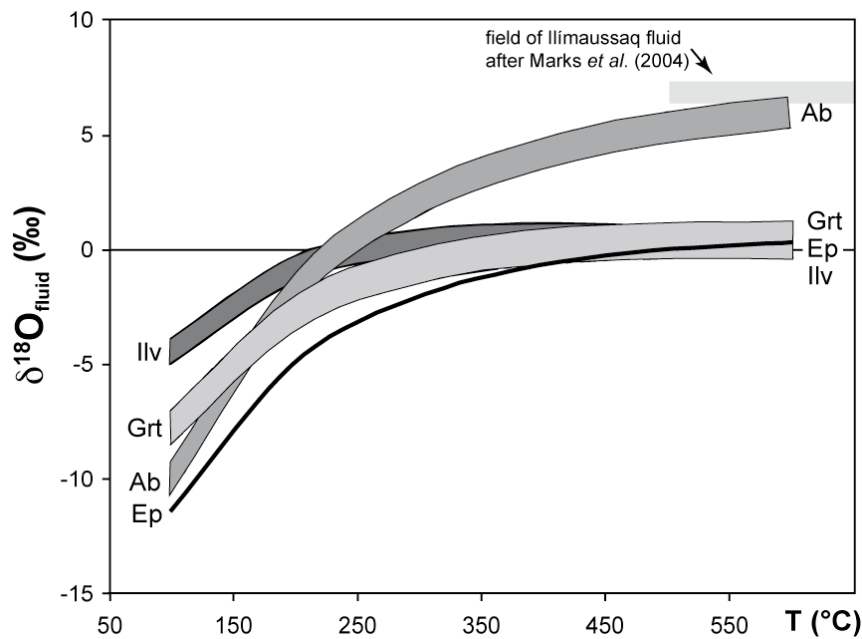
Fig. 14: $\delta^{18}O$ composition of the fluid in equilibrium with the analyzed minerals at temperatures between 50 and 600 °C calculated with fractionation coefficients of Zheng (1993a, b). The fluid compositions plot in fields rather than on lines because of the variations in the mineral analyses. Grey, frameless bar indicates fluids corresponding to the Ilímaussaq amphiboles studied by Marks *et al.* (2004) that were calculated for temperatures between 500 and 800 °C.

The hydrogen isotope signature of the ilvaite-bearing assemblage ($\delta D = -136$ to $-118\,‰$) is dominated by ilvaite ($\delta D = -148$ to $-136\,‰$) as the dominant hydrogen-bearing mineral (Table 5). The values of the ilvaite-free assemblages are accordingly higher ($\delta D = -86$ to $-55\,‰$) and in the typical range of magmatic rocks and waters (Sheppard, 1986; Taylor & Sheppard, 1986). Unfortunately, the H isotopic composition of epidote from the endoskarn assemblages could not be analysed due to lack of enough pure sample material. Based on the temperature-independent fractionation coefficient of Yaquian & Jibao (1993) for 350 to 550 °C, the δD signature of the fluid in isotopic equilibrium with ilvaite is estimated to lie between -54 and $-40\,‰$. Thus, the fluid shows a trend towards isotopically heavier waters.

The temperature independence of the coefficient and the uncertainties in hydrogen isotope fractionation coefficients in general may be the reasons that the calculated fluid does not plot on the modern meteoric water trend in Fig. 11. The δD signature of the fluid in isotopic equilibrium with the epidotes from the Eriksfjord basalts ($\delta D = -35$ and -44 ‰), however, is +6 and -3 ‰, respectively, for 400 °C and 10 and 1.4 ‰ for 500 °C (calculated with fractionation coefficients of Chacko *et al.*, 1999), which is reasonably close to modern seawater.

Admittedly, there is no indication that the stable isotope composition of modern seawater is similar to the seawater isotope composition 1.16 Ga ago, but in the absence of any proof of the contrary, and given the geological evidence of pillow-basalts of the Eriksfjord formation, it is reasonable to assume the involvement of seawater.

In summary, it appears that seawater circulating through the Eriksfjord basalts was one of the driving forces of metasomatism responsible for the formation of the endoskarns at Ilímaussaq. The structures along which seawater was circulating in the ground are arranged erratically and thus there is no uniform alteration. The pillow structures in the Eriksfjord basalts (Emeleus & Upton, 1976) and the ubiquitous occurrence of chlorite-epidote-quartz assemblages in the basalts are evidence of both a temporarily marine environment and spilitization reactions, which are the necessary prerequisites for the suggested model. Furthermore, the D and O isotopic compositions of the epidotes from basalts analyzed in the course of this study agree with equilibration with a fluid close to (modern) seawater composition.

In order to constrain the seawater alteration process quantitatively, fluid-rock equilibria were calculated by Thomas Wagner (Universität Tübingen) for a fluid of typical (modern) seawater composition during progressive fluid-rock interaction between 50 °C/300 bar and 500 °C/1000bar in the system Si-Al-Fe-Mg-Ca-Na-K-C-S-Cl-O-H. Calculations were carried out in different runs with effective fluid/rock ratios of 0.1, 1, 10 and 100 and along the constructed geotherm $P = 100+4.25*T-0.005*T^2$. It is noted that the term effective fluid/rock ratio is used here for the time-integrated fluid flux the rock has experienced. The primary seawater composition is from Millero (2004), recalculated to the system Mg-Ca-Na-K-C-S-Cl-O-H with its dissolved oxygen content constrained by equilibrium with O_2 gas at (modern) atmospheric partial pressure. The composition of a typical Eriksfjord basalt was taken from Halama *et al.* (2003, sample EF059).

Calculations were performed with the *HCh* software package (Shvarov & Bastrakov, 1999), which models heterogeneous equilibria and reaction progress by minimization of the

Gibbs free energy of the total system (Shvarov, 1978; 1981). The thermodynamic data for aqueous species are from the SUPCRT92 database and subsequent updates (Johnson *et al.*, 1992; Shock *et al.*, 1997; Sverjensky *et al.*, 1997). Data for silicate, oxide, hydroxide and carbonate minerals were taken from the internally consistent dataset of Holland & Powell (1998). An extended Debye-Hückel model using the b-gamma equation for NaCl as background electrolyte was applied for calculations of individual activity coefficients of aqueous species (Oelkers & Helgeson, 1990; Shock *et al.*, 1992).

The results of the calculations indicate that the fluids had equilibrium Ca concentrations of $6.0*10^{-3}$ and $5.2*10^{-3}$ mol/kg Ca at fluid/rock ratios of 10 and 100, respectively, for 400 °C and of $1.1*10^{-2}$ and $3.6*10^{-3}$ for 500 °C (Table 7, Fig. 15). Hence, reasonable amounts of about 10^{11} kg fluid (corresponding to a rock volume of about 100 by 100 by 100 m) would be sufficient to explain the Ca-enrichment of the endoskarns even if all Ca would have to be added. The oxygen fugacity of these fluids in equilibrium with the altered basalt is around HM ±0 and HM +4 for fluid/rock ratios of 10 and 100, respectively.

Table 7: Compositon of seawater in equilibrium with the Eriksfjord basalt along a constructed geotherm (see text for details).

T (°C)	500	450	400	300	200
P (bar)	1005	996	970	865	690
fluid/rock = 10					
Al (mol/kg)	1.13E-02	1.64E-02	6.00E-03	6.50E-03	7.69E-03
Fe (mol/kg)	3.35E-03	5.83E-04	2.26E-05	2.21E-07	2.21E-08
Mg (mol/kg)	7.99E-04	2.81E-04	3.20E-05	7.78E-06	1.46E-06
Ca (mol/kg)	1.13E-02	1.64E-02	6.00E-03	6.50E-03	7.69E-03
Na (mol/kg)	5.27E-01	5.24E-01	5.49E-01	5.52E-01	5.74E-01
K (mol/kg)	1.61E-02	1.61E-02	1.61E-02	1.61E-02	1.62E-02
log fO$_2$	-19.56	-21.90	-24.57	-31.04	-39.85
pH	5.35	5.27	5.55	5.80	6.70
fluid/rock = 100					
Al (mol/kg)	1.34E-05	3.56E-06	1.82E-06	6.19E-07	1.22E-07
Fe (mol/kg)	9.43E-03	8.07E-03	4.97E-03	3.98E-04	1.57E-04
Mg (mol/kg)	1.81E-02	2.04E-02	2.41E-02	3.03E-02	3.24E-02
Ca (mol/kg)	3.57E-03	4.59E-03	5.19E-03	5.48E-03	9.88E-03
Na (mol/kg)	5.01E-01	5.01E-01	5.01E-01	5.01E-01	5.01E-01
K (mol/kg)	1.08E-02	1.08E-02	1.08E-02	1.08E-02	1.08E-02
log fO$_2$	-15.11	-18.14	-21.29	-27.04	-34.71
pH	4.57	4.22	3.98	3.84	4.30
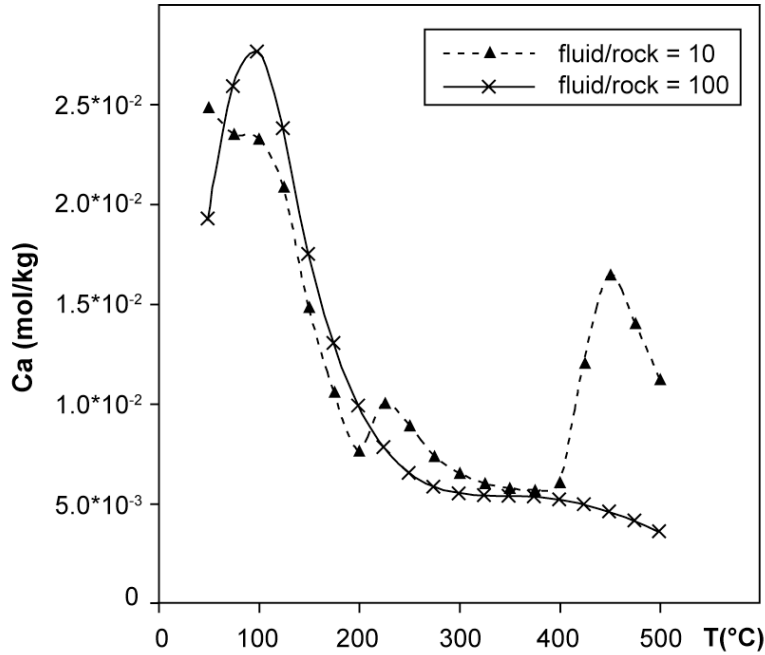
Fig. 15: Variability of the Ca content (mol/kg) of a seawater fluid passing through the Eriksfjord basalts along a constructed geotherm (see text for details). The shape of the curves is a result of variable fluid-fluid and fluid-rock equilibria.

The high fluid/rock ratio would also explain why the O isotopic signature of the fluid remained essentially unchanged during the spilitization reactions. The analyzed basalt samples, in contrast, show much lighter values (Fig. 11) than typical basalts, which are expected to have values around 5 to 7 ‰ (Taylor & Sheppard, 1986). The spread in $\delta^{18}O$ values in Fig. 11 hence probably records the intensity of the spilitization process.

The change in the isotope signature of water was calculated after the following formula of Taylor (1977):

$$W/R = \frac{\delta^f_{Rock} - \delta^i_{Rock}}{\delta^i_{H_2O} - \left(\delta^f_{Rock} - \Delta\right)}$$

where W and R are the relative atom per cent of water and rock oxygen, respectively, in the bulk system, δ^i and δ^f the initial and final isotope values, respectively, and Δ is $(\delta^f_{Rock} - \delta^f_{H_2O})$. The fresh Eriksfjord basalts have $\delta^{18}O$ values between 5 and 6 ‰ (Halama *et al.*, 2003), whereas the most altered sample has a $\delta^{18}O$ value of −1.8 ‰ (EF144, this study) The calculations after Taylor (1977) reveal that the fluid's isotope composition stays close to 0 ‰ for fluid/rock ratios of 10 (0.4 ‰) and 100 (0.04 ‰). Lower ratios result in much higher $\delta^{18}O$

values of the fluid. In analogy, the results for hydrogen isotopes are close to 0 ‰ for fluid/rock ratios of 10 (–0.1 ‰) and 100 (–0.01 ‰), when taking EF072 as fresh basalt (δD = –92 ‰) and EF144 as the most altered one (δD = –64 ‰).

3.6 Summary and conclusions

This study investigated parts of the western marginal portion of the peralkaline Ilímaussaq intrusion, where persodic rocks were altered to Ca-rich endoskarn assemblages with epidote/allanite, hydrogarnet, and ilvaite or prehnite. These endoskarns are significantly enriched in Ca in comparison with their precursor rocks, which were inferred on the basis of whole-rock compositions and textures. The very heterogeneous nepheline syenitic marginal pegmatite is the precursor for the ilvaite-bearing assemblages, whereas various other Ilímaussaq syenites (e.g. naujaite, augite syenite, foyaite) are the precursors of the ilvaite-free assemblages. The occurrence of ilvaite appears to depend on the presence of large amounts of Fe-rich amphiboles in the precursor rock. Stable isotope investigations yielded temperatures of about 500 °C and activity-corrected thermodynamic calculations revealed oxygen fugacities between FMQ +5 and FMQ +7 (slightly above the HM buffer) as conditions of formation for the endoskarn assemblage. Textures and phase relations indicate prehnite to have formed at about 300 to 340 °C during cooling of the complex and after the formation of the endoskarns. Stable isotope data of albite suggest a reequilibration at even lower temperatures.

In the absence of any carbonate rocks in the vicinity of Ilímaussaq, there remain two different possible sources of Ca: redistribution of Ca released during late- to post-magmatic breakdown of Ca-bearing magmatic phases or externally derived Ca-rich fluids, which entered the complex along faults and along the margins of the complex. Based on geological evidence, the second possibility is preferred. Stable isotope compositions of minerals from the endoskarn assemblage indicate that the fluid had the δ^{18}O signature of modern seawater, which is consistent with pillow structures in the basalts of the Eriksfjord Formation. These basalts are assumed to be only slightly older than the intrusion (Paslick *et al.*, 1993), which makes the presence of seawater at the time of intrusion plausible. Therefore, field observations and isotopic data are best explained by postulating the influx of seawater into the Ilímaussaq intrusion and, hence, the external Ca-rich fluid as major Ca source for the endoskarn assemblage is preferred. However, the possibility that some of the Ca enrichment is related to internal redistribution within the intrusion during late-magmatic autometasomatic alteration processes cannot be ruled out completely.

Fluid-rock interaction (spilitization) between seawater and the Eriksjord basalts at temperatures between 10 and 500 °C enriched the fluid in Ca necessary for the formation of the endoskarn assemblages. High fluid/rock ratios of 10 to 100 would explain both the basically unchanged $\delta^{18}O$ signature of the fluid and the highly oxidized nature of the fluid above the HM buffer. Reasonable amounts of about 10^{11} kg fluid (for a rock volume of about 100 by 100 by 100 m) with Ca contents of around 10^{-3} mol/kg Ca are sufficient to explain the Ca-enrichment in the endoskarns of, for example, the marginal pegmatite.

Earlier studies (Markl *et al.*, 2001; Marks & Markl, 2001; Marks *et al.* 2004) suggested a closed system for the evolution of the Ilímaussaq intrusion. Although evidence for the infiltration of external fluids is presented, it is important to note that this happened after fractionation and solidification of the pluton. Accordingly, magmatic crystallization proceeded in a closed system, which, however, experienced external metasomatism along its margin and along faults during cooling, while it was still at temperatures of about 300 to 500 °C.

4 ISOTOPE, MAJOR, MINOR AND TRACE ELEMENT GEOCHEMISTRY OF LATE-MAGMATIC FLUIDS IN THE PERALKALINE ILÍMAUSSAQ INTRUSION, SOUTH GREENLAND

4.1 Previous work on fluid inclusions in Ilímaussaq

A large variety of studies dealt with fluids and fluid-rock interaction processes in alkaline rocks of the Gardar Province and especially the Ilímaussaq igneous complex in South Greenland (Sobolev *et al.*, 1970; Petersilie & Sørensen, 1970; Konnerup-Madsen, 1980; 1984; 2001; Konnerup-Madsen & Rose-Hansen, 1982; 1984; Konnerup-Madsen *et al.*, 1979; 1981; 1985; 1988; Larsen & Sørensen, 1987; Markl & Baumgartner, 2001; Krumrei *et al.*, 2007). Konnerup-Madsen (1984) distinguished three different types of fluid inclusions in the granites of the Gardar complexes: (1) aqueous, (2) CO_2-CH_4, and (3) CO_2-CH_4-H_2O. Almost all of the inclusions were trapped after the main solidification. The Ilímaussaq granite contains only moderate to high-salinity aqueous inclusions. Inclusions in quartz of an alkali-granitic vein in a sandstone xenolith within the Ilímaussaq complex, however, contains predominantly CH_4 with traces of CO_2, C_2H_6, and H_2S (Konnerup-Madsen & Rose-Hansen, 1984; Konnerup-Madsen *et al.*, 1985). A quartz-vein in sandstone near the roof of the intrusion bears just pure CO_2 inclusions. In all samples from the Ilímaussaq nepheline syenites and veins formed from fluids expelled from the syenites, CH_4 is the dominant volatile component (Konnerup-Madsen, 2001). Aqueous and mixed hydrocarbon-aqueous inclusions are rarely seen. Aqueous inclusions occur in isolated patches, whereas the hydrocarbon inclusions are commonly aligned to healed fractures. Hence, the aqueous inclusions are thought to be trapped earlier than most of the hydrocarbon inclusions, but there are hydrocarbon inclusions that were clearly trapped at the magmatic stage (Krumrei *et al.*, 2007). In hydrothermal vein minerals (chkalovite), the association of hydrocarbon-rich and highly saline aqueous inclusions indicates the simultaneous entrapment of immiscible fluids (Konnerup-Madsen & Rose-Hansen, 1982). Carbon-isotope studies support an abiogenic formation for the methane (Konnerup-Madsen, 2001). Konnerup-Madsen (2001) suggested that the hydrocarbons represent the remains of a magmatic CO_2-rich volatile phase that formed during cooling and solidification of the alkaline magma. Krumrei *et al.* (2007), however, demonstrated that at least some of the hydrocarbon-rich fluid inclusions found in sodalite in naujaite have a primary high-temperature magmatic origin.

4.2   Sample description and locality

Fluid inclusions were investigated in quartz, ussingite, and fluorite from veins distributed all over the complex (Fig. 1). The ussingite samples (GM1246, GM1382 and GM1384) come from the north coast of the Tunulliarfik fjord and occur as meter-sized lenses in naujaite autoliths in the lujavrites (Fig. 1).

Quartz-bearing veins and lenses are rare in the Ilímaussaq intrusion although Ussing (1912), Ferguson (1964) and Marks & Markl (2001) described quartzitic sandstones as xenoliths in augite syenite close to the south coast of the Kangerluarsuk fjord. Most of the studied quartz veins of the present study occur within the augite syenite unit close to lake 465 in the southern part of the complex (ILM4, IlM169, ILM170 and KH2; Fig. 1). The sample KH2 was taken close to the pegmatitic margin between the augite syenite and kakortokites. The veins strike parallel to the contact and hence also parallel to the intrusion's margin. Quartz is either the main component of the veins, separated from the augite syenite by a frame of albite, aegirine, and possibly amphibole, or it occurs intergrown with these minerals (KH2). In thin section, calcite is visible in sample KH2. It occurs interstitially and is intergrown with the other minerals. Aegirine-albite veins lacking quartz are spatially associated. The quartz-bearing veins and lenses are some centimetres to some metres large with quartz occurring as anhedral masses and, less commonly, as euhedral crystals. One additional sample of a pure quartz vein (about 10 cm in thickness; ILM190; Fig. 1) comes from an alkali granite on the southwest slope of the Nakkaalaaq mountain in the northern part of the complex.

Three fluorite samples were taken from, (i) the foot of the Nakkaalaaq mountain (ILM77) where the fluorite occurs as disseminated, mm-sized grains in altered naujaite of red colour, (ii) close to lake Taseq (ILM99), occurring as small flakes in association with albite, and (iii) at Appat (ILM325), occurring as cm-sized masses in altered naujaite. In all three localities, fluorite is regarded as late-magmatic to hydrothermal, formed during reaction of the primary magmatic rock with late-stage fluids.

4.3 Analytical methods

Petrographic and microthermometric work on fluid inclusions was carried out at the Institut für Geowissenschaften, Universität Tübingen, on double-polished wafers using standard petrographic microscopes and a Linkam THMS 600 heating-freezing-stage mounted on a Leica Microscope. Calibration of the stage was done with synthetic CO_2-H_2O and pure H_2O fluid inclusions using the triple point of CO_2 (–56.6 °C), the melting point of pure H_2O (0.0 °C) and the critical point of H_2O (374.1 °C). Measurements on the fluid inclusions in the samples were done over a range of –190 to +450 °C. Freezing rates varied between 1 and 10 °C/min and heating rates between 0.5 and 1 °C/min at the points of phase transitions. Measurements were found to be reproducible to ±0.2 °C for melting temperatures (except metastable melting of hydrohalite) and ±1.0 °C for freezing and homogenisation temperatures.

A Dilor Labram 2 laser-Raman spectrometer, equipped with a 488 nm, 11 mW, Ar-laser, was used for qualitative Raman studies at the Institut für Geowissenschaften, Universität Tübingen. Calibration was done using the spectra of a diamond (1331 cm^{-1}) and a silicon standard (521 cm^{-1}). The analytical error is up to ±2 wavenumbers. Vapour and liquid phases of the inclusions were analysed from wavenumber 650 to 4500 cm^{-1} and solids beginning with wavenumber 100 cm^{-1}.

A crush-leach method was applied to handpicked and washed quartz and fluorite samples. Ion-chromatography was performed at the Institut für Geowissenschaften, Universität Tübingen, using a Dionex ICS-1000 system, with an IonPac® AS9-HC column for anions (Cl^-, Br^-, F^-, NO_3^-, SO_4^{2-}) and an IonPac® CS12A column for cations (Li^+, Na^+, K^+, Mg^{2+}, Ca^{2+}, Sr^{2+}, Ba^{2+}). Anions and cations were analysed separately from 2 g of crushed sample leached with triple deionised water. Half of the solution was taken for anion analysis, the other half was acidified with HNO_3 before injection (see Köhler *et al.*, in review, for a detailed description). Because of the inhomogeneous distribution of fluid inclusions within one sample, two or three analyses were done from different parts of the specimen. The results were recalculated based on average salinities of each samples obtained by microthermometry. The proportion of the chloride concentration revealed by microthermometry to the analysed concentration was used to recalculate all values to absolute weight ppm (wt. ppm). Bulk crush-leach analyses on additional cations of fluid inclusions in fluorite were performed on two samples only (ILM99 and ILM325) according to the method described by Bottrell *et al.* (1988), Banks and Yardley (1992) and Yardley *et al.* (1993) at the University of Leeds, UK. Na was analysed by ICP-AES (inductively coupled plasma – atom emission spectroscopy)

and Mn, Fe, Cu, Zn, Rb, Sb, Cs, Pb, Th, and U by ICP-MS. Results are presented in wt. ppm, if not quoted differently.

Oxygen-isotope compositions of quartz and ussingite were determined using a CO_2-laser, F_2 method after Sharp (1990) and Rumble & Hoering (1994), and measured as already described in chapter 3.3. The results are reported in δ-notation in permil [‰] relative to VSMOW. The analytical precision is about ± 0.2 ‰ for $δ^{18}O$ for standards and samples.

Carbon- and oxygen-isotope compositions on carbonate minerals were determined against the standard NBS-18 using a GasBench II and a Finnigan MAT 252 mass spectrometer at the Universität Tübingen. The sample material was treated at 70 °C with 99 % orthophosphoric acid to produce CO_2, which was used for isotopic determination. The results are reported in δ-notation in permil [‰] relative to Vienna PeeDee belemnite (VPDB). The analytical precision is ±0.1 ‰ for both $δ^{18}O$ and $δ^{13}C$ for standard and samples. Results for standard NBS-18 were –22.96 ‰ and –5.08 ‰ respectively.

Carbon- and hydrogen-isotope analyses on hydrocarbon-bearing inclusions were performed at the Laboratory for Stable Isotope Science at the University of Western Ontario, Canada, using the online crushing gas chromatography-isotope ratio mass spectrometry technique developed by Potter and Longstaffe (see Potter *et al.*, 2006; Potter & Longstaffe, 2007, for detailed description). At ~120 ºC, about 2 g of sample were crushed in a helium-flow. The released gases were transferred to an HP6890 gas chromatograph and separated using a Poraplot Q column. The eluting volatiles were passed through a combustion reactor and the resulting CO_2 used for $δ^{13}C$ isotopic determination. On another run the volatiles were passed through a pyrolysis reactor. The resulting H_2 was used for δD isotopic determination. Isotopic ratios were determined using a ThermoFinnigan Delta[PLUS] XL mass spectrometer. The natural gas standards RM 8559 and 8560 of the National Institute of Standards and Technology, evaluated against NBS-19 for $δ^{13}C$ and VSMOW and VSLAP (Vienna standard light antarctic precipitation) for δD, were used to calibrate the system. In-house hydrocarbon gases, evaluated against these standards, were run during sample analysis. Multiple aliquots of gas were analysed for each sample. Analytical precision was within ±0.5 ‰ for $δ^{13}C$ and ±5 ‰ for δD for all standards and most samples. The results are reported in δ-notation in permil [‰] relative to VPDB for $δ^{13}C$ and VSMOW for δD.

4.4   Results

4.4.1   Fluid inclusion petrography and microthermometric results

Based on petrographic and microthermometric work, four different types of fluid inclusions have been identified in quartz, fluorite and ussingite:

(a) Two-phase aqueous inclusions with possibly minor amounts of hydrocarbons and, in some cases, containing a third halite daughter phase.

(b) Rare aqueous inclusions with the composition of (a) plus an unidentified daughter mineral.

(c) Monophase aqueous inclusions.

(d) Monophase hydrocarbon inclusions.

These types will be used henceforward in the following sections.

Fluid inclusions in quartz veins in augite syenite

The most abundant fluid inclusions observed in the quartz veins associated with the augite syenite are aqueous inclusions of types (a) and (b) (Table 8). Most of these inclusions occur as trails or in clusters along healed fracture zones (Fig. 16a), and are interpreted to be of secondary origin. Isolated inclusions of possibly primary origin are scarce. The size of the inclusions varies from just a few to several tens of micrometers and may, in cases, be larger than 100 μm (e.g. Fig. 16e). Relatively rare monophase aqueous inclusions (type c) are present in sample ILM170. They are irregularly shaped and about 40 μm in size. More common are type (c) inclusions in ILM169. They show negative crystal shapes with varying sizes between 8 and 42 μm (Fig. 16b). Pure monophase hydrocarbon inclusions (type d) only occur in sample ILM 169 (Table 8; Fig. 16c). They occur as trails and generally show negative crystal shapes. They are interpreted to be secondary in origin.

_____

Fig. 16: Representative photographs of fluid inclusions and related Raman diagrams. a) Cluster (left) and trails (right) of two-phase aqueous inclusions in ILM4. Laser-Raman analyses indicate methane. b) Trail of monophase inclusions in ILM169. The inclusions show negative crystal shapes. c) Trail of pure hydrocarbon inclusions in ILM169. d) Two-phase aqueous inclusions in ILM170 with dissolved methane, showing negative crystal shape. e) Large, irregularly shaped three-phase aqueous inclusions in ILM170 with additional methane in the vapour phase. The solid is halite. f) Cluster of two-phase aqueous inclusions in ILM190 showing negative crystal shapes and irregularly shaped monophase aqueous inclusions. The laser-Raman diagram is typical of two-phase inclusions. g) Monophase aqueous fluid inclusions in ILM190 showing negative crystal shapes. h) Trails of monophase hydrocarbon bearing fluid inclusions in GM1246. The laser-Raman diagram proves the occurrence of not only methane but also ethane and propane. i) Hydrocarbon inclusions in ussingite in sample GM1382.
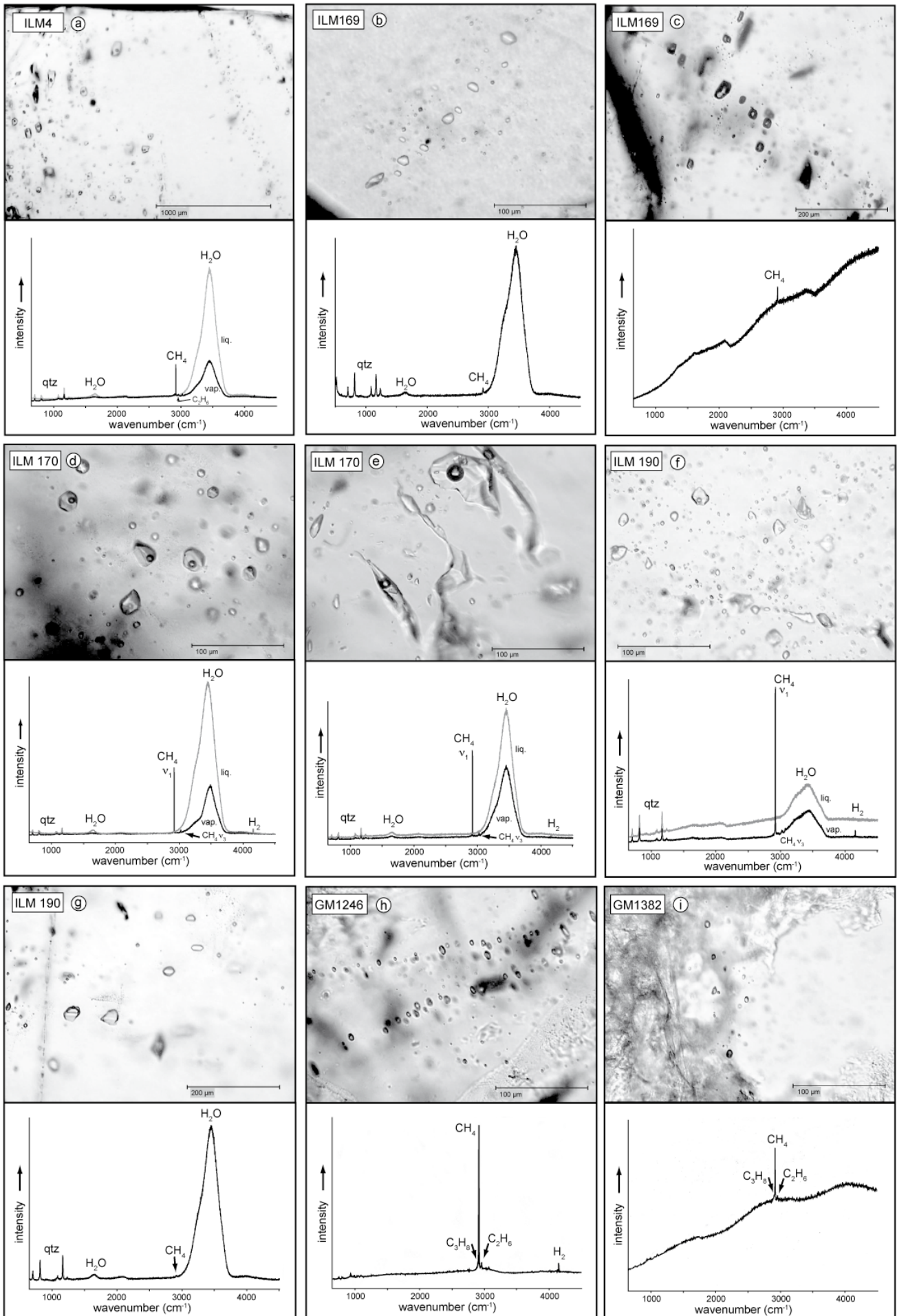
Table 8: Different fluid inclusion generations in the studied samples. All temperatures are in °C.

n	Type (see text)	Number of phases	Composition of phases	T_f	T_{fm}	$T_{m(ice)}$	$T_{m(Cl)}$	$T_{m(HH)}$	$T_{m(H)}$	T_h	F	Salinity wt.% NaCl equiv.	Comment
ILM4 - quartz vein in augite syenite													
5	b	3	aq + s	-76 – 80	-23 – 27	-21.8 – 22.5	-15.9 – 17.3 / n.o.	7.2 – 9.6	126 – 151**	117 – 190	0.80 – 0.95	28.8 – 29.7**	Raman: CH4 *
95	a	2	aq	-63 – 100	-22 – 29	-19.2 – 22.7	-9.9 – 20.0 *	-21.2 – +16.4*	-	68 – >400**	0.70 – 0.95	22.0 – 26.3°	Raman: CH4 * Th accumulated between 90 and 220°C
3	a	2	aq	-60 – 63	-28 – 36	-13.7	-5.5 / n.o.	-20.0 – 21.0	-	106 – 124	0.95	17.5	
ILM169 - quartz vein in augite syenite													
18	a	2	aq	-53 – 72	-33 – 50	-20.1 – 22.1	-	0.2 – 7.7*	-	67 – 102	0.98	22.5 – 26.3°	Raman: CH4 *
5	a	2	aq	-41 – 65	-34 – 40	-9.6 – 12.7	n.o.	-	-	50 – 96	0.96 – 0.99	13.5 – 16.6	Raman: CH4 *
		2	aq + HC			about -22	about +15						mixed aqueous-hydrocarbon inclusions with poorly visible phase transitions, see text for details
5	c	1	aq	-50 – 56	-37 – 44	-21.8 – 23.4	-	-	-	-	-	16.2 – 17.8	Raman: CH4 *
13	c	1	aq	-43 – 45	-34 – 40	-12.3 – 14.0	-	-	-	-	-	6.7 – 8.0	Raman: CH4 *
3	c	1	aq	-35 – 42	n.o.	-4.2 – 5.1	-	-	-	-	-	-	Raman: CH4 *
41	d	1	HC	-	-	-	-	-	-	-38.4 – 91.2	-	-	homogenisation to liquid
ILM170 - quartz vein in augite syenite													
1	b	4	aq + 2s	-65	-32	-24.7	-	-6.6	113	154	0.90	28.4	Tm(DX): 108
9	b	3	aq + s	-57 – 70	-29 – 30	-22.0 – 22.2	-	5.3 – 8.5	125 – 147	123 – 182**	0.95	28.8 – 29.6	Raman: CH4 *
21	a	2	aq	-62 – 85	-23 – 36	-20.1 – 24.7	n.o.	-21.9 – +6.5*	-	84 – 171	0.90 – 0.95	22.4 – 26.3°	Raman: CH4 *
8	a	2	aq	-57 – 65	-24 – 31	-15.9 – 18.0	-11 / n.o.	-	-	152-193	0.90 – 0.95	19.4 – 20.9	Raman: CH4 *
3	c	1	aq	-44 – 48	-22 – 25	-8.5 – 8.8	-	-	-	-	-	12.3 – 12.7	
ILM 190 - quartz vein in alkali granite													
1	b	4	aq + 2s	-47	-40	-3.6	-	-	400	130	0.95	47.4	Tm(DX) > 430; decrepitated
7	a	2	aq	-53 – 54	-32 – 40	-18.2 – 18.7	n.o.	-	-	84 – 142	0.95	21.1 – 21.5	
26	a	2	aq	-41 – 52	-30 – 46	-10.0 – 17.1	-10 – 14 *	-	-	35 – 116	0.95 – 0.99	13.9 – 20.3	
16	a	2	aq	-42 – 45	-24 – 35	-2.8 – 5.0	-	-	-	126 – 228	0.90 – 0.95	4.7 – 7.9	Raman: CH4 *
10	c	1	aq	-43 – 45	-32 – 45	-12.5 – 14.1	-	-	-	-	-	16.4 – 17.9	Raman: CH4 *
22	c	1	aq	n.o.	n.o.	-0.1 – 2.4	-	-	-	-	-	0.2 – 4.0	
GM1246 - ussingite													
45	d	1	HC	-	-	-	-	-	-	-77.5 – 94.1	-	-	
GM1382 - ussingite													
51	d	1	HC	-	-	-	-	-	-	-14.2 – 72.5	-	-	
GM1384 - ussingite													
20	d	1	HC	-	-	-	-	-	-	-70.1 – 89.4	-	-	
ILM77 - fluorite													
2	a	3	aq + s	-60 – 85	n.a.	-24.6 – 24.9	-	11.3 – 18.3	n.a.	n.a.	0.6-0.8	-	no salinity calculation since Tm(H) is unknown
9	a	2	aq	-60 – 85	n.a.	-22.5 – 25.0	-	-15.9 – +16.6	-	n.a.	0.6-0.8	23.2 – 26.3 °	
6	a	2	aq	-60 – 85	n.a.	-22.5 – 24.5	-	°°	-	n.a.	0.6-0.8	23.3 – 26.5°	
6	a	2	aq	-60 – 86	n.a.	-13.1 – 19.9	-	-	-	n.a.	0.6-0.8	17.0 – 22.3	
ILM99 - fluorite													
32	a	2	aq	-70 – 80	n.a.	-17.8 – 23.1	-	°°	-	n.a.	0.9-0.95	20.8 – 23.2	
12	a	2	aq	-	n.a.	-23.2 – 25.6	-	-0.5 – +7.8	-	n.a.	0.9-0.96	23.3 – 26.5°	
ILM325 - fluorite													
25	a	2	aq	-55 – 69	n.a.	-12.3 – 20.2	-	-	-	n.a.	0.7-0.8	16.2 – 22.5	

T_f — temperature of freezing
T_{fm} — temperature of first visible melting
$T_{m(ice)}$ — temperature of ice melting
$T_{m(Cl)}$ — temperature of clathrate melting
$T_{m(HH)}$ — temperature of hydrohalite melting
$T_{m(H)}$ — temperature of halite melting
T_h — temperature of homogenisation
F — degree of fill
$T_{m(DX)}$ — temperature of melting of the daughter crystal

aq — aqueous
s — solid
HC — hydrocarbons

NaCl equiv. NaCl equivalente in weight %
n.o. — not observable
- — phase not present
n.a. — not analysed

* — not in every inclusion present
** — phase transition not exactly observable
°) — because of metastable melting of hydrohalite, the maximum salinity of hydrohalite bearing inclusions is taken as upper limit
°°) — Tm(ice) is so low that hydrohalite should have formed in the pure NaCl-H₂O system and is metastable absent or, otherwise, additional salts are dissolved

*) — not in every inclusion present
**) — some inclusions decrepitated prior to melting of solid
comment: — decrepitation is common, thus Th was not measurable in all inclusions

Fig. 17: Histograms of the studied fluid inclusions samples, showing the ice melting temperature ($T_{m(ice)}$) in relation to the amount of phases and the homogenization temperature of hydrocarbons ($T_{h(HC)}$).

Microthermometric results are shown in Table 8. Most of the aqueous inclusions (type a and b) freeze between –53 and –100 °C to a dark mass of microcrystalline ice and hydrohalite or to a bright mass which commonly recrystallises to a dark mass on heating to about –30 °C. Initial melting is visible between –50 and –22 °C. Last ice-melting temperatures are between –24.7 and –19.2 °C (Fig. 17b - d), leaving usually hydrohalite and in some cases a clathrate. Each sample contains another minor generation of fluid inclusions with ice melting temperatures ranging from –18.0 to –15.9, –12.7 to –9.6 and of –13.7 °C in ILM170, ILM169 and ILM4, respectively. Clathrate melting occurs in the temperature range of –20.0 to –5.5 °C. Hydrohalite melting takes place between –21.9 and +16.4 °C, indicating metastable behaviour. Halite melts between 113 and 151 °C. In one fluid inclusion of sample ILM170, a second solid occurred besides halite. It dissolved at 108 °C prior to halite and liquid-vapour homogenisation. Total homogenisation to the liquid phase occurs over a wide temperature range of 50 to more than 400 °C, with the majority homogenising between 90 and 220 °C. During heating, a large number of inclusions decrepitated.

In sample 169 occur two-phase mixed aqueous-hydrocarbon inclusions of variable mixing proportions (Fig. 18). Microthermometric analyses of these inclusions were difficult. Phase separation within the hydrocarbon phase was visible but homogenisation could not be observed in detail because the shrinking vapour bubbles hid in the thick dark margins of the hydrocarbon-rich liquid phase. The point of homogenisation has to be much higher than the critical temperature of methane at –82.45 °C (Mullis, 1979), since the vapour bubble is still visible up to –40 °C. Last ice-melting temperatures are about –22 °C, and clathrate melting temperatures about +15 °C. Total homogenisation was not achieved before the inclusions started to decrepitate.

Monophase aqueous liquid inclusions (type c) are common in ILM169. Last ice-melting temperatures were variable, with populations around –22 °C, –13 °C and –4 °C, indicating varying fluid compositions (Fig. 17d). In ILM170, monophase inclusions occur in small numbers only and show last ice-melting temperatures between –8.8 and –8.5 °C (Fig. 17b).

The monophase hydrocarbon inclusions (type d) in sample ILM169 generally contain only one phase at room temperature. A second phase nucleates during cooling. Homogenisation into the liquid phase and, rarely, critical homogenisation occurs during heating between –91.2 and –38.4 °C with the majority of measurements falling in the range between –52 and –38 °C (Fig. 17d).
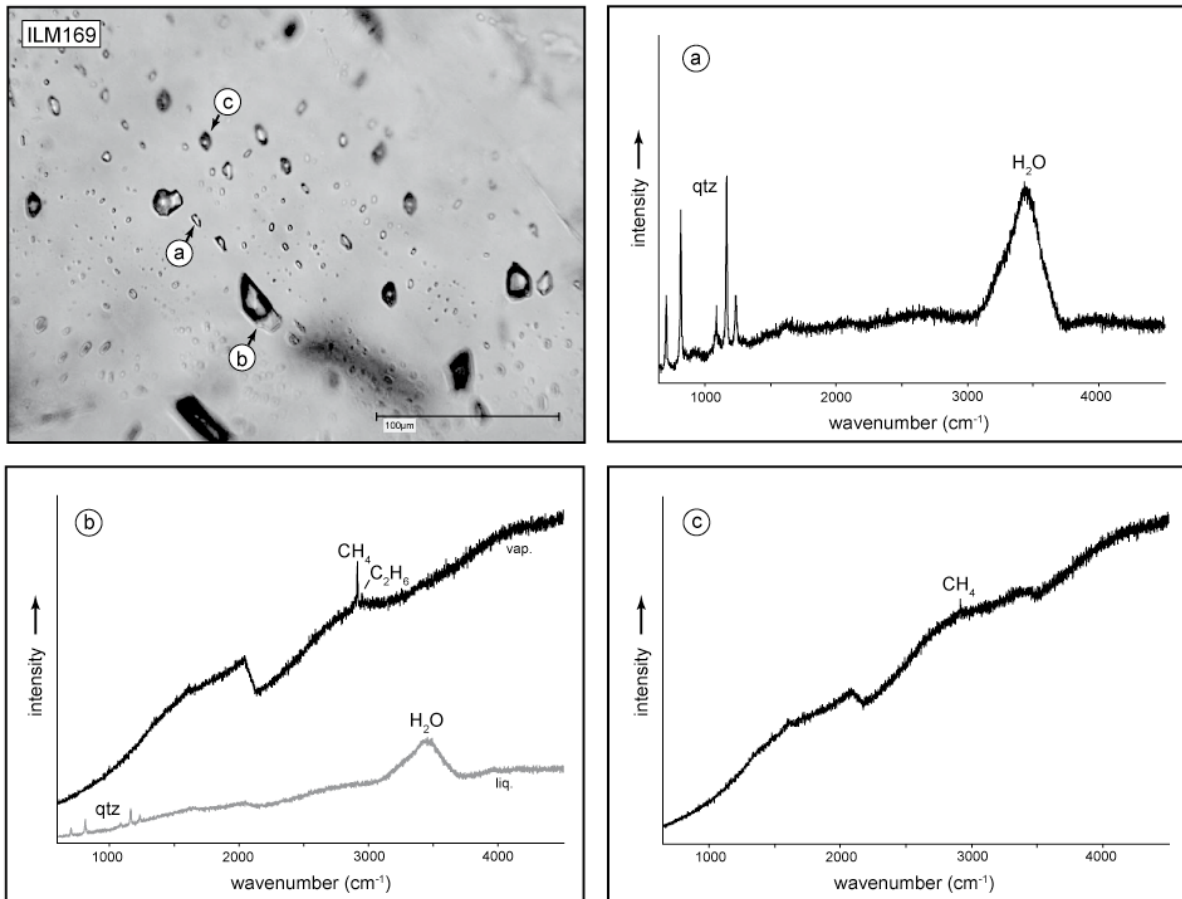
Fig. 18: Representative photograph and related Raman diagrams of mixed aqueous-hydrocarbon inclusions in sample ILM169. a) Pure aqueous inclusions with no detectable hydrocarbons. b) Inclusion with a liquid aqueous phase on the lower right side and a hydrocarbon dominated vapour phase (with a dark rim). c) Pure hydrocarbon inclusion.

Fluid inclusions in quartz veins in the alkali granite

Fluid inclusions of type (a) and (c), without the presence of halite crystals, and in very rare cases, type (b), are present in this sample. Monophase aqueous inclusions of type (c) are very abundant and commonly occur as trails (Fig. 16g), which occasionally cross each other. They typically have negative crystal shapes of compact form but both monophase and two-phase inclusions occur also in irregular shapes (Fig. 16f). Because of missing grain boundaries, an unequivocal classification as primary, secondary or pseudosecondary is not possible. The occurrence of crosscutting trails proves that at least some of the inclusions are of secondary origin. Type (a) inclusions contain at least 90 vol.-% liquid. The analysed inclusions are about 20 μm in diameter. There are a large number of inclusions < 5 μm, which were too small for microthermometric analysis.

Two generations of aqueous-inclusions (type a and b) can be distinguished based on their last ice-melting and homogenisation temperatures. A high salinity population have last ice-melting temperatures ~ -14 °C and a low salinity population have last ice-melting temperatures ~ -3 °C (Fig. 17a). Total homogenisation into the liquid phase takes place between 35 and 142 °C in the high salinity population and between 126 and 228 °C in the low salinity population (Table 8). However, missing textural relationships makes it difficult to determine their relative timing. Neither of the two fluid generations forms observable hydrohalite during the heating-freezing cycle, but the high salinity generation usually forms a poorly visible clathrate. If clearly visible, final clathrate melting occurs at about –11 °C. During heating a couple of inclusions of the latter generation decrepitated or leaked. One high salinity fluid inclusion contained two daughter crystals, halite, which melted at 400 °C after liquid-vapour homogenisation at 130 °C, and an unknown solid that did not melt before decrepitation at 430 °C (Table 8).

Monophase aqueous inclusions (type c) are abundant. Two different last ice-melting points were distinguished (about –14 °C and close to 0 °C, Fig. 17a), indicating two fluid generations, similar to the type (a) and (b) two-phase aqueous inclusions.

Fluid inclusions in ussingite veins

Monophase liquid hydrocarbon-bearing fluids of type (d) are the only type of fluid inclusions found in ussingite. The inclusions are commonly up to 20 μm in size, oval shaped and arranged in clusters or along trails (Fig. 16h).

The inclusions in ussingite homogenise in the range of –94.1 to –14.2 °C. Most of the inclusions in GM1246 homogenise ~ -92 °C (Fig. 17e), whereas, the majority of inclusions in GM1382 homogenise ~ -65 °C (Fig. 17g). Sample GM1384 shows a uniform distribution of homogenisation temperatures between –70 and –90 °C (Fig. 17f).

Fluid inclusions in fluorite

Only one type of fluid inclusion was observed in fluorite. The inclusions are aqueous and contain two or three phases, similar to type (a) inclusions in quartz. Commonly, the inclusions occur as trails or in clusters along healed fracture zones. The inclusions are up to 50 μm in size and negative crystal shapes are common. These are interpreted as being predominantly of secondary, and less commonly of primary origin.

It was only possible to determine the last ice-melting temperature and the melting point of hydrohalite in these aqueous inclusions (Table 8, Fig. 17h-j). Most of the ice in the inclusions

melt between –25.6 and –17.8 °C but can melt as high as –12.3 °C (ILM325). Hydrohalite melting takes place between –15.9 and +18.3 °C (Table 8).

4.4.2   Laser-Raman microprobe analysis results

Result from inclusions in quartz veins in augite syenite

The occurrence of clathrate in several of the aqueous inclusions (type a and b) in the quartz samples already indicates the presence of a volatile phase in addition to water (Table 8). The typical ν_1 peak of methane (2917 cm^{-1} at atmospheric conditions) is detectable by laser-Raman in most of the analysed bubbles, independent of the occurrence of clathrate (e.g. Fig. 16a, d). The ν_3 peak (3019 cm^{-1}) is also visible in some inclusions (Fig. 16d). Occasionally, the methane ν_1 peak is detectable in the liquid phase as well. Two peaks for water (3219 and 3657 cm^{-1}) appear close to each other, forming one broad peak. This peak and a peak at 1640 cm^{-1} are detectable in the liquid and commonly in the vapour phase as well. The H_2 peak (4256 cm^{-1}) could be detected in several cases in the vapour phase (e.g. Fig. 16d). Less common is the occurrence of detectable amounts of ethane (2954 cm^{-1}) and propane (2890 cm^{-1}, Fig. 16h). Peaks typical of CO_2 are not seen in any inclusion in this study. In the monophase aqueous inclusions (type c), a weak methane signal is commonly visible in addition to the two water peaks (Fig. 16b).

The monophase hydrocarbon-bearing inclusions (type d) in quartz of sample ILM169 show a small peak for methane (Fig. 16c). Fluorescence of, most likely, complex higher hydrocarbons, produces a broad, high intensity Raman signal in some of these inclusions, even when analysed with short measurement times and filters (e.g. Fig. 16c). The fluorescence may mask signals of other trace components, e.g. higher hydrocarbons.

Result from inclusions in quartz veins in the alkali granite

The vapour bubble in the aqueous inclusions (type a and b) in the quartz veins associated with the alkali granite commonly show a clear signal for methane, with not only the ν_1 peak but quite commonly the ν_3 peak (Fig. 16f). The typical peak of H_2 may occur as well (Fig. 16f). The halite daughter mineral in the inclusion with two solids showed no Raman signal and the unknown solid could not be identified by its peak positions (973, 1027, 1086 cm^{-1}).

The two different monophase fluid generations (type c) identified by different last ice-melting temperatures were also analysed by laser-Raman. The generation with last ice-melting temperatures close to 0 °C reveal peaks for H_2O only. The generation with lower last

ice-melting temperatures, however, commonly shows a weak methane peak in addition to the dominating water peaks (Fig. 16g).

Results from inclusions in ussingite

The inclusions in the ussingite samples may show peaks for ethane, propane, and hydrogen in some cases, too, but they are much lower in intensity than the dominating methane peak (Fig. 16h, i). Even if the three samples have different homogenisation temperatures of the inclusions, they behave quite similar in the laser-Raman study.

4.4.3   Stable isotope results

Oxygen- and carbon-isotope results from quartz and carbonate

The $\delta^{18}O$ values for ILM4, ILM169 and ILM170 vein quartz are close to 10 ‰ (Table 9). The $\delta^{18}O$ of KH2 is 5.8 ‰. ILM190 vein quartz has a $\delta^{18}O$ value of 8.5 ‰. Associated albite and aegirine in samples ILM4 and KH2 have values of 6.9 and 1.4 ‰, 7.9 and 2.7 ‰, respectively. Ussingites from sample GM1246 and GM1382 have $\delta^{18}O$ values of 8.4 ‰ and 11.5 ‰, respectively.

The study of the thin section of sample KH2 revealed minor amounts of calcite. This carbonate has a $\delta^{18}O$ value of –24.0 ‰ relative to VPDB, which is 6.1 ‰ relative to VSMOW according to Coplen *et al.* (1983), and a $\delta^{13}C$ value of –2.6 ‰.

Table 9: Stable isotope data of selected minerals.

Sample no.	Mineral	Origin	$\delta^{18}O$ [‰]	$\delta^{13}C$ [‰]
KH2	quartz	vein in augite syenite	5.8	
KH2	albite	vein in augite syenite	7.9	
KH2	aegirine	vein in augite syenite	2.7	
KH2	calcite	vein in augite syenite	6.1	-2.6
ILM169	quartz	vein in augite syenite	10.2	
ILM170	quartz	vein in augite syenite	10.5	
ILM4	quartz	vein in augite syenite	10.0	
ILM4	albite	vein in augite syenite	6.9	
ILM4	aegirine	vein in augite syenite	1.4	
ILM190	quartz	vein in alkali granite	8.5	
GM1246	ussingite	vein in naujaite autolith	8.4	
GM1382	ussingite	vein in naujaite autolith	11.5	

Carbon- and hydrogen-isotope results for the hydrocarbon-bearing fluids

The $\delta^{13}C$ values of CH_4 in inclusions in vein quartz from the augite syenite are between –43.4 and –34.9 ‰ (ILM4, ILM169, ILM170) and –22.6 ‰ (KH2), in vein quartz in alkali granite –12.3 ‰ (ILM190), and in the two ussingite samples –5.9 and –3.1 ‰ (GM1246, GM1382; Table 10, Fig. 19). The $\delta^{13}C$ values of C_2H_6 in inclusions in vein quartz in augite syenite are between –42.3 and –32.2 ‰ (ILM4, ILM169, ILM170) and –28.2 ‰ (KH2), and in ussingite –14.7 and –10.1 ‰. In alkali granite, C_2H_6 is below the detection limit. $\delta^{13}C$ values for C_3H_8 could be determined in three samples: quartz in augite syenite –41.4 ‰ (ILM169) and –27.3 ‰ (KH2), and in ussingite –17.3 ‰ (GM1246). A $\delta^{13}C$ value for C_4H_{10} was determined in just one quartz sample (ILM169). A value of –42.6 ‰ was obtained for the first sample and –41.7 ‰ for a duplicate sample.

Table 10: $\delta^{13}C$ results in ‰ of gas chromatography studies on hydrocarbons and CO_2.

Sample no.	Mineral	$\delta^{13}C_{CH4}$	2σ	δD_{CH4}		$\delta^{13}C_{C2H6}$	2σ	δD_{C2H6}		$\delta^{13}C_{C3H8}$	2σ	$\delta^{13}C_{C4H10}$	2σ	$\delta^{13}C_{CO2}$	2σ	$\Delta_{CO2-CH4}$
ILM4	quartz	-43.4	0.2	-148	±2	-37.0	1.4	-	-	-	-	-	-	-14.7	0.9	28.8
ILM169	quartz	-36.2	1.2	-172	±0.5	-43.3	0.1	-216	-	-41.4	-	-42.6	-	-5.8	0.3	30.4
ILM169-dupl	quartz	-34.9	1.5	-	-	-42.2	0.7	-	-	-41.4	-	-41.7	-	-4.6	0.3	30.3
ILM170	quartz	-37.3	0.5	-121	-	-32.2	0.2	-	-	-	-	-	-	-21.0	0.3	16.3
ILM190	quartz	-12.3	-	-	-	-	-	-	-	-	-	-	-	-21.6	0.6	-9.3
KH2	quartz	-22.6	0.1	-176	±1	-28.2	0.5	-	-	-27.3	-	-	-	-12.1	0.2	10.5
GM1246	ussingite	-3.1	0.1	-121	±0.5	-10.1	0.5	-133	±0.5	-17.3	-	-	-	-17.3	0.8	-14.1
GM1382	ussingite	-5.9	0.5	-	-	-14.7	1.0	-	-	-	-	-	-	-7.4	0.9	-1.5

Even though there was no CO_2 detectable by laser-Raman spectroscopy, small amounts were detected by gas chromatography-mass spectroscopy, in particular in sample ILM169 that had a similar yield for CO_2 as CH_4. In the inclusions in vein quartz in augite syenite (ILM4, ILM169, ILM170 and KH2), CO_2 has $\delta^{13}C$ values between –21.0 and –4.6 ‰, in alkali granite, –21.6 ‰, and in the ussingites, –17.3 and –7.4 ‰. δD values of methane in inclusions in quartz are –148 ‰ (ILM4), –172 ‰ (ILM169), –121 ‰ (ILM170), –176 ‰ (KH2) and in ussingite –121 ‰ (GM1246). In ILM169 and GM1246, δD values for ethane were –216 and –133 ‰, respectively. Reproducibility of $\delta^{13}C$ results obtained from multiple aliquots of gas released from the same sample are generally better than ±0.7 ‰. The exception is sample ILM169 that shows errors up to ±1.5 ‰ for CH_4 (Table 10). A duplicate run produced the same results. This may indicate that the fluid is heterogeneous in this sample, with slightly different fluid generations released at each crush. Reproducibility of δD results is good (≤±2 ‰). This indicates, that in most cases, the fluids released represent a single, homogeneous fluid.
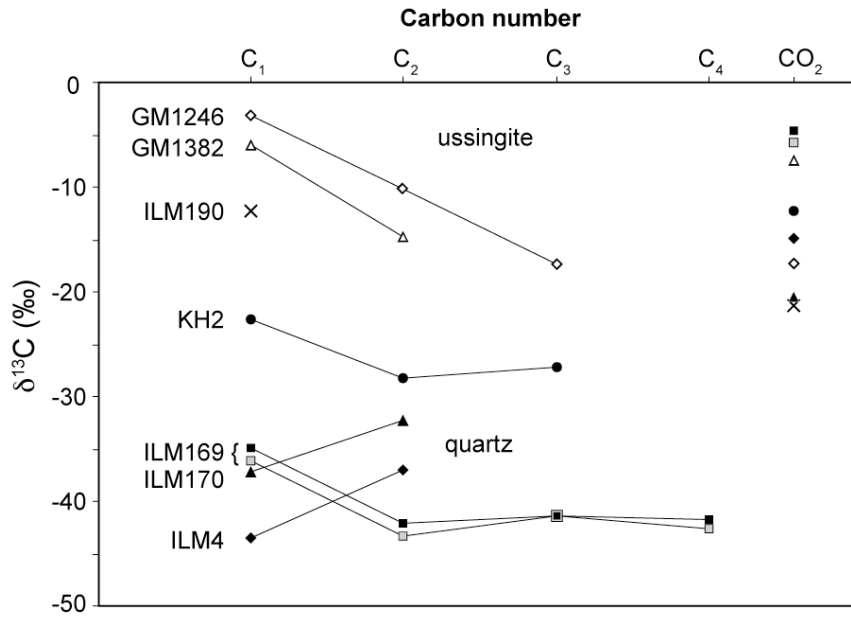
Fig. 19: Variability of $\delta^{13}C$ within the hydrocarbons of each sample.

4.4.4 Results from ion-chromatography and ICP-AES/MS

The concentrations derived from crush-leach analyses have been recalculated based on average salinities calculated from the microthermometric data from the individual samples (Table 8, 11). The dissolved constituents are dominated by NaCl (108 621 to 149 655 ppm chloride, 77 505 to 254 657 ppm sodium).

In fluorite, fluorine and calcium cannot be analysed due to contamination from the host mineral. In quartz, nitrogen, fluorine, bromine, and sulphur occur in minor amounts (571 to 15 847 ppm NO_3, 52 to 20 731 ppm F, up to 1 455 ppm Br, and up to 905 ppm SO_4). Bromine is lacking in inclusions in quartz (ILM190) and in fluorite (ILM325), as sulphur is lacking in inclusions in ILM190, KH2, ILM77, and ILM99. Cl/Br ratios are between 101 and 132 (molar: 228 and 298) and exceed 1000 where the Br concentration is small, Cl/SO_4 varies between 165 and 964 (Table 11).

Besides sodium, the inclusions contain also potassium (3 966 to 21 966 ppm), calcium (3 299 to 34 193 ppm), magnesium (58 to 3 476 ppm), lithium (18 to 401 ppm), barium (up to 2 312 ppm), and strontium (up to 412 ppm). Na/K ratios range from 9 to 35, Na/Ca from 6 to 40 and Na/Br from 63 to 190 and up to 1 716 in ILM77 (molar: 219 to 662 and up to 5 965). Additional data for minor cations from fluorite samples ILM99 and ILM325 are presented in Table 12. Noteworthy are the amounts of iron (212 and 584 ppm), zinc (191 and 240 ppm), and the amount of uranium (188 ppm in ILM99).

Table 11: Composition of the fluid in ppm.

Sample no.	ILM170#1	ILM170#2	ILM99	ILM325	ILM190#1	ILM190#2	ILM77	ILM169#1	ILM169#2	ILM169#3	KH2
Mineral	quartz	quartz	fluorite	fluorite	quartz	quartz	fluorite	quartz	quartz	quartz	quartz
average Salinity	23.8	23.8	23.1	19.3	18.0	18.0	22.4	24.8	24.8	24.8	24.0
(wt.% NaCl$_{equiv.}$)											
F	4522	52	-	-	20731	10509	-	2703	1179	1049	1164
Cl	143621	143621	139397	116466	108621	108621	135172	149655	149655	149655	144828
Br	1375	1423	1283	b.d.l.	b.d.l.	b.d.l.	45	1337	1455	1419	1094
SO$_4$	259	149	b.d.l.	50	b.d.l.	b.d.l.	b.d.l.	366	905	390	b.d.l.
NO$_3$	571	653	2602	830	6729	15847	7838	4987	2557	3933	7328
Na	93649	89590	85595	81630	220641	133256	77505	254657	198078	187525	135211
K	5155	5189	3966	6858	21966	9538	8625	8932	6953	5427	7831
Li	23	82	18	43	126	401	101	57	45	37	119
Mg	1555	58	240	214	1139	1070	3476	211	272	297	260
Ca	3299	4208	-	-	15125	10824	-	34193	32616	8200	3375
Sr	106	133	b.d.l.	b.d.l.	b.d.l.	133	b.d.l.	118	412	335	31
Ba	b.d.l.	35	41	567	b.d.l.	2312	160	1861	1774	667	675
TDS (ppm)	254135	245192	-	-	395077	292510	-	459077	395901	358934	301915
+/- (molar)	1.0	1.0	-	-	2.6	1.7	-	2.9	2.4	2.0	1.5
Cl/Br (wt.)	104	101	109	>> 1000	>> 1000	>> 1000	2993	112	103	105	132
Cl/Br (molar)	235	228	245	>> 1000	>> 1000	>> 1000	6747	252	232	238	298
Cl/SO$_4$ (wt.)	554	964	-	2344	-	-	-	408	165	384	-
Na/Br (wt.)	68	63	67	-	-	-	1716	190	136	132	124
Na/Br (molar)	237	219	232	-	-	-	5965	662	473	459	430
Na/K (wt.)	18	17	22	12	10	14	9	29	28	35	17
Na/Ca (wt.)	28	21	-	-	15	12	-	7	6	23	40

TDS total dissolved solids   b.d.l. below detection limit
+/- charge balance

Table 12: Cation composition of the fluid in fluorite in ppm.

Sample no.	ILM99	ILM325
Mineral	fluorite	fluorite
Salinity	23.1	19.3
(wt.% NaCl$_{equiv.}$)		
Na	85595	81630
K	3966	6858
Li	18	43
Mg	240	214
Sr	b.d.l.	b.d.l.
Ba	41	567
Mn	27	49
Fe	212	584
Cu	3	12
Zn	191	240
Rb	30	68
Sb	b.d.l.	b.d.l.
Cs	27	77
Pb	72	31
Th	b.d.l.	b.d.l.
U	188	b.d.l.

b.d.l. below detection limit

4.5   Discussion

4.5.1   Isotopic constraints on the formation of the quartz veins

The quartz in the two different regions shows distinct differences in their $\delta^{18}O$ values, indicating different origins of the quartz veins in augite syenite and alkali granite. It is also noteworthy that sample KH2 has a much lower isotopic value (5.8 ‰) than the other three samples from veins in augite syenite (~10 ‰). Calculated isotopic mineral equilibria using the fractionation coefficients of Zheng (1993b) between quartz and surrounding albite and aegirine for ILM4 reveal that albite is in isotopic equilibrium with quartz at about 160 °C, and aegirine and quartz at about 60 °C (Fig. 20). This suggests a later, diffusive reequilibration of at least one of the phases. In the case of KH2, the calculated equilibrium temperature of quartz and aegirine is about 430 °C, whereas no equilibrium temperature can be calculated for albite and quartz. This might be caused by low-temperature alteration of albite. The values of aegirine have to be handled with care, since they are among the lowest $\delta^{18}O$ values for aegirine ever measured in Ilímaussaq. However, Marks *et al.* (in review) report similarly low values for late aegirines in the peralkaline Ilímaussaq granite (3.7 ‰) and in an Ilímaussaq aegirine vein in the basement granite (3.1 ‰) indicating late aegirines have much lower $\delta^{18}O$ values than early magmatic ones.
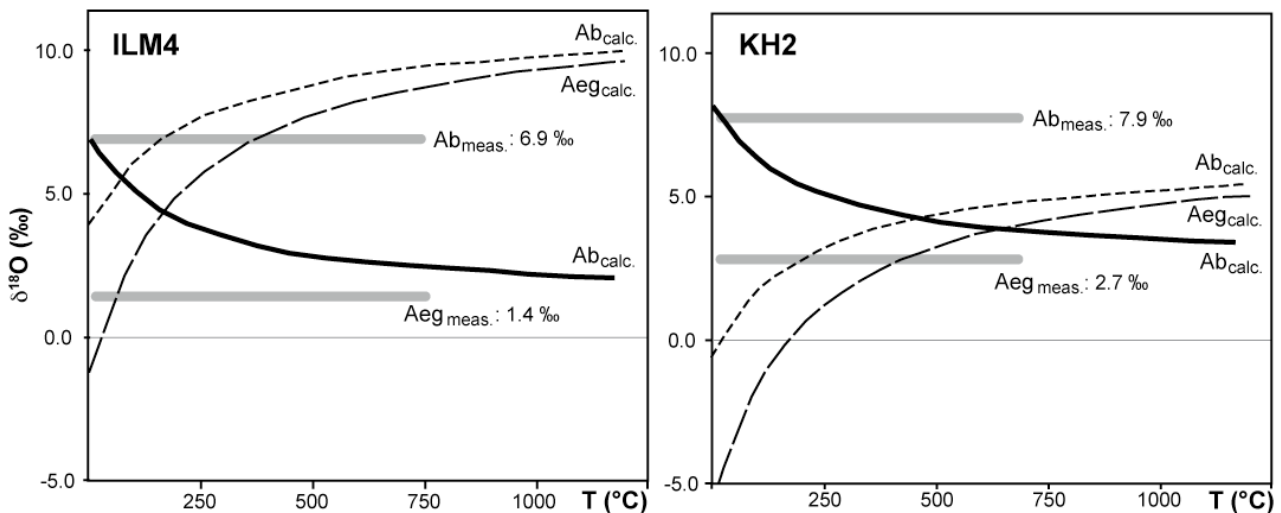
Fig. 20: Isotope mineral-mineral equilibria calculated with fractionation factors of Zheng (1993b). Dashed lines indicate the calculated isotope signature for albite (Ab) and for aegirine (Aeg) in equilibrium with analysed quartz of sample ILM4 and KH2 (10.0 and 5.8 ‰, respectively). The black line indicates the calculated signature for albite in equilibrium with analysed aegirine of sample ILM4 and KH2 (1.4 and 2.7 ‰, respectively). Grey bars indicate the measured $\delta^{18}O$ values of aegirine and albite in the same sample.

The $\delta^{18}O$ signature of a fluid corresponding to the studied quartz in augite syenite (ILM4, ILM169 and ILM170) was calculated using the fractionation coefficients of Matsuhisa *et al.* (1979) for the temperature range of 250 to 500 °C. The range of $\delta^{18}O$ of this hypothetical fluid lies between 1.1 (250 °C) and 8.2 ‰ (500 °C). Using the fractionation coefficients of Zheng (1991) the range is 1.0 (250 °C) to 7.4 ‰ (500 °C). A fluid corresponding to quartz in KH2, at 430 °C, has a $\delta^{18}O$ value of 2.3 ‰ (Matsuhisa *et al.*, 1979) or 1.8 ‰ (Zheng, 1991).

Quartzitic sandstones are found as xenoliths of varying size in the augite syenite unit of Ilímaussaq (Ussing, 1912; Ferguson, 1964; Marks & Markl, 2001). Ussing (1912) described reaction phenomena between the xenoliths and the augite syenite host, which resulted in up to 2 m wide reaction rims of *soda-granite,* i.e. alkali granite consisting of feldspar, quartz, alkali pyroxene and alkali amphibole, around the xenoliths and veining therein. Commonly, however, the alkali granitic rims and veins in and around the xenoliths are just a few centimetres wide and they do not resemble the structures of the studied veins. As the augite syenite itself is saturated to undersaturated with respect to quartz, the occurrence of quartz-bearing veins in this unit is likely to be related to either influx of an external SiO_2-saturated fluid or to mobilisation of quartz from the sandstone xenoliths. Quartz from such xenoliths have $\delta^{18}O$ values of 11.5 ‰ (Halama *et al.*, 2003) and 10.3 to 10.7 ‰ (Konnerup-Madsen, 1980; Konnerup-Madsen & Rose-Hansen, 1984; Marks *et al.*, in review). All of these values are close, or even identical, to the values of the vein quartz of this study, which, however, does not support or disprove direct mobilisation of xenolithic quartz, as the $\delta^{18}O$ value would not survive a mobilisation event – the oxygen from the quartz would mix and equilibrate with the oxygen of the mobilising melt or fluid. However, it is interesting to note that quartz and feldspar in an alkali granitic reaction vein in a sandstone xenolith studied by Konnerup-Madsen (1980), Konnerup-Madsen & Rose-Hansen (1984), and Konnerup-Madsen *et al.* (1985) have isotopic and fluid inclusion characteristics similar to sample ILM169: their quartz has a $\delta^{18}O$ value of 10.5 ‰, their associated feldspar a value of 7.7 ‰, and the fluid inclusions comprise pure carbonic (dominated by methane) and mixed aqueous – carbonic fluids (however, with a salinity of only 4 to 11 wt.% $NaCl_{equiv}$).

Based on the fractionation coefficients of Zheng (1993b), an average vein quartz with a $\delta^{18}O$ of 10.2 ‰ is in equilibrium with pyroxenes of the augite syenite at about 450 °C (mineral data from Marks *et al.*, 2004). Interestingly, this is almost the temperature at which quartz and aegirine in sample KH2 are in isotopic equilibrium and it is the temperature

interval, which was suggested for Be mineral-bearing late-magmatic veins in Ilímaussaq based on phase-petrological constraints (Markl, 2001b). It is therefore reasonable to assume that a late-magmatic Ilímaussaq fluid either reacted with the quartzite xenoliths in the augite syenite unit or with a quartz-saturated fluid from the granitic country rocks and thereby locally produced quartz-bearing veins at temperatures around 400 to 450 °C.

The $\delta^{18}O$ value of quartz from the quartz vein in alkali granite analysed in this study (8.5 ‰) is close to quartz in the alkali granite (9.3 ± 0.2 ‰, Konnerup-Madsen, 1980). It is clearly different from the quartz veins in the augite syenite and the vein is interpreted to be of orthomagmatic origin.

Although the formation of the quartz veins from the two different localities is not related to each other, both types of veins clearly formed as part of the Ilímaussaq complex, they are contemporaneous with the magmatic activity and their fluid inclusions reflect fluid compositions directly related to the peralkaline activity (late-magmatic to hydrothermal).

4.5.2   *Isotopic constraints on the origin of the hydrocarbon-bearing fluids*

The carbon-isotope results of the hydrocarbon-bearing fluids differ depending on the type of sample. The lowest isotopic compositions are measured in fluids in quartz veins from the augite syenite ($\delta^{13}C_{CH4}$ between –43.4 and –34.9 ‰ and $\delta^{13}C_{C2H6}$ between –43.3 and –32.2 ‰; Table 10). Samples ILM4 and ILM170 have higher $\delta^{13}C$ values for C_2H_6 in respect to CH_4 (Table 10; Fig. 19). These values would be in agreement with a thermogenic origin for these hydrocarbons (e.g. Schoell, 1988), but since analyses of further higher hydrocarbons are lacking, this statement is weakly founded. ILM169, however, shows a zigzag trend, in which C_2 to C_4 are depleted with respect to C_1 (Fig. 19). This pattern is typical of abiogenic hydrocarbon generation (Sherwood Lollar *et al*., 2002). This trend is found in sample KH2 as well, but in comparison to the other three quartz veins, the hydrocarbons in KH2 are generally more enriched in ^{13}C (Table 10; Fig. 19).

The $\delta^{13}C$ results for hydrocarbons in inclusions in quartz in augite syenite are much lower than any of the Ilímaussaq gases studied before by Konnerup-Madsen *et al*. (1988). Even the fluid captured in the quartz vein in alkali granite of the present study has a $\delta^{13}C_{CH4}$ value of –12.3 ‰, still lower than other analysed Ilímaussaq fluids. Konnerup-Madsen *et al*. (1988) reported $\delta^{13}C$ values between –7.0 and –1.0 ‰ for CH_4 in lujavrite, kakortokite, naujaite, sodalite foyaite, and augite syenite and $\delta^{13}C$ between –5.9 and –18.2 ‰ for other hydrocarbons. The values of hydrocarbons in quartz veins in the augite syenite of sample

ILM4, ILM169 and ILM170 are even lower than most of the measured values from the agpaitic Khibina complex, Russia (Potter & Konnerup-Madsen, 2003; Beeskow *et al.*, 2006; Potter & Longstaffe, 2007, and references therein). In a $\delta^{13}C$ - δD plot for methane (Fig. 21) the data for inclusions in quartz scatter close to the range of thermogenic methane and are far away from the Ilímaussaq fluid investigated by Konnerup-Madsen (2001) or from the mantle field. The isotopic values of hydrocarbons from fluid inclusions in ussingite, however, are close to the range of other Ilímaussaq gases reported in Konnerup-Madsen *et al.* (1988; Fig. 21), with $\delta^{13}C_{CH4}$ between −5.9 and −3.1 ‰, and $\delta^{13}C_{C2H6}$ between −14.7 and −10.1 ‰, consistent with an abiogenic origin.
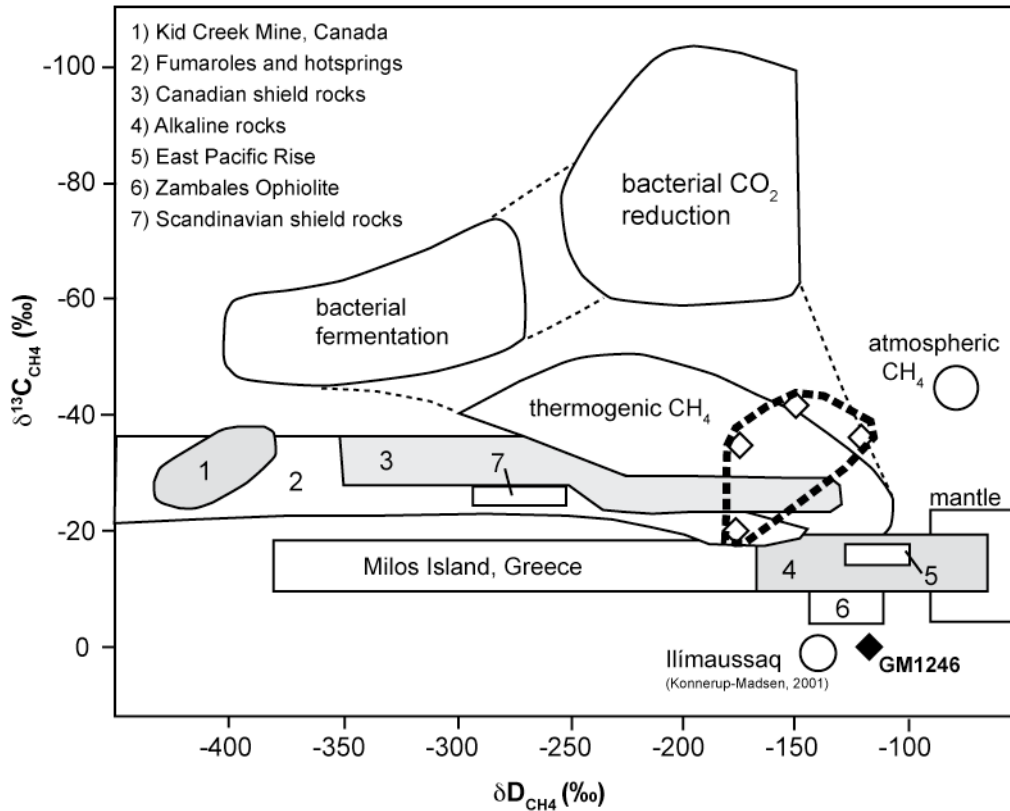
Fig. 21: $\delta^{13}C$ versus δD of the studied samples (rhombs) in comparison to other environments after Potter & Konnerup-Madsen (2003) (data from Wehlan & Craig, 1983; Schoell, 1988; Abrajano *et al.*, 1990; Voytov, 1992; Sherwood-Lollar *et al.*, 1993; 2002; Nivin *et al.*, 1995; Botz *et al.*, 1996; Potter, 2000; Konnerup-Madsen, 2001).

The δD values for CH_4 in all samples range from –121 to –176 ‰. These are typical values of "magmatic" CH_4, although they are lower than mantle values (–80 to –50‰; Kyser & O'Neil, 1984; Fig. 21). The δD values of C_2H_6 are 10-40 ‰ lower than the δD values of the associated CH_4 (Table 10). This kind of D-depletion is uncommon in nature, because higher hydrocarbons are generally more enriched in D than CH_4, whether they formed thermogenically or abiogenically (e.g. Sherwood-Lollar *et al.*, 2002). Nevertheless, large D-depletions of about 70 ‰ have been observed in C_2H_6 in hydrocarbon-bearing fluids from Khibina (Potter & Longstaffe, 2007). Hence, this depletion may be characteristic of hydrocarbon-bearing fluids in peralkaline systems. Potter & Longstaffe (2007) suggested that it formed due to low temperature polymerisation reactions. But a complete understanding of the fractionation in these fluids remains elusive at present.

Mantle-derived abiogenic methane is known to have $\delta^{13}C$ values above –25 ‰, but not all abiogenic hydrocarbons are mantle-derived and methane produced by low-temperature (< 200 °C) water-rock interactions can have values as low as –57 ‰ due to large fractionations at low temperatures and mixing with microbial-generated CH_4 (Sherwood-Lollar *et al.*, 2006). However, the process, which enriched the lighter carbon isotope in the fluid in the quartz veins, is unclear, as the incorporation of microbially-generated CH_4 appears unreasonable in these magmatic rocks.

The reequilibration of CH_4 with a CO_2 fluid during late-magmatic processes as proposed by e.g. Konnerup-Madsen (2001) is another possibility. Gas chromatography-mass spectrometry revealed traces of CO_2 in all samples. $\Delta_{CO2-CH4}$ is positive for most of the quartz samples (~10, 17 and 30 ‰; Table 10) and indicates equilibration temperatures of ~600, 450 and 250 ℃, respectively, using the fractionation factor of Bottinga (1969). This seems, except for 450 ℃, unreasonable with respect to petrological and fluid inclusion evidence. Additionally, the rest of the samples has negative $\Delta_{CO2-CH4}$ values (–15 to –1 ‰), indicating that the CH_4 and CO_2 are not in equilibrium. Interestingly, the negative $\Delta_{CO2-CH4}$ values resemble $\Delta_{CO2-CH4}$ values from hydrocarbon-bearing fluids in Khibina (Beeskow *et al.*, 2006; Potter & Longstaffe, 2007). However, the origin of this CO_2 is problematic.

Traces of CO_2 found in the Khibina fluids are suggested to have generated by abiogenic oxidation during post-magmatic modification of the primary CH_4 fluid (Potter & Longstaffe, 2007). In this study, however, CO_2 could not be determined by microthermometry and also laser-Raman showed no CO_2 peaks. Anyhow, the trace amounts of CO_2 detected by gas chromatography-mass spectrometry may be below the laser-Raman detection limit but the elevated homogenisation temperatures of methane ($Th_{CH4} > -82.45$ ℃) may suggest the

presence of higher hydrocarbons as well as the presence of CO_2. The strong disequilibrium and the large range of $\delta^{13}C_{CO2}$ values (–21.6 to –4.6 ‰), however, may indicate that the CO_2 is not a primary component of the fluid inclusions. During bulk crushing, CO_2 stored along grain boundaries or CO_2 from the crystal structure and, thus, not related to the late-magmatic fluid, may have been released.

Calcite intergrown with quartz, albite, aegirine and amphibole in sample KH2 must also be taken into account, as it unequivocally proves the existence of CO_2 during the formation of this vein (if the calcite texture is not interpreted as a later replacement growth). Using the calcite-CO_2 fractionation factor of Chacko *et al.* (1991), however, there is no isotopic equilibrium between the calcite (–2.6 ‰) and the CO_2 (–12.1 ‰) in KH2. Generally, calcite has been described only from one other place at Ilímaussaq at the north coast of the Kangerluarsuk Fjord (Ussing, 1912; Petersen *et al.*, 1995) in a Ca-rich assemblage containing ilvaite, epidote and hydrogarnet which most likely involves the influx of externally derived, Ca-rich fluids, as shown in the first part of this study. Hence, the magmatic, late-magmatic and hydrothermal fluids at Ilímaussaq are supposed to have been devoid of CO_2 as a consequence of the strongly reduced nature of the melt. The ^{13}C-depleted CH_4 values for the fluids in the quartz samples remain enigmatic. They may represent a migrated, fractionated late-stage magmatic fluid where $\delta^{13}C_{CH4}$ values have shifted away from early magmatic CH_4 carbon-isotope compositions.

4.5.3   *Calculation of trapping conditions for the fluids*

Exact trapping temperatures and pressures can only be determined from microthermometric data, if the characteristics of the liquid-vapour isopleth and the isochore of the fluid system are well known; otherwise, only minimum estimates are possible. Pressure is constrained by the reconstructed Eriksfjord Formation overburden over the intrusion (3-4 km = 1-1.5 kbar, Poulsen, 1964) and Konnerup-Madsen & Rose-Hansen (1984) independently came to a pressure estimate of 1.0 kbar based on their investigation of purely aqueous inclusions.

Deriving trapping temperatures from the measured homogenisation temperatures of the present study at this pressure estimate is rendered difficult. Dubessy *et al.* (2001) and Pironon *et al.* (2003) noted that disregarding even small amounts of methane in liquid inclusions can result in a misinterpretation of the position of the liquid-vapour isopleth and thus create wrong P-T estimates. Since the exact amount and composition of the hydrocarbons in the studied fluid inclusions is unknown, the trapping conditions cannot be easily quantified. Inclusions in

ILM190 homogenise at temperatures as low as 35 °C into the liquid phase, which most likely indicates trapped meteoric water or simply metastable behaviour of the fluid. Nevertheless, most homogenisation temperatures are in the range up to 220 °C, which gives a pressure corrected trapping temperature of about 275 °C in the pure H_2O-NaCl system (calculated for 1 kbar with the program *MacFlinCor*; Brown, 1989). If the fluid inclusions were trapped during the time of formation of the quartz veins, the respective temperature estimate based on oxygen isotope thermometry of 400 to 450 °C applies to them as well. This indicates, that pressure correction in CH_4-bearing systems should be higher than in the pure H_2O-NaCl system. Earlier studies on late-magmatic fluid activity at Ilímaussaq fit nicely into this temperature frame: Markl & Baumgartner (2002) described hydrothermal veins and replacement textures generated by late-magmatic fluids at temperatures of 300 to 500 °C, Markl (2001b) estimated late-magmatic liquids and fluids to have formed Be-enriched veins at 200 to 400 °C, and the first part of this study presents evidence for a hydrothermal overprinting at temperatures of 300 to 500 °C, in the course of which a Ca-rich mineral assemblage with ilvaite formed. Hence, circumstantial evidence indicates that the fluids investigated here represent late-magmatic to hydrothermal fluids.

4.5.4   Composition of the fluids I: major components

The observation that the last phase to melt in the fluid inclusions is either ice, clathrate, hydrohalite or, in rare cases, halite clearly proves extreme salinity variations in the late-magmatic fluids. Gas hydrates (clathrates) exclude salts from their structure (Hand *et al.*, 1974) and, hence, the residual solution is more saline than the pristine one. The presence of hydrocarbons and clathrates can thus strongly affect the interpretation of microthermometric data like density and composition of the fluid (Hollister & Burruss, 1976; Collins, 1979; Seitz & Pasteris, 1990). Moreover, CH_4, CO_2 and other gases may form complete solid solution clathrates with different behaviour (especially $T_{m(Cl)}$) depending on the composition of the clathrate and the concentration of salt (e.g. NaCl) dissolved in the liquid (Unruh & Katz, 1949; Hollister & Burruss, 1976; Collins, 1979; Dubessy *et al.*, 2001).

Since it is impossible to calculate the exact salinity in clathrate-bearing fluids without knowing the relative amounts of fluid components, and since clathrates are common but not always present in the inclusions studied, the occurrence of hydrocarbons has to be neglected if one wants to obtain at least an approximate estimate of the salinity. Hence, the salinity of inclusions without hydrohalite and halite was calculated using the depression of the ice

melting point after Bodnar (1993). The range in which hydrohalite appears, from 23.3 to 26.3 wt.% NaCl, is taken as a salinity estimate for the inclusions which form metastably melting hydrohalite. Otherwise it was calculated after Sterner *et al.* (1988) using the hydrohalite melting point. The salinity of inclusions containing halite daughter crystals was calculated after Sterner *et al.* (1988) using the melting point of halite. Since the eutectic melting (T_e) was very hard to observe, the temperature of the first visible melting (T_{fm}) was taken instead as reference for the composition of the fluid system.

Fluid composition of inclusions in quartz veins in augite syenite

The eutectic melting temperature of the pure H_2O-NaCl system is –21.2 °C (Davis *et al.*, 1990). Most of the studied inclusions in the quartz samples ILM4 and ILM170 have a composition close to it with T_{fm} within the interval of –30 to –22 °C (Table 8). The salinity of most of these inclusions corresponds to 20 to 30 wt.% $NaCl_{equiv.}$. Raman studies provided evidence for a fraction of hydrocarbons (e.g. Fig. 16a, d, e), which is supported by clathrate formation during microthermometric studies. Both samples contain minor amounts of probably late and exsolved fluid inclusions with lower salinities and no detectable hydrocarbons (Table 8). The fluids in quartz ILM169 start melting between –50 and –33 °C and, hence, indicate the presence of minor amounts of other dissolved salts in addition to NaCl. There are also mono- and two-phase inclusions, which are very similar, with salinities from 22 to 26 wt.% $NaCl_{equiv.}$ and 14 to 18 wt.% $NaCl_{equiv}$ (Table 8). Mono- and two-phase inclusions with the same salinity are interpreted to have trapped the same fluid with a potential metastable absence of the vapour bubble in the monophase inclusions as described by Roedder (1984). Moreover, ILM169 contains monophase inclusions with about 8 wt.% $NaCl_{equiv.}$, showing, like all other brines in this sample, the Raman signal of CH_4. Finally, ILM169 contains pure hydrocarbon inclusions and mixed aqueous-hydrocarbon inclusions with a large hydrocarbon-bearing bubble in an aqueous liquid. The pure hydrocarbon inclusions generally homogenise between –53 and –38 °C into the liquid phase (Fig. 17d). Since the critical temperature of pure methane is –82.45 °C (Mullis, 1979), higher homogenisation temperatures indicate the presence of other hydrocarbons. Their presence could also be the reason for the strong fluorescence in these inclusions during Raman studies (Fig. 16c; Wopenka *et al.* 1990; Pironon *et al.*, 1991). As mentioned above, mixed aqueous-hydrocarbon inclusions could not be studied in detail. Nevertheless, the occurrence of pure hydrocarbons, aqueous brines and mixed aqueous-hydrocarbon inclusions of variable mixing proportions in spatial vicinity proves the coexistence of immiscible hydrocarbon-rich and

aqueous liquid phases at the time of entrapment. This interpretation was also suggested by Konnerup-Madsen & Rose-Hansen (1982), who described the occurrence of saline aqueous inclusions and hydrocarbon inclusions close to each other in hydrothermal vein minerals in the Ilímaussaq intrusion.

Lamb *et al.* (1996) studied the phase relations at 1 kbar and from 400 to 600 °C in the CH_4-H_2O-NaCl system. Since all quartz samples of the present study contain dominantly liquid-rich inclusions only, the bulk composition of these inclusions is suggested to lie in the one-phase field on the opposite site of the CH_4 apex (Fig. 22).
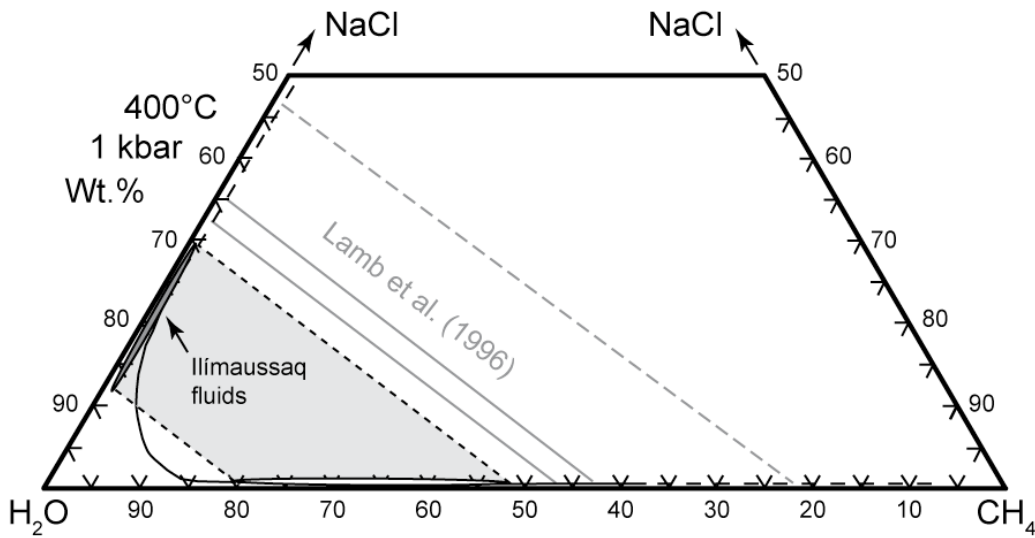
Fig. 22: Results of this study in the diagram after Lamb *et al.* (1996).

Fluid composition of inclusions in quartz veins in alkali granite

The inclusions start melting between –46 and –30 °C, indicating the presence of other dissolved salts in addition to NaCl (Table 8). Salinities peak for both mono- and two-phase inclusions at about 18 wt.% $NaCl_{equiv.}$, additional peaks for two-phase inclusions are at 21 wt.% $NaCl_{equiv.}$ and 6 wt.% $NaCl_{equiv.}$, and for monophase inclusions at about 1 wt.% $NaCl_{equiv.}$ (Table 8). Except for the latter, Raman studies show peaks for methane in all different fluid types (Fig. 16d, f). In rare cases, clathrates are visible. Thus, fluid inclusion studies reveal three different hydrocarbon-bearing brines and a weakly saline monophase aqueous fluid. The latter is interpreted to be a late fluid generation, which may have no relation to the formation of the quartz vein or to the magmatic activity at all, and which may represent infiltrating meteoric water. Inclusions in magmatic quartz from the alkali granite

itself, studied by Konnerup-Madsen (1980) and Konnerup-Madsen & Rose-Hansen (1984), vary in salinity from 7 to more than 64 wt.% $NaCl_{equiv.}$ for primary inclusions and from 1 to 35 wt.% $NaCl_{equiv.}$ for the more common secondary inclusions. They are of aqueous composition only (with possible daughter and/or captured crystals) and free of carbonic components. Based on stable isotope analyses, Konnerup-Madsen (1980) concluded that at least some inclusions may reflect stages of circulation of meteoric fluids and that a part of the dissolved salts may be of non-magmatic origin. The fact that no hydrocarbons were found in the quartz vein in the alkali granite indicates, that the vein most likely trapped a mixture of syenitic, hydrocarbon-bearing and alkali granitic fluids of variable salinity.

Fluid composition of inclusions in ussingite veins

The inclusions in each of the three ussingite samples have different homogenisation temperatures, indicating different compositions of the captured fluid. The majority of homogenisation temperatures of GM1246 are below the critical temperature of methane, which indicates a methane-dominated fluid with additional hydrogen (e.g. Potter & Konnerup-Madsen, 2003), which is confirmed by laser-Raman analyses (Fig. 16h). In comparison, GM1382 and GM1384 have, as do the hydrocarbon-bearing inclusions in quartz ILM169, homogenisation temperatures largely above the critical temperature, indicating the presence of higher hydrocarbons, again supported by laser-Raman spectroscopy (Fig. 16i). Interestingly, any aqueous fluid component is completely missing.

4.5.5   Composition of the fluid II: minor components in the aqueous fluids

Cations

Sodium and chlorine are by far the dominant ions in the investigated fluid (Table 11). The large variability in the absolute amounts is a consequence of the difficulty to precisely estimate the inclusions salinity and that different types of fluids in a single sample were analysed by the bulk method applied here. Although these facts render the results less quantitative than desirable, the numbers presented here nevertheless give an impression of the late-magmatic fluid composition in a Na-dominated peralkaline system. As such data are very scarce, it is worth considering them despite the problems inherent to the method. It is important to note, that - as discussed in detail above - even different fluids trapped in a single sample are interpreted to be related to the same late-magmatic processes. The only exception are aqueous inclusions with very lowest salinity, which, however, are scarce. It is assumed

that their low salinity does not strongly affect the analysed element ratio from the high-salinity inclusions.

Microthermometry has already indicated that there must be dissolved solids other than NaCl present. This is confirmed by crush-leach analyses, which show the additional presence of calcium (3 299 to 34 193 ppm), potassium (3 966 to 21 966 ppm), and minor amounts of magnesium (58 to 3476 ppm) and lithium (18 to 401 ppm) as well as significant amounts of barium (up to 2 312 ppm), and strontium (up to 412 ppm). Additional analyses of cations, e.g. iron (212 and 584 ppm), manganese (27 and 49 ppm), zinc (191 and 240 ppm), and uranium (188 ppm) in two fluorite samples quantify the typical contents of such minor cations (Table 12).

Anions

The dominating anion in the fluids is chlorine (108 621 to 149 655 ppm; Table 11). Other analysed ions are fluorine (52 to 20 731 ppm), bromine (up to 1 455 ppm), nitrogen (571 to 15 847 ppm NO_3), and sulphur (up to 905 ppm SO_4).

Quartz sample ILM170 and fluorite sample ILM99 are the "best guess" of a typical late-stage, agpaitic, Ilímaussaq fluid, as the charge balance of these samples fits best. With decreasing Cl/Ca ratio, the charge balance gets worse, suggesting a relation between the charge balance and the amounts of NaCl and $CaCl_2$ dissolved in the fluid. The fact, that the two analyses from different aliquots of ILM170 show different concentrations of fluorine and magnesium probably has to be attributed to variable proportions of different trapped fluids.

Chlorine and bromine in fluids are of special interest since bromine is supposed to behave largely conservatively in most geochemical systems (Oosting & Von Damm, 1996) and therefore, the Cl/Br ratio has commonly been used as a geochemical tracer to provide information on the various source possibilities of a fluid's salinity (Kesler *et al.*, 1996; Nesbitt & Prochaska, 1998; Stober & Bucher, 1999; Liebscher *et al.*, 2006). The Cl/Br signature for present-day seawater is 288 (in weight ppm, molar: 649; Stober & Bucher, 1999; Millero, 2004).

Cl/Br ratios in the Ilímaussaq samples are surprisingly constant (typically between 101 and 112, and 132 in KH2, molar: 228 to 252 and 298 in KH2) in spite of the problems with the various fluid generations. This points to a common source and the inert geochemical behaviour of the Cl/Br ratio in this magmatic system. The high values of >1000 in quartz sample ILM190 and fluorite samples ILM77 and ILM325 are due to their extremely small

concentrations of bromine, which are close to, or even below the detection limit. These values could reflect mixing with a high-Cl fluid, but they have to be treated with great care.

The Cl/Br data of this study are plotted with Cl/Br data from various geofluids in Fig. 23. Based on Cl/Br data close to 300 (molar: 676), the high salinity in many brines from fractured crystalline rocks is explained by the concentration of seawater during water-rock interactions (Stober & Bucher, 1999; Bottomley *et al*., 1999; 2002; 2003; 2005). Typical hydrothermal MOR fluids have Cl/Br values between 232 and 467 (molar: 523 and 1053; German & Von Damm, 2003) and basinal brines may range from about 14 to 1130 (molar: 32 to 2565; Kesler *et al*., 1995; 1996). Data for Cl, Br and Na in primary magmatic fluids are very scarce. The only known study that presents such data is the one of Campbell *et al*. (1995) who explained high Cl/Br ratios (823-3554, molar: 1855-8010; Fig. 23) in the magmatic fluids in the Capitan pluton, New Mexico, by assimilation of evaporites during intrusion. This fluid is more enriched in Na and Cl than the investigated Ilímaussaq fluid.

Data on two other peralkaline Gardar complexes from South Greenland (Ivigtut and Motzfeldt from Köhler *et al*., in review and Schönenberger *et al*., in prep, respectively) show very similar values around 100 (molar: 225, Fig. 23), which indicates an underlying feature of the peralkaline Gardar magmas and may reflect the Cl/Br ratio of the lithospheric mantle beneath Gardar. Interestingly, this value of about 100 does not appear to be influenced by magmatic processes in spite of the fact that Cl- and Br-bearing minerals like sodalite and amphibole crystallise from the Ilímaussaq magma. While preliminary analyses of an Ilímaussaq amphibole in naujaite (Schönenberger, pers. com.) gives a Cl/Br ratio of about 120 and hence indicates that amphibole crystallisation does not fractionate the two elements. Sodalite has values from 500 to 1700 (Krumrei *et al*., 2007) and should accordingly lead to Br enrichment during fractionation. There is no such trend in the present fluid study or in the whole-rock values provided by Bailey *et al*. (2001) who reported Cl/Br ratios for representative coarse augite syenite (300), for fine augite syenite (>420), for alkali granite (>240) and for naujaite (197). The difference between sodalite, whole-rock, amphibole and fluid Cl/Br ratios is still unexplained and will be the topic of a larger study in the future.
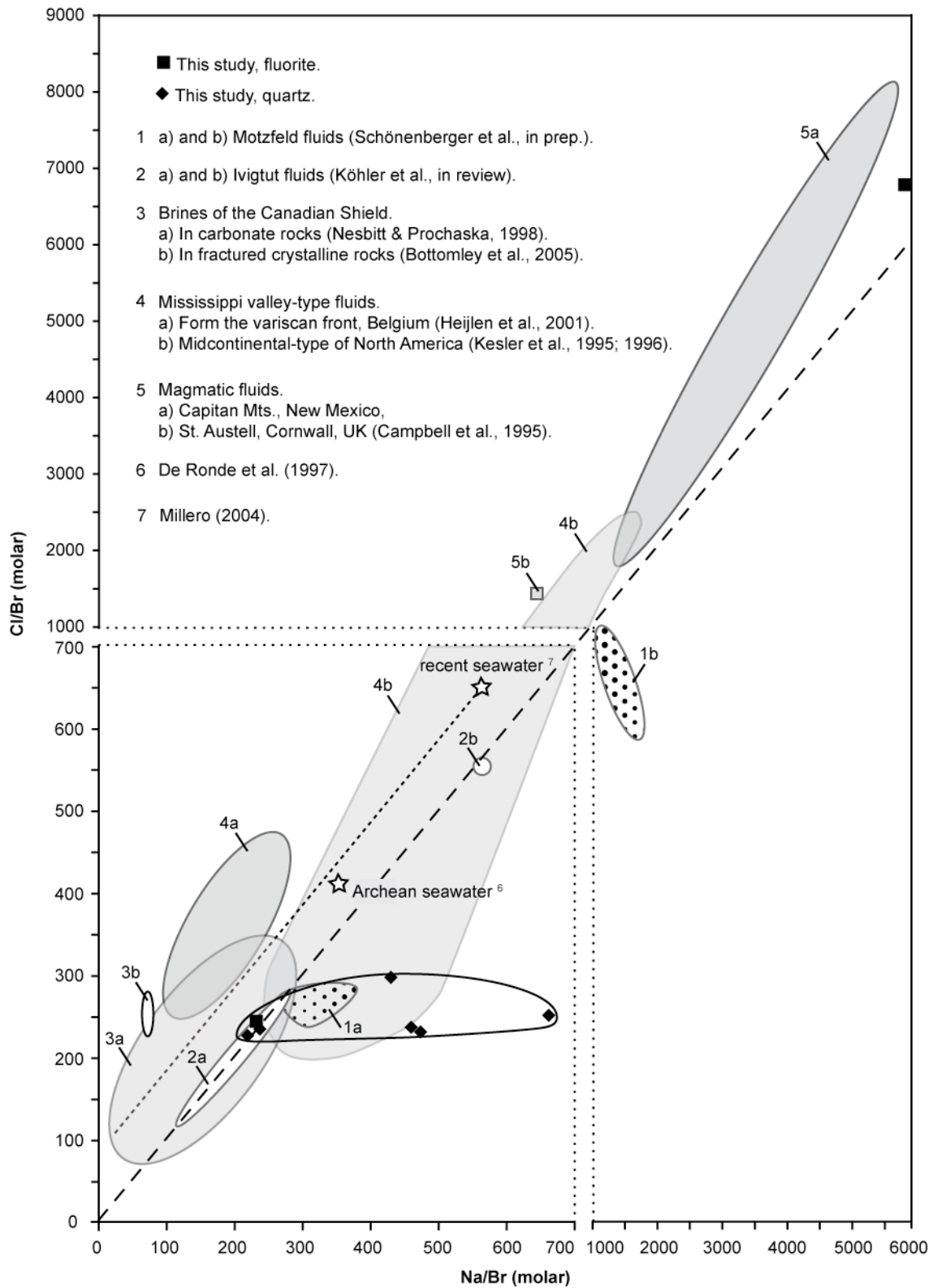
Fig. 23: Na/Br versus Cl/Br ratios of this study in comparison to the ratios of other settings.

4.6   Summary and conclusions

Microthermometric and laser-Raman investigations in fluid inclusions in late-magmatic to hydrothermal vein minerals in the Ilímaussaq intrusion reveal aqueous brine solutions that contain small amounts of hydrocarbons and monophase hydrocarbon-bearing inclusions dominated by CH_4. Gas chromatography-mass spectrometry reveals in some samples minor amounts of CO_2, which, however, is most likely not related to the late-magmatic fluids. The brines are dominated by dissolved NaCl and minor amounts of $CaCl_2$ and KCl.

Most of the inclusions are interpreted to be of secondary origin, but their chemical characteristics (occurrence of hydrocarbons, high salinity, similar Cl/Br ratios, similar trapping conditions) indicate that they reflect the typical late-magmatic to hydrothermal fluids in this persodic system. The common occurrence of hydrocarbons appears to be typical of agpaitic rocks in general (Beeskow *et al.*, 2006; Ryabchikov & Kogarko, 2006; Salvi & Williams-Jones, 2006) and of the very reduced Ilímaussaq intrusion, in specific (Marks & Markl, 2001b; Markl *et al.*, 2001; Krumrei *et al.*, 2007). Based on carbon- and hydrogen-isotope analyses the hydrocarbons in ussingite are of typical abiogenic origin, while those in quartz have slightly different carbon-isotope characteristics, but can also be explained by an abiogenic origin.

Crush-leach analyses indicate that the typical late-stage fluids have Na/K ratios from 10 to 34, Na/Ca from 6 to 40, Ba/Sr of 0.3 to 22 and Li, Mg, K, Ca, Ba and Sr contents of 18 to 401, 58 to 3 479, 3 966 to 21 966, 3 299 to 34 193, up to 2 312 and up to 412 ppm, respectively. Fluorine appears to be largely variable which nicely fits with the observations of Schönenberger *et al.* (2006) who showed that F is easily mobilised and reprecipitated during late-magmatic metasomatic reactions. Cl/Br ratios are surprisingly constant between 100 and 130, which nicely corresponds to results from other peralkaline complexes in the Gardar Province of South Greenland (Köhler *et al.*, in review; Schönenberger *et al.*, in prep). Apparently, this Cl/Br ratio is governed by a common source and is not modified by magmatic to hydrothermal processes other than mixing with external fluids. Probably, it reflects the Cl/Br ratio of the Gardar lithospheric mantle.

REFERENCES

Abrajano, T.A., Sturchio, N.C., Kennedy, B.M., Lyon, G.L., Muehlenbachs, K., Bohlke, J.K. (1990). Geochemistry of reduced gas related to serpentinization of the Zambales ophiolite, Philippines. *Applied Geochemistry* **5**, 625-630.

Andersen, S., Bohsen, H., Steenfelt, A. (1988). Geological map of Greenland 1:20 000 the southern part of the Ilímaussaq complex, South Greenland. *Grønlands Geologiske Undersøgelse* / Geodætisk Institut, Denmark.

Andersen, T., Sørensen, H. (2005). Stability of naujakasite in hyperagpaitic melts, and the petrology of naujakasite lujavrite in the Ilímaussaq alkaline complex, South Greenland. *Mineralogical Magazine* **69**, 125-136.

Armour-Brown, A., Steenfelt, A., Kunzendorf, H. (1983). Uranium districts defined by reconnaissance geochemistry in south Greenland. *Journal of Geochemical Exploration* **19**, 127-145.

Armstrong, J.T. (1991). Quantitative element analysis of individual microparticles with electron beam instruments. In: Heinrich, K.F.J., Newbury, D.E. (Eds.), Electron Probe Quantitation. Plenum Press, New York and London, 261-315.

Bailey, J.C., Gwozdz, R., Rose-Hansen, J., Sørensen, H. (2001). Geochemical overview of the Ilímaussaq alkaline complex, South Greenland. In: Sørensen, H. (Ed.), The Ilímaussaq alkaline complex. South Greenland: status of mineralogical research with new results. *Geology of Greenland Survey Bulletin* **190**, 35-53.

Bailey, J.C., Sørensen, H., Andersen, T., Kograko, L.N., Rose-Hansen, J. (2006). On the origin of microrhythmic layering in arfvedsonite lujavrite from the Ilímaussaq alkaline complex, South Greenland. *Lithos* **91**, 301-318.

Banks, D.A., Yardley, B.W.D. (1992). Crush-leach analysis of fluid inclusions in small natural and synthetic samples. *Geochimica et Cosmochimica Acta* **56**, 245-248.

Bartholomé, P., Dimanche, F. (1967). On the paragenesis of ilvaite in Italian skarns. *Annales de la Societe Geologique de Belgique* **90**, 533-558.

Beeskow, B., Treloar, P.J., Rankin, A.H., Vennemann, T.W., Spangenberg, J., (2006). A reassessment of models for hydrocarbon generation in the Khibiny nepheline syenite complex, Kola Peninsular, Russia. *Lithos* **91**, 1-18.

Bird, D.K., Helgeson, A.C. (1980). Chemical interaction of aqueous solutions with epidote-feldspar mineral assemblages in geologic systems. 1. Thermodynamic analysis of phase relations in the system CaO-FeO-Fe_2O_3-Al_2O_3-SiO_2-H_2O-CO_2. *American Journal of Science* **280**, 907-941.

Bodnar, R.J. (1993). Revised equation and table for determining the freezing point depression of the H_2O-NaCl solutions. *Geochimica et Cosmochimica Acta* **57**, 683-684.

Bøggild, O.B. (1902). On ilvaite from Siorarsuit at Julianehaab, Greenland. *Meddelelser om Grønland* **25**, 43-90.

Bohse, H., Andersen, S. (1981). Review of the stratigraphic divisions of the kakortokite and lujavrite in southern Ilímaussaq. *Rapport Grønlands Geologiske Undersøgelse* **103**, 53-62.

Bohse, H., Brooks, C.K., Kunzendorf, H. (1971). Field observations on the kakortokites of the Ilímaussaq intrusion, south Greenland, including mapping and analyses by portable x-ray fluorescence equipment for zirconium and niobium. *Grønlands Geologiske Undersøgelse Rapport* **38**, 42pp.

Boily, M., Williams-Jones, A.E. (1994). The role of magmatic and hydrothermal processes in the chemical evolution of the Strange Lake plutonic complex, Québec-Labrador. *Contributions to Mineralogy and Petrology* **118**, 33-47.

Bottinga, Y. (1969). Calculated fractionation factors for carbons and hydrogen isotope exchange in the system calcite - carbon dioxide - graphite - methane - hydrogen - water vapor. *Geochimica et Cosmochimica Acta* **33**, 49-64.

Bottomley, D.J., Katz, A., Chan, L.H., Starinsky, A., Douglas, M., Clark, I.D., Raven, K.G. (1999). The origin and evolution of Canadian Shield brines. Evaporation or freezing of seawater? New lithium isotope and geochemical evidence from the Save craton. *Chemical Geology* **155**, 295-320.

Bottomley, D.J., Renaud, R., Kotzer, T., Clark, I.D. (2002). Iodine-129 constraints on residence times of deep marine brines in the Canadian Shield. *Geology* **30**, 587-590.

Bottomley, D.J., Chan, L.H., Katz, A., Starinsky, A., Clark, I.D. (2003). Lithium isotope geochemistry and origin of Canadian Shield brines. *Ground Water* **41**, 847-856.

Bottomley, D.J., Clark, I.D., Battye, N., Kotzer, T. (2005). Geochemical and isotopic evidence for a genetic link between Canadian Shield brines, dolomitization in the Western Canada Sedimentary Basin, and Devonian calcium-chloridic seawater. *Canadian Journal of Earth Sciences* **42**, 2059-2071.

Bottrell, S.H., Yardley, B., Buckley, F. (1988). A modified crush-leach method for the analysis of fluid inclusion electrolytes. *Bulletin de Minéralogie* **111**, 279-290.

Botz, R., Stüben, D., Winckler, G., Bayer, R., Schmitt, M., Faber, E. (1996). Hydrothermal gases offshore Milos Island, Greece. *Chemical Geology* **130**, 49-64.

Brown, P.E. (1989). FLINCOR; a microcomputer program for the reduction and investigation of fluid inclusion data. *American Mineralogist* **74**, 1390-1393.

Campbell, A.R., Banks, D.A., Philipps, R.S., Yardley, B.W.D. (1995). Geochemistry of Th-U-REE mineralizing magmatic fluids, Capitan Mountains, New Mexico. *Economic Geology* **90**, 1271-1287.

Chacko, T., Mayeda, T.K., Clayon, R.N., Goldsmith, J.R. (1991). Oxygen isotope fractionations between CO_2 and calcite. *Geochimica et Cosmochimica Acta* **55**, 2867-2882.

Chacko, T., Riciputi, R., Cole, R., Horita, J. (1999). A new technique for determining equilibrium hydrogen isotope fractionation factors usig the ion microprobe: Application to the epidote-water system. *Geochimica et Cosmochimica Acta* **63**, 1-10.

Clayton, R.N., Mayeda, T.K. (1963). The use of bromine pentafluoride in the extraction of oxygen from oxides and silicates for isotope analysis. *Geochimica et Cosmochimica Acta* **27**, 43-52.

Collins, P.L.F. (1979). Gas hydrates in CO_2-bearing fluid inclusions and the use of freezing data for estimation of salinity. *Economic Geology* **74**, 1435-1444.

Coplen, T.B., Kendall, C., Hoppe, J. (1983). Comparison of stable isotope reference samples. *Nature* **302**, 236-238.

Coulson, I.M. (1997). Post-magmatic alteration in eudialyte form the North Qôroq centre, South Greenland. *Mineralogical Magazine* **61**, 99-109.

Coulson, I.M. (2003). Evolution of the North Qôroq centre nepheline syenites, south Greenland: alkali-mafic silicates and the role of metasomatism. *Mineralogical Magazine* **67**, 873-892.

Davis, W.D., Lowenstein, T.K., Spencer, R.J. (1990). Melting behaviour of fluid inclusions in laboratory-grown halite crystals in the systems $NaCl-H_2O$, $NaCl-KCl-H_2O$, $NaCl-MgCl_2-H_2O$ and $NaCl-CaCl_2-H_2O$. *Geochimica et Cosmochimica Acta* **54**, 591-601.

De Ronde, C.E.J., Channer, D.M.DeR., Faure, K., Bray, C.L., Spooner, E.T.C. (1997). Fluid chemistry of Archean seafloor hydrothermal vents; implications for the composition of circa 3.2 Ga seawater. *Geochimica et Cosmochimica Acta* **61**, 4025-4042.

Dubessy, J., Buschaert, S., Lamb, W., Pironon, J., Thiéry, R. (2001). Methane-bearing aqueous fluid inclusions: Raman analysis, thermodynamic modeling and application to petroleum basins. *Chemical Geology* **173**, 193-205.

Edgar A.D., Parker, L.M. (1974). Comparison of melting relationship of some plutonic and volcanic peralkaline undersaturated rocks. *Lithos* **7**, 263-273.

Einaudi, M.T., Burt, D.M. (1982). Introduction – terminology, classification, and composition of skarn deposits. *Economic Geology* **77**, 745-754.

Einaudi, M.T., Meinert, L.D., Newberry, R.J. (1981). Skarn deposits. *Economic Geology*, 75th Anniversary Volume, 317-391.

Emeleus, C.H., Upton, B.G.J. (1976). The Gardar period in southern Greenland. In: Escher, A., Watt, W.S. (Eds.), Geology of Greenland. Geological Survey of Greenland, Copenhagen, 153-181.

Engell, J., Hansen, J., Jensen, M., Kunzendorf, H., Løvborg, L. (1971). Beryllium mineralization in the Ilímaussaq intrusion, South Greenland, with description of a field beryllometer and chemical methods. *Grønlands Geologiske Undersøgelse Rapport* **33**, 40pp.

Esche, A., Watt, W.S. (1976). Geology of Greenland. Geological Survey of Greenland, Copenhagen, 603 pp.

Ferguson, J. (1964). Geology of the Ilímaussaq alkaline intrusion, South Greenland. *Bulletin Grønlands Geologiske Undersøgelse* **39**, 82pp.

Finch, A. (1995). Metasomatic overprinting by juvenile igneous fluids, Igdlerfigsalik, South Greenland. *Contributions to Mineralogy and Petrology* **122**, 11-24.

Friedman, I., O'Neil, J.R. (1977). Compilation of stable isotope fractionation factors of geochemical interest. In: Fleischer, M. (Ed.), Data of geochemistry. *U.S. Geological Survey Professional Paper* **440-KK**, 12 pp.

Garde, A.A., Hamilton, M.A., Chadwick, B., Grocott, J., McCaffrey, K.J.W. (2002). The Ketilidian orogen of South Greenland: geochronology, tectonics, magmatism, and fore-arc accretion during Palaeoproterozoic oblique convergence. *Canadian Journal of Earth Sciences* **39**, 765-793.

Giletti, B.J., Semet, M.P., Yund, R.A. (1978). Studies in diffusion – III. Oxygen in feldspars: an ion microprobe determination. *Geochimica et Cosmochimica Acta* **42**, 45-57.

Gieré, R. & Sorensen, S.S. (2004). Allanite and other REE-rich epidote-group minerals. In: Liebscher, A., Franz, G. (Eds.), Epidotes. *Reviews in Mineralogy & Geochemistry* **56**, 431-493.

German, C.R., Von Damm, K.L. (2003). Hydrothermal processes. In: Elderfield, H., Holland, H.D., Turekian, K.K. (Eds.), Treatise on Geochemistry, Volume 6, The Oceans and Marine Geochemistry. Elsevier Ltd, 145-180.

Gustafson, W.I. (1974). The stability of andradite, hedenbergite, and related minerals in the system Ca-Fe-Si-O-H. *Journal of Petrology* **15**, 455-496.

Halama, R., Wenzel, T., Upton, B.J.G., Siebel, W., Markl, G. (2003). A geochemical and Sr-Nd-O isotopic study of the Proterozoic Eriksfjord Basalts, Gardar Province, South Greenland: Reconstruction of an OIB signature in crustally contaminated rift-related basalts. *Mineralogical Magazine* **67**, 831-854.

Hand, J.H., Katz, D.L., Verma, V.K. (1974). Review of gas hydrates with implication for ocean sediments. In: Kaplan, I.R. (Ed.), Natural gases in marine sediments. Plenum Press, New York, 179-194.

Hansen, J. (1968). A Study of Radioactive Veins containing rare-earth minerals in the area surrounding the Ilímaussaq alkaline intrusion in South Greenland. *Meddelelser om Grønland* **181**, 47 pp.

Heijlen, W., Muchez, P., Banks, D.A. (2001). Origin and evolution of high-salinity, Zn-Pb mineralising fluids in the Variscides of Belgium. *Mineralium Deposita* **36**, 165-176.

Holland, T.J.B. (1990). Activities of components in omphacitic solid solutions; an application of Landay theory of mixtures. *Contributions to Mineralogy and Petrology* **105**, 446-453.

Holland, T.J.B., Powell, R. (1998). An internally consistent thermodynamic data set for phases of petrological interest. *Journal of Metamorphic Geology* **16**, 309-343.

Holland, T.J.B., Powell, R. (2000). AX – Mineral activity calculations for thermobarometry. Computer program for Apple MacIntosh and PC.

Hollister, L.S., Burruss, R.C. (1976). Phase equilibria in fluid inclusions from the Khtada Lake metamorphic complex. *Geochimica et Cosmochimica Acta* **40**, 163-175.

Johnsen, O., Gault, R.A. (1997). Chemical variation in eudialyte. *Neues Jahrbuch für Mineralogie Abhandlungen* **171**, 215-237.

Johnson, J.W., Oelkers, E.H., Helgeson, H.C. (1992). SUPCRT92: A software package for calculating the standard molal thermodynamic properties of minerals, gases, aqueous species, and reactions from 1 to 5000 bars and 0 to 1000 °C. *Computing Geosciences* **18**, 899-947.

Karup-Møller, S. (1978). The ore minerals of the Ilímaussaq intrusion: their mode of occurrence and their conditions of formation. *Bulletin Grønlands Geologiske Undersøgelse* **127**, 51 pp.

Kesler, S.E., Appold, M.S., Walter, L.M., Martini, A., Huston, T.S., Kyle, J.R. (1995). Na-Cl-Br systematics in Mississippi Valley-type brines. *Geology* **23**, 641-644.

Kesler, S.E., Martini, A.M., Appold, M.S., Walter, L.M., Huston, T.J., Furman, C. (1996). Na-Cl-Br systematics of fluid inclusions form Mississippi Valley-type deposits, Appalachian Basin: constraints on solute origin and migration paths. *Geochimica et Cosmochimica Acta* **66**, 22-233.

Khadem Allah, B., Fontane, F., Kadar, M., Monchoux, P. & Sørensen, H. (1998). Reactions between agpaitic nepheline syenitic melts and sedimentary carbonate rocks, exemplified by the Tamazeght Complex, Morocco. *Geochemistry International* **36**, 569-581.

Kieffer, S.W. (1982). Thermodynamics and lattice vibrations of minerals: 5. Applications to phase equilibria, isotopic fractionation and high-pressure thermodynamic properties. *Reviews of Geophysics and Space Physics* **20**, 827-849.

Köhler, J., Konnerup-Madsen, J., Markl, G. (in review). Fluid geochemistry in the Ivigtut cryolite deposit, South Greenland. *Lithos*.

Konnerup-Madsen, J. (1980). Fluid inclusions in minerals from igneous rocks belonging to the Precambrian continental Gardar rift province, South Greenland: the alkaline Ilímaussaq intrusion and the alkaline acidic igneous complexes. PhD Thesis, University of Copenhagen, 140 p.

Konnerup-Madsen, J. (1984). Composition of fluid inclusions in granites and quartz syenites from the Gardar continental rift province (South Greenland). *Bulletin de Minéralogie* **107**, 327-340.

Konnerup-Madsen, J. (2001). A review of the composition and evolution of hydrocarbon gases during solidification of the Ilímaussaq alkaline complex, South Greenland. *Geology of Greenland Survey Bulletin* **190**, 159-166.

Konnerup-Madsen, J., Rose-Hansen, J. (1982). Volatiles associated with alkaline igneous rift activity; fluid inclusions in the Ilímaussaq intrusion and the Gardar granitic complex (South Greenland). *Chemical Geology* **37**, 79-93.

Konnerup-Madsen, J., Rose-Hansen, J. (1984). Composition and significance of fluid inclusions in the Ilímaussaq peralkaline granite, South Greenland. *Bulletin de Minéralogie* **107**, 317-326.

Konnerup-Madsen, J., Larsen, E., Rose-Hansen, J. (1979). Hydrocarbon-rich fluid inclusions in minerals from the alkaline Ilímaussaq intrusion, South Greenland. *Bulletin de Minéralogie* **102**, 642-653.

Konnerup-Madsen, J., Rose-Hansen, J., Larsen, E. (1981). Hydrocarbon gases associated with alkaline igneous activity: evidence from compositions of fluid inclusions. *Rapport Grønlands Geologiske Undersøgelse* **103**, 99-108.

Konnerup-Madsen, J., Dubessy, J., Rose-Hansen, J. (1985). Combined Raman microprobe spectrometry and microthermometry of fluid inclusions in minerals from igneous rocks of the Gardar province (south Greenland). *Lithos* **18**, 271-280.

Konnerup-Madsen, J., Kreulen, R., Rose-Hansen, J. (1988). Stable isotope characteristics of hydrocarbon gases in the alkaline Ilímaussaq complex, South Greenland. *Bulletin de Minéralogie* **111**, 567-576.

Kretz, R. (1983). Symbols for rock-forming minerals. *American Mineralogist* **68**, 277-279.

Krumrei, T.V., Villa, I.M., Marks, M.A.W., Markl, G. (2006). A $^{40}Ar/^{39}Ar$ and U/Pb isotopic study of the Ilímaussaq complex, South Greenland: implications for the ^{40}K decay constant and for the duration of magmatic activity in a peralkaline complex. *Chemical Geology* **227**, 258-273.

Krumrei, T.V., Pernicka, E., Kaliwoda, M., Markl, G. (2007). Volatiles in a peralkaline system: abiogenic hydrocarbons and F-Cl-Br systematics in the naujaite of the Ilímaussaq intrusion, South Greenland. *Lithos* **95**, 298-314.

Kunzendorf, H., Nyegaard, P., Nielsen, B.L. (1982). Distribution of characteristic elements in the radioactive rocks of the northern part of Kvanefjeld, Ilímaussaq instrusion, South Greenland. *Rapport Grønlands Geologiske Undersøgelse* **109**, pp.32.

Kyser, T.K., O'Neil, J.R. (1984). Hydrogen isotope systematics of submarine basalts. *Geochimica et Cosmochimica Acta* **48**, 2123-2133.

Lager, G.A., Armbruster, T., Rotella, F.J., Rossman, G.R. (1989). OH substitution in garnets: X-ray and neutron diffraction, infrared, and geometric-modeling studies. *American Mineralogy* **74**, 840-851.

Lamb, W.M., Popp, R.K., Boockoff, L.A. (1996). The determination of phase relations in the CH_4-H_2O-NaCl system at 1 kbar, 400 to 600 °C using synthetic fluid inclusions. *Geochimica et Cosmochimica Acta*, **60**, 1885-1897.

Larsen, L.M. (1976). Clinopyroxenes and coexisting mafic minerals from the alkaline Ilímaussaq Intrusion, south Greenland: chemistry and petrological implications. *Journal of Petrology* **17**, 258-290.

Larsen, L.M. (1981). Chemistry of feldspars in the Ilímaussaq augite syenite with additional data on some other minerals. *Rapport Grønlands Geologiske Undersøgelse* **103**, 31-37.

Larsen, L.M., Sørensen, H. (1987). The Ilímaussaq Intrusion – progressive crystallization and formation of layering in an agpaitic magma. In: Fitton, J.G., Upton, B.G.J. (Eds.), Alkaline igneous rocks. *Geological Society Special Publications* **20**, 473-488.

Leake, B.E., Woolley, A.R., Arps, C.E.S., Birch, W.D., Gilbert, M.C., Grice, J.D., Hawthorne, F.C., Kato, A., Kisch, H.J., Krivovichev, V.G., Linthout, K., Laird, J., Mandarino, J., Marsch, W.V., Nickel, E.H., Rock, N.M.S., Schumacher, J.C., Smith, D.C., Stephenson, N.C.N., Ungaretti, L., Whittaker, E.J.W., Youzhi, G. (1997). Nomenclature of amphiboles. Report of the Subcommittee on Amphiboles of the International Mineralogical Association Commission on New Minerals and Mineral Names. *European Journal of Mineralogy* **9**, 623-651.

Leake, B.E., Woolley, A.R., Brich, W.D., Burke, E.A.J., Ferraris, G., Grice, J.D., Hawthorne, F.C., Kisch, H.J., Krivovichev, V.G., Schumacher, J.C., Stephenson, N.C:N., Whittaker, E.J.W. (2004). Nomenclature of amphiboles: additions and revisions to the International Mineralogical Association's amphibole nomenclature. *European Journal of Mineralogy* **16**, 191-196.

Liebscher, A., Lüders, V., Heinrich, W., Schettler, G. (2006). Br/Cl signature of hydrothermal fluids: liquid-vapour fractionation of bromine revisited. *Geofluids* **6**, 113-121.

Liou, J.G., Kim, H.S., Maruyama, S. (1983). Prehnite-epidote equilibria and their petrologic applications. *Journal of Petrology* **24**, 321-342.

Liferovich, R.P., Mitchell, R.H. (2006). Apatite-group minerals from nepheline syenites, Pilansberg alkaline complex, South Africa. *Mineralogical Magazine* **70**, 463-484.

Lorenzen, L. (1881). Undersøgelse of nogle Mineralier i Sodalith-Syenite fra Julianehaabs Distrikt (in Danish). *Meddelelser om Grønland* **2**, 43-79.

Markl, G. (2001a). A new type of silicate liquid immiscibility macroscopically visible in Proterozoic peralkaline rocks from Ilímaussaq, South Greenland. *Contributions to Mineralogy and Petrology* **141**, 458-472.

Markl, G. (2001b). Stability of Na-Be minerals in late-magmatic fluids of the Ilímaussaq alkaline complex. South Greenland. *Geology of Greenland Survey Bulletin* **190**, 145-158.

Markl, G., Baumgartner, L. (2002). pH changes in peralkaline late-magmatic fields. *Contributions to Mineralogy and Petrology* **144**, 331-346.

Markl, G., Marks, M., Schwinn, G., Sommer, H. (2001). Phase Equilibrium Constraints on Intensive Crystallization Parameters of the Ilímaussaq Complex, South Greenland. *Journal of Petrology* **42**, 2231-2258.

Marks, M., Markl, G. (2001). Fractionation and assimilation processes in the alkaline augite syenite unit of the Ilímaussaq intrusion, South Greenland, as deduced from phase equilibria. *Journal of Petrology* **42**, 1947-1969.

Marks, M., Vennemann, T., Siebel, W., Markl, G. (2003). Quantification of magmatic and hydrothermal processes in a peralkaline syenite-alkali granite complex based on textures, phase equilibria, and stable and radiogenic isotopes. *Journal of Petrology* **44**, 1247-1280.

Marks, M., Vennemann, T., Siebel, W., Markl, G. (2004). Nd-, o-, and H-isotopic evidence for complex, closed-system fluid evolution of the peralkaline Ilímaussaq intrusion, South Greenland. *Geochimica et Cosmochimica Acta* **68**, 3379-3395.

Marks, M.A.W., Rudnick, R.L., McCammon, C., Vennemann, T., Markl, M. (in review). Arrested kinetic Li isotope fractionation at the margin of the Ilímaussaq complex, South Greenland: evidence for open-system processes during final cooling of peralkaline igneous. *Chemical Geology*.

Matsuhisa, Y., Goldsmith, J.R., Clayton, R.N. (1979). Oxygen isotope fractionation in the system quartz-albite-anorthite-water. *Geochimica et Cosmochimica Acta* **43**, 1131-1140.

McDonough, W.F., Sun, S.S. (1995). The composition of the Earth. *Chemical Geology* **120**, 223-253.

Meinert, L.D., Dipple, G.M. & Nicolescu, S. (2005). World skarn deposits. 100th anniversary volume, *Economic Geology,* 299-336.

Metcalf-Johansen, J. (1983). Prehnite from the Ilímaussaq alkaline intrusion. *Mineralogical Magazine* **47**, 403-404.

Millero, F.J. (2004). Physicochemical Controls on Seawater. In: Elderfield, H., Holland, H.D., Turekian, K.K. (Eds.), Treatise on Geochemistry, Volume 6, The Oceans and Marine Geochemistry. Elsevier Ltd, 1-22.

Mitchell, R.H., Liferovich, R.P. (2006). Subsolidus deuteric/hydrothermal alteration of eudialyte in lujavrites from the Pilansberg alkaline complex, South Africa. *Lithos* **91**, 352-372.

Müller-Loch, D., Marks, M.A.W., Markl, G. (2007). Na and K distribution in agpaitic pegmatites. *Lithos* **95**, 315-330.

Mullis, J. (1979). The system methane-water as a geologic thermometer and barometer from the external part of the Central Alps. *Bulletin de Minéralogie* **102**, 526-536.

Nesbit, B.E., Prochaska, W. (1998). Solute chemistry of inclusions fluids from sparry dolomites and magnesites in Middle Cambrian carbonate rocks of the southern Canadian Rocky Mountains. *Canadian Journal of Earth Sciences* **35**, 546-555.

Nivin, V.A., Devirts, A.L., Lagutina, Y.P. (1995). Hydrogen generation from mantle source rocks in Oman. *Earth and Planetary Science Letters* **60**, 315-321.

Nivin, V.A., Treloar, P.J., Konopleva, N.G., Ikorsky, S.V. (2005). A review of the occurrence, form and origin of C-bearing species in the Khibiny Alkaline Igneous Complex, Kola Peninsula, NW Russia. *Lithos* **85**, 93-112.

Oelkers, E.H., Helgeson, H.C. (1990). Triple-ion anions and polynuclear complexing in supercritical electrolyte solutions. *Geochimica et Cosmochimica Acta* **54**, 727-738.

Oosting, S.E., Von Damm, K.L. (1996). Bromide/chloride fractionation in seafloor hydrothermal fluids from 9-10°N East Pacific Rise. *Earth and Planetary Science Letters* **144**, 133-145.

Parsons, I., Mason, R.A., Becker, S.M., Finch, A.A. (1991). Biotite equilibria and fluid circulation in the Klokken Intrusion. *Journal of Petrology* **32**, 1299-1333.

Paslick, C.R., Halliday, A.N., Davies, G.R., Mezger, K., Upton, B.G.J. (1993). Timing of proterozoic magmatism in the Gardar Province, southern Greenland. *Bulletin of the Geological Society of America* **105**, 272-278.

Pauly, H., Bailey, J.C. (1999). Genesis and evolution of the Ivigtut cryolite deposit, SW Greenland. *Meddelelser om Grønland Geoscience* **37**, 60pp.

Petersen, O.V., Micheelsen, H.I., Leonardsen, E.S. (1995). Bavenite, $Ca_4Be_3Al[Si_9O_{25}(OH)_3]$, from the Ilímaussaq alkaline complex, South Greenland. *Neues Jahrbuch Mineralogie Monatsheft* **7**, 321-335.

Petersilie, I.A., Sørensen, H. (1970). Hydrocarbon gases and bituminous substances in rocks from the Ilímaussaq alkaline intrusion, South Greenland. *Lithos* **3**, 59-76.

Pironon, J., Sawatzki, J., Dubessy, J. (1991). NIR FT-Raman microspectroscopy of fluid inclusions: Comparison with VIS Raman and FT-IR microspectroscopies. *Geochimica et Cosmochimica Acta* **55**, 3885-3891.

Pironon, J., Grimmer, J.O.W., Teinturier, S., Guillaume, D., Dubessy, J. (2003). Dissolved methane in water: temperature effect on Raman quantification in fluid inclusions. *Journal of Geochemical Exploration* **78-79**, 111-115.

Piotrowski, J.M. & Edgar, A.D. (1970). Melting relations of undersaturated alkaline rocks from South Greenland, *Meddelelser om Grønland* **181**, 62 pp.

Potter, J. (2000). The characterisation and origin of hydrocarbons in the alkaline igneous complexes in the Kola Alkaline Province. PhD thesis, Kingston University, London, UK.

Potter, J., Rankin, A.H., Treloar, P.J., Nivin, V.A., Ting, W., Ni, P. (1998). A preliminary study of methane inclusions in alkaline igneous rocks of the Kola igneous province, Russia: implication for the origin of methane in igneous rocks. *European Journal of Mineralogy* **10**, 1167-1180.

Potter, J., Konnerup-Madsen, J. (2003). A review of the occurrence and origin of abiogenic hydrocarbons in igneous rocks. In: Petford, N., McCaffrey. K.J.W. (Eds.), Hydrocarbons in Crystalline Rocks. *Geological Society, London, Special Publications* **214**, 151-173.

Potter, J., Rankin, A.H., Treloar, P.J. (2004). Abiogenic Fischer-Tropsch synthesis of hydrocarbons in alkaline igneous rocks; fluid inclusion, textural and isotopic evidence from the Lovozero complex, N.W. Russia. *Lithos* **75**, 311-330.

Potter, J., Longstaffe, J., Treloar, P.J., Beeskow, B., Rankin, A.H. (2006). A method for determination of stable isotope compositions of volatile in fluid inclusions: Results from hydrocarbon-bearing fluids of the Khibina alkaline complex, northwest Russia. GAC-MAC *Annual Meeting, Program with abstracts* **31**, 122-123.

Potter, J., Longstaffe, J. (2007). A gas-chromatograph, continuous flow-isotope ratio mass-spectrometry method for $\delta^{13}C$ and δD measurement of complex fluid inclusion volatiles: Examples from the Khibina alkaline igneous complex, northwest Russia and the south Wales coalfields. *Chemical Geology* **244**, 186-201.

Poulsen, V. (1964). The sandstones of the Precambrian Eriksfjord Formation in Southern Greenland. *Rapport Grønlands Geologiske Undersøgelse*, **2**, 16 pp.

Rae, D.A., Coulson, I.M., Chambers, A.D. (1996). Metasomatism in the North Qôroq centre, South Greenland: apatite chemistry and rare-earth element transport. *Mineralogical Magazine* **60**, 207-220.

Ranløv, J., Dymek, R.F. (1991). Compositional zoning in hydrothermal aegirine from fenites in the Proterozoic Gardar Province, South Greenland. *European Journal of Mineralogy* **3**, 837-853.

Roedder, E. (1984). Fluid Inclusions. *Reviews in Mineralogy* **12**, 646 pp.

Rossman, G.R., Aines, R.D. (1986). Spectroscopy of a birefringent grossular from Asbestos, Quebec, Canada. *American Mineralogist* **71**, 779-780.

Rumble, D., Hoering, T.C. (1994). Analysis of oxygen and sulfur isotope ratios in oxide and sulfide minerals by spot heating with a carbon dioxide laser in a fluorine atmosphere. *Accounts of Chemical Research* **27**, 237-241.

Ryabchikov, I.D., Kogarko, L.N. (2006). Magnetite compositions and oxygen fugacities of the Khibina magmatic system. *Lithos* **91**, 35-45.

Salvi, S., Williams-Jones, A.E. (1990). The role of hydrothermal processes in the granite-hosted Zr, Y, REE deposit at Strange Lake, Quebec / Labrador: Evidence from fluid inclusions. *Geochimica et Cosmochimica Acta* **54**, 2403-2418.

Salvi, S., Williams-Jones, A.E. (1992). Reduced orthomagmatic C-O-H-NaCl fluid in the Strange Lake rare-metal granitic complex, Quebec / Labrador, Canada. *European Journal of Mineralogy* **4**, 1155-1174.

Salvi, S., Williams-Jones, A.E. (1996). The role of hydrothermal processes in concentration high-field strength elements in the Strange Lake peralkaline complex, northeastern Canada. *Geochimica et Cosmochimica Acta* **60**, 1917-1932.

Salvi, S., Williams-Jones, A.E. (1997). Fischer-Tropsch synthesis of hydrocarbons during sub-solidus alteration of the Strange Lake peralkaline granite, Quebec / Labrador, Canada. *Geochimica et Cosmochimica Acta* **61**, 83-99.

Salvi, S., Williams-Jones, A.E. (2006). Alteration, HFSE mineralisation and hydrocarbon formation in peralkaline igneous systems: Insights from the Strange Lake Pluton, Canada. *Lithos* **91**, 19-34.

Salvi, S., Fontan, F., Monxhoux, P., Williams-Jones, A.E., Moine, B. (2000). Hydrothermal mobilization of high field strength elements in alkaline igneous systems: Evidence from the Tamazeght Complex (Morocco). *Economic Geology* **95**, 559-676.

Savatenkov, V.M., Morozova, I.M., Levsky, L.K. (2004). Behavior of the Sm-Nd, Rb-Sr, K-Ar, and U-Pb isotopic systems during alkaline metasomatism: Fenites in the outer-contact zone of an ultramafic-alkaline intrusion. *Geochemistry International* **42**, 899-920.

Schoell, M. (1988). Multiple origins of methane in the earth. *Chemical Geology* **71**, 1-10.

Schönenberger, J., Marks, M., Wagner, T., Markl, G. (2006). Fluid-rock interaction in autoliths of agpaitic nepheline syenites in the Ilímaussaq intrusion, South Greenland. *Lithos* **91**, 331-351.

Seitz, J.C., Pasteris, J.D. (1990). Theoretical and practical aspects of different partitioning of gases by clathrate hydrates in fluid inclusions. *Geochimica et Cosmochimica Acta* **54**, 631-639.

Sharp, Z.D. (1990). A laser-based microanalytical method for the in-situ determination of oxygen isotope rations of silicates and oxides. *Geochimica et Cosmochimica Acta* **54**, 1353-1357.

Sindern, S., Kramm, U. (2000). Volume characteristics and element transfer of fenite aureoles: a case study from the Iivaara alkaline complex, Finland. *Lithos* **51**, 75-93.

Sheppard, S.M.F. (1986). Characterization and isotopic variations in natural waters. In: Valley, J.W., Taylor Jr., H.P., O'Neil, J.R. (Eds.), Stable Isotopes. *Reviews in Mineralogy* **16**, 165-181.

Sherwood-Lollar, B., Frape, S.K., Weise, S.M., Fritz, P., Macko, S.A., Welhan, W.A. (1993). Abiogenic methanogenesis in crystalline rocks. *Geochimica et Cosmochimica Acta* **57**, 5087-5097.

Sherwood-Lollar, B., Westgate, T.D., Ward, J.A., Slater, G.F., Lacrampe-Couloume, G. (2002). Abiogenic formation of alkanes in the Earth's crust as a minor source for global hydrocarbon reservoirs. *Nature* **416**, 522-524.

Sherwood-Lollar, B., Lacrampe-Couloume, G., Slater, G.F., Ward, J., Moser, D.P., Gohring, T.M., Lin, L.-H., Onstott, T.C. (2006). Unravelling abiogenic and biogenic sources of methane in the Earth's deep subsurface. *Chemical Geology* **226**, 328-339.

Shimazaki, H. (1982). The Sasano hastingsite-bearing copper skarn deposit formed in aluminous sediment, at the Yoshioka mine, Japan. *Economic Geology* **77**, 868-876.

Shock, E.L., Oelkers, E.H., Johnson, J.W., Sverjensky, D.A., Helgeson, H.C. (1992). Calculation of the thermodynamic properties of aqueous species at high pressures and temperatures. *Journal of the Chemical Society Faraday Transactions* **88**, 803-950.

Shock, E.L., Sassani, D.C., Willis, M., Sverjensky, D.A. (1997). Inorganic species in geological fluids: correlation among standard molal thermodynamic properties of aqueous ions and hydroxide complexes. *Geochimica et Cosmochimica Acta* **61**, 907-950.

Shvarov, Y.V., Bastrakov, E.N. (1999). HCh: a software package for geochemical equilibrium modelling. User's Guide. Australian Geological Survey Organisation, Record 1999/25, 61 p.

Shvarov, Y.V. (1978). Minimization of the thermodynamic potential of an open chemical system. *Geochemistry International* **15**, 200-203.

Shvarov, Y.V. (1981). A general equilibrium criterion for an isobaric-isothermal model of a chemical system. *Geochemistry International* **18**, 38-45.

Sindern, S., Kramm, U. (2002). Volume characteristics and element transfer of fenite aureoles: A case study from the Iivaara alkaline complex, Finland. *Lithos* **51**, 75-93.

Sobolev, V.S., Bazarova, T.Y., Shugurova, N.A., Bazarov, L.S., Dolgov, Y.A., Sørensen, H. (1970). A preliminary examination of fluid inclusions in nepheline, sørensenite, tugtupite and chkalovite from the Ilímaussaq alkaline intrusion, South Greenland. *Bulletin Geological Survey of Greenland* **81**, 1-21.

Sood, M.K., Edgar, A.D. (1970). Melting relations of undersaturated alkaline rocks from the Ilímaussaq intrusion and Grønnedal-Ika complex, South Greenland, under water vapour and controlled partial oxygen pressure. *Meddelelser om Grønland* **181**, 41pp.

Sørensen, H. (1962). On the occurrence of streenstrupine in the Ilímaussaq massif, southwest Greenland. *Meddelelser om Grønland* **167**, 251pp.

Sørensen, H. (1969). Rythmic igneous layering in peralkaline intrusions. *Lithos* **2**, 261-283.

Sørensen, H. (1992). Agpaitic nepheline syenites: a potential source of rare elements. *Applied Geochemistry* **7**, 417-427.

Sørensen, H. (1997). The agpaitic rocks – an overview. *Mineralogical Magazine* **61**, 485-498.

Sørensen, H. (2001). Brief introduction to the geology of the Ilímaussaq alkaline complex, South Greenland, and its exploration history. *Geology of Greenland Survey Bulletin* **190**, 7-24.

Sørensen, H. (2006). The Ilímaussaq Alkaline Complex, South Greenland – an Overview of 200 years of Research and an Outlook. *Meddelelser om Grønland* **45**, 70 pp.

Sørensen, H., Larsen, L.M. (2001). The hyperagpaitic stage in the evolution of the Ilímaussaq alkaline complex, South Greenland. In: Sørensen, H. (Ed.), The Ilímaussaq Alkaline Complex, South Greenland, status of mineralogical research with new results, *Geology of Greenland Bulletin* **190**, 83-94.

Sørensen, H., Rose-Hanse, J., Nielsen, B.L., Løvborg, L., Sørensen, E., Løvborg, T. (1974). The uranium, deposit at Kvanefjeld, the Ilímaussaq intrusion, South Greenland. Geology, reserves, beneficiation. *Rapport Grønlands Geologiske Undersøgelse* **60**, 54 pp.

Sørensen, H., Bailey, J.C., Kogarko, L.N., Rose-Hansen, J., Karup-Møller, S. (2003). Spheroidal structures in arfvedsonite lujavrite, Ilímaussaq alkaline complex, South Greenland – an example of macro-scale liquid immiscibility. *Lithos* **70**, 1-20.

Sørensen, H., Bohse, H., Bailey, J.C. (2006). The origin and mode of emplacement of lujavrites in the Ilímaussaq alkaline complex, South Greenland. *Lithos* **91**, 286-300.

Sterner, S.M., Hall, D.L., Bodnar, R.J. (1988). Synthetic fluid inclusions. V. Solubility relations in the system NaCl-KCl-H$_2$O under vapor-saturated conditions. *Geochimica et Cosmochimica Acta* **52**, 989-1005.

Stevenson, R., Upton, B.G.J., Steenfelt, A. (1997). Crust-mantle interaction in the evolution of the Ilímaussaq Complex, South Greenland: Nd isotopic studies. *Lithos* **40**, 189-202.

Stober, I., Bucher, K. (1999). Origin of salinity of deep groundwater in crystalline rocks. *Terra Nova* **11**, 181-185.

Sverjensky, D.A., Shock, E.L., Helgeson, H.C. (1997). Prediction of the thermodynamic properties of aqueous metal complexes to 1000 °C and 5 kb. *Geochimica et Cosmochimica Acta* **61**, 1359-1412.

Taylor, B.E. (1976). Origin and significance of C-O-H fluids in the formation of Ca-Fe-Si skarn, Osgood Mountains, Humboldt County, Nevada. PhD Dissertation, Stanford University.

Taylor Jr., H.P. (1997). Water/rock interactions and the origin of H$_2$O in granitic batholiths. *Journal of the Geological Society of London* **133**, 509-558.

Taylor Jr., H.P., Sheppard, S.M.F. (1986). Igneous Rocks: I. Processes of isotopic fractionation and isotope systematics. In: Valley, J.W., Taylor Jr., H.P., O'Neil, J.R. (Eds.), Stable Isotopes in high temperature geological processes. *Reviews in Mineralogy* **16**, 227-271.

Unruh, C.H., Katz, D.L. (1949). Gas hydrates of carbon dioxide-methane mixtures. *Journal of Petroleum Technology* **1**, 83-86.

Upton, B.G.J., Emeleus, C.H. (1987). Mid-Proterozoic alkaline magmatism in southern Greenland: the Gardar province. In: Fitton, J.G., Upton, B.G.J. (Eds.), The Alkaline Rocks. *Geological Society of London Special Publication* **30**, 449-471.

Upton, B.G.J., Emeleus, C.H., Heaman, L.M., Goodenough, K.M., Finch, A. (2003). Magmatism of the mid-Proterozoic Gardar Province, South Greenland: chronology, petrogenesis and geological setting. *Lithos* **68**, 43-65.

Ussing, N.V. (1912). Geology of the country around Julianehaab, Greenland. *Meddelelser om Grønland* **38**, 376pp.

Valley, J.W., Essene, E.J., Peacor, D.R. (1983). Fluorine-bearing garnets in Adirondack calc-silicates. *American Mineralogist* **68**, 444-448.

Valley, J.W., Kitchen, N., Kohn, M.J., Niendorf, C.R., Spicuzza, M. (1995). UWG-2, a garnet standard for oxygen isotope ratios: Strategies for high precision and accuracy with laser heating. *Geochimica et Cosmochimica Acta* **59**, 5223-5231.

Veksler, I.V. (2004). Liquid immiscibility and its role at the magmatic-hydrothermal transition: A summary of experimental studies. *Chemical Geology* **210**, 7-31.

Vennemann, T.W., O'Neil, L.R. (1993). A simple and inexpensive method of hydrogen isotope and water analyses of minerals and rocks based on zinc reagent. *Chemical Geology* **103**, 227-234.

Vennemann, T.W., Smith, H.S. (1990). The rate and temperature of reaction of CIF3 with silicate minerals, and their relevance to oxygen isotope analysis. *Chemical Geology* (Isotope Geoscience Section) **86**, 83-88.

Voytov, G.I. (1992). Chemical and carbon-isotope fluctuations in free gases (gas jets) in the Khibiny. *Geochemistry International*, 14-24.

Wegmann, C.E. (1938). Geological investigations in southern Greenland. Part I. On the structural divisions of southern Greenland. *Meddelelser om Grønland* **113**, 148 pp.

Welhan, J.A., Craig, H. (1983). Methane, hydrogen and helium in hydrothermal fluids at 21°N, East Pacific Rise. In: Rona, P.A., Boström, K., Laubier, L., Smith Jr, K.L. (Eds.), Hydrothermal processes at seafloor spreading centres. Plenum, New York, 391-409.

Wopenka, B., Pasteris, J.D., Freeman, J.J. (1990). Analysis of individual fluid inclusions by Fourier transform infrared and Raman microspectroscopy. *Geochimica et Cosmochimica Acta* **54**, 519-533.

Yaqian, Q., Jibao, G. (1993). Study of hydrogen isotope equilibrium and kinetic fractionation in the ilvaite-water system. *Geochimica et Cosmochimica Acta* **57**, 3073-3082.

Yardley, B.W.D., Banks, D.A., Bottrell, S.H. (1993). Post-metamorphic gold-quartz veins from NW Italy: the composition and origin of the ore fluid. *Mineralogical Magazine* **57**, 407-422.

Zheng, Y.F. (1991). Calculation of oxygen isotope fractionation in metal oxides. *Geochimica et Cosmochimica Acta* **55**, 2299-2307.

Zheng, Y.F. (1993a). Calculation of oxygen isotope fractionation in hydroxyl-bearing silicates. *Earth Planetary Science Letters* **120**, 247-263.

Zheng, Y.F. (1993b). Calculation of oxygen isotope fractionation in anhydrous silicate minerals. *Geochimica et Cosmochimica Acta* **57**, 1070-1091.